The Dissertation Committee for Si Chon Lao Certifies that this is the approved version of the following dissertation:

Multifunctional Cyanate Ester/MWNT Nanocomposites: Processing and Characterization

Committee:

Tess J. Moon, Supervisor

Joseph H. Koo, Co-Supervisor

Paulo J. Ferreira

Donald R. Paul

Rodney S. Ruoff

Multifunctional Cyanate Ester/MWNT Nanocomposites: Processing and Characterization

by

Si Chon Lao, B.S.Ch.; M.S.E.

Dissertation

Presented to the Faculty of the Graduate School of

The University of Texas at Austin

in Partial Fulfillment

of the Requirements

for the Degree of

Doctor of Philosophy

The University of Texas at Austin

December 2013

Dedication

To my mother, elder brother, friends, and brothers and sisters in Christ, who supported me during my graduate study.

Acknowledgements

First and foremost, the author would like to thank Dr. Koo and Dr. Moon for the many years of patient supervising and generous teaching. The author would also like to thank Dr. Louis Pilato, Dr. Wei Li, Dr. Jinyong Lee, Dr. Mourad Krifa, and Dr. Jitendra Tate for their advices and assistances throughout the project. Gratitude extends to the colleagues of the Koo Research Group, particularly Dr. Ayou Hao, Hao Wu, Chris Lam, Eric Yao, and Brian Lisco, who shared the many research projects over the past years and assisted in many ways the making of this project. Lastly and most importantly, the author would like to thank his family for the continual support. Partial financial support from Air Force Office of Scientific Research (AFOSR) and KAI, LLC is greatly appreciated.

Multifunctional Cyanate Ester/MWNT Nanocomposites: Processing and Characterization

Si Chon Lao, Ph.D.

The University of Texas at Austin, 2013

Supervisor: Tess J. Moon

Co-Supervisor: Joseph H. Koo

Tomorrow's lightweight, high-performance composite systems will be made of structures built with materials that have unprecedented intrinsic properties for performing a wide range of functions, such as EMI shielding, thermal management, flame resistance, lightning strike protection, acoustic damping, and health-monitoring. Current structures require parasitic components, e.g., metal strips, copper wire meshes, strain gauges, and heat sinks to provide these functions. By eliminating parasitic components, future high-performance multifunctional systems can achieve the intended objectives, while maintaining optimum weight, reliability, cost, and fuel efficiency. With the continuing growth of polymer composites in industries, such as aerospace, automotive, and wind energy, research and development on lightweight, high-performance composites that possess extraordinary properties for future multifunctional systems has generated considerable interest and excitement. Recent advances in nanomaterial synthesis and functionalization have shown that tailored property combinations are possible with reduced parasitic content to achieve multifunctionality.

Cyanate ester (CE), a class of high-performance thermosetting resins (high T_g, >250°C), has received considerable attention due to its good mechanical properties,

thermal stability, flammability properties, ease of process, and volatile-free curing process. Multiwall carbon nanotubes were selected due to their unique combination of excellent mechanical, electrical, and thermal properties. The principal objective of this work is to determine the extent to which several different processing techniques will affect the MWNT dispersion and corresponding nanocomposite properties, such as thermal, flammability, mechanical, and electrical properties. A *processing-structure-property* relationship, as well as performance of this class of carbon-based CE nanocomposite, will be established. Therefore, a major scientific contribution of this study will be the development and characterization of a novel, multifunctional CE nanocomposite.

Different mixing instruments, such as high shear mixer, ultrasonicator, planetary centrifugal mixer, etc. were used to disperse the nanotubes in the cyanate ester resin matrix. Microstructural morphology characterizations by SEM, STEM, and TEM show that various degrees of dispersions of MWNTs were obtained by the different mixing techniques. An attempt to quantify the MWNT dispersion was made. Electrical resistivity of samples processed by both stand mixer and three-roll mill passes the ESD requirement; however, the MWNT percolation thresholds by the two techniques are different. Thermal analysis shows that the addition of the Fe^{3+} catalyst or the coupling agent lowers the glass transition temperature and degrades the mechanical properties (e.g., storage modulus, tangent of phase angle delta) of the CE resin. On the other hand, processing techniques only affect the mechanical properties of the resin. Thermal stability of CE is only slightly affected by different processing techniques, as well as the addition of MWNTs. Much more significantly, flammability characterization shows that the incorporation of either the Fe^{3+} catalyst or the coupling agent substantially increases the peak heat release rate (PHRR) relative to the neat CE resin value.

Table of Contents

List of Tables

List of Figures

Chapter 1

Introduction

Similar to conventional polymer composite materials, polymer nanocomposites (PNCs) consist of a polymer resin matrix and reinforcing phases. In PNCs, the polymer matrix is often composed of thermoplastics, thermosets, elastomers, or their blends, while the reinforcing phase is often different types of nanomaterials. The introduction of inorganic nanomaterials as additives into polymer matrix systems has resulted in polymer nanostructured materials exhibiting multifunctional, high-performance polymer characteristics beyond what traditional polymer composites possess [1-2]. Improvements attributable to polymer nanocomposites consist of improved thermal stability, flame and ablation resistance, mechanical properties, thermal and electrical conductivities, moisture resistance, permeability, charge dissipation, and chemical resistance. These composites are of interest in military, aerospace, and commercial flight applications, since composite structures of aerospace vehicles require thermally stable, electrically conductive, and high-performance resins [3-5].

Generally, the properties of the resulting PNCs depend on the compatibility between the polymer resin and nanomaterials, the fractional weight loading of the nanomaterials, and the processing techniques. In nanocomposites, most desirable properties result from a uniform dispersion of nanomaterials in the polymer matrix. Moreover, for conductive properties like electrical and thermal conductivity, a network of nanomaterials dispersed throughout the matrix reaching a percolation threshold is needed. If not well dispersed, the nanomaterial agglomerates may perform just like conventional micron-size particles. In fact, in some cases agglomeration of nanomaterials can result in polymer composite materials with inferior properties as compared to the neat polymer resin. This may result in reinforcement like conventional composite materials.

Fortunately, due to nanomaterials' generally high aspect ratio, PNCs require much lower fractional loadings of reinforcing nanomaterials than conventional composites.

Polyimide, a thermosetting resin with a high glass transition temperature (T_g~230-370°C) [5] has been the leading candidate for these demanding military and commercial aerospace/aviation applications. Polyimide nanocomposites—reinforced with carbon nanotubes (CNTs) and carbon nanofibers (CNFs)—have demonstrated superior thermal and mechanical properties as compared to neat polyimide resin [6]. Moreover, by incorporating high-strength, continuous carbon fibers into these nanocomposites, they can be further strengthened to create structural fiber-reinforced components [7]. Mo *et al*. incorporated various weight loadings (0.5 – 15 wt%) of MWNTs into polyimide resin via in-situ polymerization process and found that the glass transition temperature and decomposition temperature are unaffected by the incorporation of MWNTs [8]. Tensile strength increases as the amount of MWNT, up to 7 wt%, increases. The storage modulus increases 30% when 0.5wt% MWNT is added and an increase of 200% when 10 wt% is added. The polyimide polymer also gradually changes to a conductive system at a percolation threshold at 10 wt% MWNTs. However, polyimides are difficult to process and some release toxic materials, such as m-PDA, MDA, and NMP, during the curing process [9]. Nanocomposites that are toxin-free, cured in volatile-free processes and possessing thermal properties and glass transition temperatures similar to, or better than, the polyimide nanocomposites are desirable.

Cyanate ester (CE), a class of high-performance thermosetting resins, has received considerable attention due to its good mechanical properties, thermal stability, flammability properties, ease of process, and volatile-free curing process [10]. Its relatively high glass transition temperature (>250°C) falls between that of epoxy and polyimide. With proper nano-modification and cure, CE has a potential to replace the hard-to-process polyimide resin. Multiwall carbon nanotubes (MWNTs) were selected due to their unique combination of excellent mechanical, electrical, and thermal

properties [11], and it is anticipated that the incorporation of MWNTs will enhance the mechanical properties and thermal properties as well as reducing the electrical resistivity of the resulting CE-MWNT nanocomposites. Ultimately, the high-performance carbon fiber-reinforced CE-MWNT nanocomposites will be fabricated for the structural applications, as in the aerospace/aviation industries, military, etc., which require excellent mechanical, thermal, and flammability properties as well as good electrical conductivity.

The principal objective of this work is to determine the extent to which several standard processing techniques will affect/improve MWNT dispersion and attendant nanocomposite properties, such as the thermal, mechanical, and electrical properties, as well as flammability. A *processing-structure-property* relationship, as well as performance of this class of carbon-based CE nanocomposite, is established. Effects of different standard functionalizations of MWNTs (i.e. -OH, -COOH, and $-NH_2$) on MWNT dispersion in the CE resin are studied. In addition to aiding dispersion, these functionalizations have the potential to differentially affect/improve nanocomposite properties (such as mechanical properties, flammability properties, electrical conductivity, and thermal conductivity) due to the resulting improved interfacial bonding or adhesion between the CE resin and MWNTs. Finally, a major scientific contribution of this study is the development and characterization of a novel, multifunctional CE nanocomposite.

Most processing techniques for nano-modifications aim to disperse nanomaterials uniformly in the polymer resin. Dispersion techniques vary for different polymer resins and different nanomaterials. Common methods include emulsion polymerization, in-situ polymerization, melt compounding, solvent blending, ultrasonication, mechanical mixing, and high shear mixing. For example, polyhedral oligomeric silsesquioxane (POSS®) is usually functionalized, specifically tailored to the chosen polymer resin, and processed by in-situ polymerization. On the other hand, nanoclay usually requires shearing force, so that layers of clay platelets can be sheared apart. In the case of carbon

nanotubes, vigorous stirring or high shear mixing are believed to debundle the nanotubes aggregates. More details regarding these processing techniques and properties enhancement of the resulting polymer nanocomposites are discussed in the subsequent Chapters.

In this study, several processing instruments—including ultrasonicator, planetary centrifugal mixer, high shear mixer, three-roll mill, and stand mixer—are used to disperse the carbon nanotubes into the cyanate ester resin. The PNC morphology and MWNT dispersion are characterized by transmission electron microscopy (TEM) and scanning electron microscopy (SEM). Further, the thermal stability is assessed by thermogravimetric analysis (TGA), while combustion characteristics are examined by microscale combustion calorimetry (MCC). The glass transition temperature is determined by dynamic mechanical analysis (DMA), while the electrical conductivity is measured by megohmmeter and plate electrodes. Details of the characterization methods are discussed in Chapter 3, while results are discussed in Chapter 4. A preliminary study of the fabrication of carbon fiber-reinforced CE-MWNT nanocomposites was also performed. Processing and characterizations of these structural composite materials are discussed in Chapter 5. A brief summary and potential future work of this polymer nanocomposite research are provided in Chapter 6.

REFERENCES

1. J. H. Koo, *Polymer Nanocomposites: Processing, Characterization, and Applications,* McGraw-Hill, New York, 2006.
2. J. Leng, and A. K. Lau, *Multifunctional Polymer Nanocomposites*, CRC Press, Boca Raton, 2011.
3. J. Cheng, S. Lao, J. Yong, J. H. Koo, P. Ferreira, L. Pilato, G. Wissler, and Z. P. Luo, "Cyanate Ester-Buckytubes Nanocomposites: Processing and Characterization," *Proc. SAMPE 2007 ISSE*, SAMPE, Covina, CA (2007).
4. K. A. Watson, J. G. Smith Jr., and J. W. Connell, *Soc. Adv. Mat. Proc. Eng. Ser.*, 48: 1145, 2003.
5. D. A. Scola, "Polyimide Resins," *ASM Handbook, Composites*, 21: 105-119, 2001.
6. S. Ghose, K. A. Watson, H. A. Elliott, D. C. Working, J. M. Criss, K. L. Dudley, E. J. Siochi, and J. W. Connell, "Fabrication and Characterization of High Temperature Resin/Carbon Nanofiller Composites," *Proc. Multifunctional Nanocomposites 2006*, Sept 20-22, Honolulu, HI, 2006.
7. Y. Lu, M. Zhan, and W. Zheng, "Preparation and Properties of T300 Carbon Fiber- Reinforced Thermoplastic Polyimide Composites," *J. Appl. Polym. Sci.*, 102: 646- 654, 2006.
8. T.-C. Mo, H.-W. Wang, S.-Y. Chen, and Y.-C. Yeh, "Synthesis and Characterization of Polyimide/Multi-Walled Carbon Nanotube Nanocomposites," *Polymer Composites*, 29(4): 451-457, 2008.
9. D. Kohli, R. Mayhew, S. L. Peake, M. Bucchi, T. Vuong, F. Riel, and E. Delaney, *Proc. SAMPE 1993 ISSE*, 25: 318-326, SAMPE, Covina, CA (1993).
10. L. Christodoulou and J. D. Venables, "Multifunctional Material Systems: the First Generation," *Journal of Materials*, 55: 39-45, 2003.
11. M. Moniruzzaman and K. I. Winey, "Polymer Nanocomposites Containing Carbon Nanotubes," *Macromolecules*, 39: 5194-5205, 2006.

Chapter 2

Background

OVERVIEW AND LITERATURE REVIEW

Cyanate ester (CE), a class of high-performance thermosetting resins (glass transition temperature T_g >250°C), has received considerable attention due to its good mechanical properties, thermal stability, flammability properties, ease of process, and volatile-free curing process [1]. Cyanate ester can be cured by heating at a temperature above 165°C. During the cure process, it undergoes cyclotrimerization [2] to form triazine ring structure (Figure 2.1) and there is no decomposition by products [3]. According to the vendor, this material is suitable for resin transfer molding (RTM), vacuum-assisted resin transfer molding (VARTM), filament winding, resin liquid infiltration, pultrusion, abrasive coating, high voltage potting compound, liquid encapsulation, and reactive diluent. A carbon-carbon composite can be fabricated with cyanate ester as shown by previous studies by Shivakumar *et al.* [4-5] and Koo *et al.* [6-7].

Fabrication of nanocomposites with cyanate ester resin with different nanoparticles, such as clay, POSS®, carbon nanotubes, silicon nanoparticles, fumed silica, and zirconium tungstate, was conducted by a several groups [8-40]. In these studies, the research objectives were variously to enhance the glass transition temperature (T_g) and decomposition temperature, to improve the mechanical properties, and to lower

the dielectric constant of the polymer resin by incorporating conductive nanoparticles. Assorted processing techniques, such as mechanical blending, shear mixing, and sonication were used, but a direct comparison of these techniques on the same PNC system was not conducted. The polymer nanocomposites were usually characterized by thermogravimetric analysis (TGA), differential scanning calorimetry (DSC), and dynamic mechanical analysis (DMA) for materials properties and examined by scanning electron microscopy (SEM), transmission electron microscopy (TEM), Ramen spectroscopy, and x-ray diffraction (XRD) for nanoparticles dispersion. In some cases, mechanical properties were also tested.

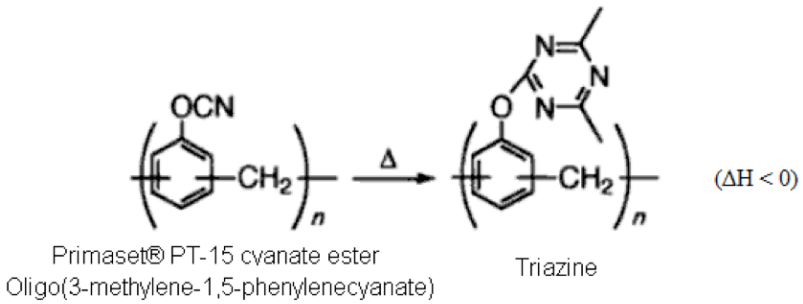

Figure 2.1. Molecular structure of Primaset® PT-15 polycyanate ester (Lonza Corporation) and its cyclotrimerization.

Cyanate Ester-Clay Nanocomposites

Gangulo *et al*. fabricated and characterized cyanate ester nanocomposites with montmorillonite organo-clay [8-13]. Mechanical force and blend/mix were usually used to exfoliate a few weight percent (wt%) of clay in the polymer resin. The clay enhanced both the thermal properties and thermal stability of the cyanate ester, since clay

simultaneously exhibits low thermal conductivity and high melting temperature. The glass transition temperature and decomposition temperature of the cyanate ester nanocomposite increase 10-15°C over that of the neat cyanate ester. Gilman *et al*. [14] showed that the montmorillonite organo-clay dramatically alters the flammability properties. For example, the peak heat release rate of the phenolic cyanate ester is reduced by over 50%. Nanoclay also alters the curing kinetics of the cyanate ester resin as shown by Lin *et al*. [15]; the cure of cyanate ester is accelerated to various degrees depending on the treatment of the nanoclay. Similar catalytic cyclotrimerization of the cyanate ester was reported by Pan *et al*. [16], who also found the flexural modulus, flexural strength, and fracture toughness of cyanate ester clay nanocomposites are increased 40%, 42%, and 55%, respectively, as compared to the neat resin. Wooster *et al*. [17] found that the crack resistance of the cyanate ester is improved by 80% by the addition of 4 wt% nanoclay without a sacrifice of flexural strength. Others have shown that the incorporation of nanoclay has similar enhancement on mechanical properties, toughness, and thermal properties of cyanate ester modified epoxy resin or cyanate/epoxy blends [18-21].

Cyanate Ester-POSS® Nanocomposites

Liang *et al*. [22-24] incorporated 1-15 wt% of POSS® into cyanate ester resin to synthesize cyanate ester-POSS® nanocomposites and conducted characterization. Since the POSS® was functionalized to mix favorably with the cyanate ester used, simple stirring and blending were sufficient to disperse the POSS® in the resin. The POSS®

enhances the glass transition and decomposition temperatures of the cyanate ester without compromising the viscosity beyond processing threshold. Dynamic mechanical analysis shows a general increase of glass transition temperature of more than 10°C, while in some cases the glass transition temperature increases twice as much from 360 to 380°C. The decomposition temperature given by the TGA also increases 15-20°C. Therefore, similar to clay, cyanate ester nanocomposites show promising thermal property improvement resulting from the incorporation of POSS®. Seetharaman *et al*. [25] incorporated different weight percentages (1, 3, 5, and 10 wt%) of octafunctional maleimide POSS® (OMPS) into bisphenol-A based CE resin and reported that the resulting nanocomposite with 5 wt% OMPS possesses higher values of glass transition temperature as compared to those filled with small amounts of OMPS. Similar to nanoclay, Zhang *et al*. [26] and Lin *et al*. [27], respectively, found that POSS® exhibits a catalytic effect on the cure of CE (lowering cure temperature and activation energy). The most effective catalytic effect was observed at 5 wt% of the POSS®. Zhang also reported that by incorporating 1 wt% POSS®, the dielectric constant of the cyanate ester is significantly lowered and the dielectric loss is reduced. Glass transition temperature increases at lower POSS® content (<5 wt%) and reaches a plateau beyond 5 wt%. Some research work of introducing POSS® into cyanate ester modified epoxy or cyanate ester/epoxy polymer blends were also conducted [28-31]. In general, POSS® increases the decomposition temperature, the glass transition temperature, and the storage modulus, but decreases dielectric constant of these polymer systems, similar to the effect of POSS® on the neat cyanate ester.

Cyanate Ester-Carbon Nanotubes Nanocomposites

Some research has been conducted on CE-CNT nanocomposites. Cheng *et al*. [32] attempted to disperse 1-3 wt% non-functionalized, small diameter (~3.5nm) CNTs (or buckytubes) into Primaset® PT-15 cyanate ester using a high shear mixer at 5000-7900rpm, but was unsuccessful due to CNT dispersion. The buckytubes agglomerated in the CE matrix, probably due to the high aspect ratio and entanglement of nanotubes, as well as insufficient interfacial adhesion between the nanotubes and the matrix [33]. Phase separation of neat resin from the buckytube nanocomposite was observed in the cured nanocomposite materials. Notably phase separation was not observed immediately after mixing, suggesting that it occurred during the 16-hour curing process. This phenomenon may be due to the weak interfacial adhesion between the nanotubes and the resin matrix, as well as the long (16 hours) cure time required for catalyst-free CE curing. Further, the thermal properties of these processed nanocomposites were inferior to those of the neat CE resin.

Dominguez *et al*. [34] mixed 0.01-3 wt% of MWNT into cyanate ester resin using a high intensity (20kHz, 500W) ultrasonic mixer. He reported improved viscoelastic behavior and thermal properties of the MWNT-reinforced cyanate ester polymer. Glass transition temperature and decomposition temperature increased 7-13% and 5-8%, respectively, while the storage modulus at 40°C increased 12-50%. Wang *et al*. [35] reported a 10% increase in the storage modulus and a 40% increase in the flexural strength when incorporating 2 wt% of functionalized MWNT into the cyanate ester resin by ultrasonication. Han *et al*. [36] dispersed various weight loadings of MWNTs into

cyanate ester resin with vigorous stirring by a homogeneous agitator. The electrical conductivity increased by as much as five orders of magnitude and a percolation threshold of 0.5-0.65 wt% MWNT for these CE-MWNT nanocomposites was reported.

Similar to clay and POSS®, MWNT may also alter the cure dynamics of the cyanate ester. Lin *et al*. [37] reported that pristine MWNT does not have any effect on the cure behavior of the cyanate ester, while functionalized MWNT decreases the cure temperature and activation energy by as much as 20% and 50%, respectively.

Cyanate Ester Nanocomposites with Other Nanoparticles

There are a few research reports on cyanate ester nanocomposites made with other nanoparticles, such as fumed silica [38], zirconium tungstate [39], and silicon nanoparticles [40]. Most of these published work focus on the material properties and the processing techniques and methodologies are not well documented.

Carbon Fiber-Reinforced Cyanate Ester Nanocomposites

Some carbon fiber-reinforced cyanate ester nanocomposites have been fabricated and variously characterized [41-44]. However, the fabrication techniques, conditions, and methodologies, which are generally not the subject of investigation, are scarcely documented. Further, the cyanate ester resin used varies from study to study. Therefore, there is a need to conduct a preliminary study on the fabrication of the carbon fiber-reinforced composite with the cyanate ester and cyanate ester nanocomposites used and fabricated in this study. This will provide guidelines for future studies.

In summary, nanoclay and POSS® can enhance the glass transition temperature and decomposition temperature of cyanate ester resin, while carbon nanotubes may or may not exhibit a similar improvement—depending on the type of carbon nanotube and nanotube functionalization, if any. That said, it is clear that carbon nanotubes can increase the electrical conductivity of the relatively low-electrical conductivity cyanate ester polymer. Nanoclay, POSS®, and carbon nanotubes can affect the cure behavior of the cyanate ester. Existing cyanate ester nanocomposites research reports relatively simple and standard processing techniques. A detailed comparison and examination of different processing techniques for manufacturing CE-MWNT nanocomposites is lacking in the literature. This research attempts to address that void.

REFERENCES

1. D. Dean, M. O. Abdalla, S. Ganguli, M. Jose, S. Campbell, J. Gillman, W. H. Awad, and R. Vaia, "High Temperature Thermoset Nanocomposites," *Proc. SAMPE 2003 ISSE*, SAMPE, Covina, CA (2003).
2. I. Hamerton, *Chemistry and Technology of Cyanate Ester Resins*, Blackie Academic & Professional, New York, 1994, p. 122.
3. Primaset® PT-15 Brochure. Lonza Inc. Fair Lawn, NJ.
4. K. Shivakumar, F. Abali, R. Sadler, and J. McCoy, "Development of Cyanate Ester Based Carbon/Carbon Composites," *Proc. SAMPE 2000 ISESE*, SAMPE, Covina, CA (2000), p. 1005.
5. F. Abali, K. Shivakumar, N. Hamidi, and T. Sadler, "An RTM Densification Method of Manufacturing Carbon-Carbon Composites Using PT-30 Resin," *Carbon*, 41 (5), 893 (2003).
6. Koo *et al*. "Thermo-Oxidative Studies of Nanomodified Carbon/Carbon Composites," The University of Texas at Austin, Dept. of Mechanical Engineering, Austin, TX. *Proc. SAMPE 2004 ISSE*, SAMPE, Covina, CA (2004).
7. Koo *et al*. "Nanomodified Carbon/Carbon Composites for Intermediate Temperature: Processing and Characterization," Texas A&M University, Dept. of Mechanical Engineering, College Station, TX. *Proc. SAMPE 2003 ISTC*, SAMPE, Covina, CA (2003).
8. S. Ganguli, D. Derrick; K. Jordan, G. Price, and R. Vaia, "Cyanate Ester Resins - A Candidate for High Temperature Space Applications," TCAM, Tuskegee University, Tuskegee, AL. *Proc. NATAS Annual Conference on Thermal Analysis and Applications* (2001), 29th, 250-256.
9. D. Dean, M. O. Abdalla, S. Ganguli, M. Jose, S. Campbell, J. Gillman, W. H. Awad, and R. Vaia, "High Temperature Thermoset Nanocomposites," Tuskegee-Center for Advanced Materials, Tuskegee University, Tuskegee, AL. *PMSE Preprints* (2003), 89, 729-732.
10. S. Ganguli, D. Dean, K. Jordan, G. Price, and R. Vaia, "Chemorheology of Cyanate Ester-Organically Layered Silicate Nanocomposites," *Polymer* (2003), 44(22), 6901-6911.
11. D. R. Dean, S. Ganguli, M. Abdalla, S. Campbell, R. Vaia, and M. Jose, "High Temperature Thermoset Nanocomposites," Tuskegee University, Tuskegee, AL. *226th ACS National Meeting*, New York, NY, September 7-11, 2003 (2003), PMSE-433.
12. S. Ganguli, D. Dean, K. Jordan, and G. Price, "Structure Processing Property Relationships of Cyanate Ester-Organically Layered Silicates Nanocomposites,"

Center for Advanced Materials, Tuskegee University, Tuskegee, AL. *Proc. SAMPE 2003 ISSE*, 48 (Advancing Materials in the Global Economy--Applications, Emerging Markets and Evolving Technologies, Book 1), 1132-1144.

13. S. Ganguli, D. Dean, K. Jordan, G. Price, and R. Vaia, "Mechanical Properties of Intercalated Cyanate Ester-Layered Silicate Nanocomposites," *Polymer* (2003), 44(4), 1315-1319.

14. J. W. Gilman, R. H. Harris, Jr., C. L. Jackson, A. B. Morgan, L. D. Brassell, and D. L. Hunter, "Phenolic Cyanate Ester Clay Nanocomposites: Effect of Ammonium Ion Structure on Flammability and Nano-dispersion," *Polymeric Materials Science and Engineering*, 82: 276-277, 2000.

15. Y. Lin, M. Song, C. A. Stone, and S. J. Shaw, "A Comprehensive Study on the Curing Kinetics and Network Formation of Cyanate Ester Resin/Clay Nanocomposites," *Thermochimica Acta*, 552: 77-86, 2013.

16. P. Yongzheng, Y. Xu, L. An, H. Lu, Y. Yang, W. Chen, and S. Nutt, "Hybrid Network Structure and Mechanical Properties of Rodlike Silicate/Cyanate Ester Nanocomposites," *Macromolecues,* 41(23): 9245-9258, 2008.

17. T. Wooster, S. Abrol, and D. R. MacFarlane, "Rheological and Mechanical Properties of Percolated Cyanate Ester Nanocomposites," *Polymer*, 46: 8011-8017, 2005.

18. H. Lu, and Z. Zhou, "Research on Cyanate Ester Modified Epoxy Resin/Clay Nanocomposites," *Wuhan Ligong Daxue Xuebao*, 31(21): 89-92, 97, 2009.

19. S. Nagendiran, C. K. Chozhan, M. Alagar, and I. Hamerton, "Inorganic/Organic Hybrid Nanocomposites Involving OMMT clay and Cyanate Ester-Siloxane-Modified Epoxy Resin: Thermal, Dielectric and Morphological Properties," *High Performance Polymers*, 20(3): 323-347, 2008.

20. S. Nagendiran, S. Premkumar, and M. Alagar, "Mechanical and Morphological Properties of Organic, Inorganic, Hybrid, Clay-filled, and Cyanate Ester/Siloxane Toughened Epoxy Nanocomposites," *Journal of Applied Polymer Science*, 106(2): 1263-1273, 2007.

21. K. Dinakaran, and M. Alagar, "Preparation and Characterization of Epoxy-Cyanate Ester Interpenetrating Network Matrices/Organoclay Nanocomposites," *Polymers for Advanced Technologies*, 14(8): 574-585, 2003.

22. K. Liang, G. Li, H. Toghiani, J. H. Koo, C. U. Pittman Jr., and C. Dave, "Cyanate Ester/Polyhedral Oligomeric Silsesquioxane (POSS) Nanocomposites: Synthesis and Characterization," *Chemistry of Materials* (2006), 18(2), 301-312.

23. H. S. Cho, K. Liang, S. Chatterjee, and C. U. Pittman Jr., "Synthesis, Morphology, and Viscoelastic Properties of Polyhedral Oligomeric

Silsesquioxane Nanocomposites with Epoxy and Cyanate Ester Matrices," *Journal of Inorganic and Organometallic Polymers and Materials* (2006), Volume Date 2005, 15(4), 541-553.

24. K. Liang, H. Toghiani, G. Li, C. U. Pittman Jr., and C. Dave, "Synthesis, Morphology, and Viscoelastic Properties of Cyanate Ester/Polyhedral Oligomeric Silsesquioxane Nanocomposites," *Journal of Polymer Science, Part A: Polymer Chemistry* (2005), 43(17), 3887-3898.
25. J. Seetharaman, D. Subramani, R. V. Muthukumaraswamy, C. Ayyavu, A. K. Achimuthu, and A. Muthukaruppan, "Thermal, Thermomechanical and Morphological Behavior of Octa(maleimidophenyl) Silsesquioxane (OMPS) Cyanate Ester Nanocomposites," *High Performance Polymers*, 24(5): 379-388, 2012.
26. Z. Zhang, G. Liang, X. Wang, S. Adhikari, and J. Pei, "Curing Behavior and Dielectric Properties of Amino-functionalized Polyhedral Oligomeric Silsesquioxane/Cyanate Ester Resin Hybrids," *High Performance Polymers*, 25(4): 427-435, 439, 2013.
27. Y. Lin, J. Jin, M. Song, S. J. Shaw, C. A. Stone, "Curing Dynamics and Network Formation of Cyanate Ester Resin/Polyhedral Oligomeric Silsesquioxane Nanocomposites," *Polymer*, 52(8): 1716-1724, 2011.
28. S. Rakesh, C. R. Sakthi Dharan, M. Selladurai, V. Sudha, P. R. Sundararajan, and M. Sarojadevi, "Thermal and Mechanical Properties of POSS®-Cyanate Ester/Epoxy Nanocomposites," *High Performance Polymers*, 25(1): 87-96, 2013.
29. C. Ayyavu, D. Kanniyan, A. K. Achimuthu, and A. Muthukaruppan, "Synthesis and Characterization of Epoxy modified Cyanate Ester POSS Nanocomposites," *High Performance Polymers*, 24(5): 405-417, 2012.
30. K. Liang, H. Toghiani, and C. U. Pittman, Jr., "Synthesis, Morphology and Viscoelastic Properties of Epoxy/Polyhedral Oligomeric Silsesquioxane (POSS) and Epoxy/Cyanate Ester/POSS Nanocomposites," *Journal of Inorganic and Organometallic Polymers and Materials*, 21(1): 128-142, 2011.
31. Z. P. Zhang, J. Z. Pei, C. Q. Fang, and S. F. Chen, "Enhanced Thermal Properties of Cyanate Ester Resin by Epoxy-Functionalized POSS," *Advanced Materials Research*, 549: 647-650, 2012.
32. J. Cheng, S. Lao, J. Yong, J. H. Koo, P. Ferreira, L. Pilato, G. Wissler, and Z. P. Luo, "Cyanate Ester-Buckytubes Nanocomposites: Processing and Characterization," *Proc. SAMPE 2007 ISSE*, SAMPE, Covina, CA (2007).
33. M.-L. Sham and J.-K. Kim, "Surface Functionalities of Multi-wall Carbon Nanotubes after UV/Ozone and TETA Treatments," *Carbon*, 44: 768-777, 2006.

34. D. D. Dominguez, M. Laskoski, and T. M. Keller, "Modification of Oligomeric Cyanate Ester Polymer Properties with Multi-Walled Carbon Nanotube-Containing Particles," *Macromolecular Chemistry and Physics*, 210: 1709-1716, 2009.

35. J. Wang, G. Liang, H. Yan, and S. He, "Mechanical and Thermal Properties of Functionalized Multiwalled Carbon Nanotubes/Cyanate Ester Composites," *Polymer Engineering & Science*, 49(4): 680-684, 2009.

36. C. Han, A. Gu, G. Liang, L. Yuan, "Carbon Nanotubes/Cyanate Ester Composites with Low Percolation Threshold, High Dielectric Constant and Outstanding Thermal Property," *Composites: Part A*, 41: 1321-1328, 2010.

37. Y. Lin, C. A. Stone, S. J. Shaw, and M. Song, "Effect of Carbon Nanotubes on the Curing Dynamics and Network Formation of Cyanate Ester Resin," *Journal of Polymer Research*, 20: 106, 2013.

38. E. Taha, J. Wu, K. Gao, and L. Guo, "Preparation and Properties of Fumed Silica/Cyanate Ester Nanocomposites," *Chinese Journal of Polymer Science*, 30(4): 530-536, 2012.

39. P. Badrinarayanan, and M. R. Kessler, "Zirconium Tungstate/Cyanate Ester Nanocomposites with Tailored Thermal Expansivity," *Composites Science and Technology*, 71(11): 1385-1391, 2011.

40. W. Sun, J. E. D. Leon, C. Ma, X. Tan, and M. R. Kessler, "Novel Si/Cyanate Ester Nanocomposites with Multifunctional Properties," *Composites Science and Technology*, 72: 1692-1696, 2012.

41. P. Badrinarayanan, M. K. Rogalski, and M. R. Kessler, "Carbon Fiber-Reinforced Cyanate Ester/Nano-ZrW_2O_8 Composites with Tailored Thermal Expansion," *Applied Materials & Interfaces*, 4: 510-517, 2012.

42. C. D. Blasi, C. Branca, A. Galgano, R. Moricone, and E. Milella, "Oxidation of a Carbon/Glass Reinforced Cyanate Ester Composite," *Polymer Degradation and Stability*, 94: 1962-1971, 2009.

43. W. K. Goertzen, and M. R. Kessler, "Thermal and Mechanical Evaluation of Cyanate Ester Composites with Low-Temperature Processability," *Composites Part A*, 38: 779-784, 2007.

44. K. Chung, and J. C. Seferis, "Evaluation of Thermal Degradation on Carbon Fiber/Cyanate Ester Composites," *Polymer Degradation and Stability*, 71: 425-434, 2001

Chapter 3

Experimental Approach and Characterization of MWNTs

MATERIALS

Polymer Resin: Cyanate Ester

Cyanate ester [Primaset® PT-15, Lonza Corporation] was selected for this study. This resin matrix is an off-white, waxy solid at room temperature. It has less than 0.5% volatiles, no decomposition by-products during curing, and yields an amber cured solid (when cured without using catalyst) [1].

Carbonization of cyanate esters occurs at about 400-500°C, resulting in char (carbon) yields of 63-65 wt%. These are considerably higher carbon yields than the customary phenolic resins (e.g., Momentive's SC-1008 phenolic resin with a char yield of 43 wt%) that are used as carbon-carbon composite (CCC) precursors [2-3].

This resin is waxy solid at room temperature (25°C) with a density of 1.25g/mL, while the melt density, measured at room temperature, is 1.05g/mL. The resin is partially soluble in acetone, which could be used to some advantage in the polymer nanocomposite processing. It has very low viscosities in its molten state at elevated temperatures: 35mPA-s at 80°C, 15mPa-s at 100°C, and 8mPa-s at 120°C.

Low neat-resin viscosity is an advantage in MWNT nanocomposite processing, since the viscosity of the nanocomposite usually increases dramatically when MWNTs are well dispersed in the polymer resin. Increased viscosity impedes the fabrication of prepregs, fiber-reinforced composites, or carbon-carbon composites. Processing at very low viscosity initially, it is anticipated that the increased viscosity due to the MWNT filler will still fall in the processable range of industrial composite fabrication.

The decomposition temperature of the cured product as determined by thermogravimetric analysis is 420°C; the glass transition temperature (T_g) is 300 - 350°C, depending on the cure procedures.

Nanoparticles: Multiwall Carbon Nanotubes

Multiwall carbon nanotubes from four different sources were obtained, some of which were surface functionalized by a plasma technique. These MWNTs were (1) ILjin Nanotech Co., Ltd.'s CM95, (2) Arkema's Graphistrength® C100, (3) Bayer MaterialScience's Baytubes® C150P, and (4) Cheap Tubes Inc.'s MWNT. The MWNTs obtained and their sources are summarized in Table 3.1 [4].

Table 3.1 Seven Types of MWNTs Used in this Study [4]

MWNT		Functionalized	Source
MWNT-1	(CM-95 neat) [7]	No	ILjin Nanotech
MWNT-2	(CM-95-OH) [8]	Hydroxyl	ILjin Nanotech
MWNT-3	(CM-95-COOH) [8]	Carboxyl	ILjin Nanotech
MWNT-4	(CM-95-NH_2) [8]	Amine	ILjin Nanotech
MWNT-5	(Graphistrength® C100) [9]	No	Arkema
MWNT-6	(Baytubes® C 150 P) [10]	No	Bayer MaterialScience
MWNT-7	(Cheap Tubes-COOH) [11]	Carboxyl	Cheap Tubes

Before initiating the polymer nanocomposites (PNC) research, the morphology, thermal stability, and kinetics parameters of each MWNT were examined [4]. Further, these MWNTs were mixed into the cyanate ester resin using ultrasonication to investigate the compatibility of these as-received MWNTs with the PT-15 cyanate ester resin.

It is generally accepted that proper functionalization of nanoparticles is the key for achieving good dispersion, as well as better interfacial adhesion of nanoparticles to the polymer matrix. These will, in turn, result in improved nanocomposite properties [5]. Consequently, aliquots of the CM95 MWNTs were functionalized with the hydroxyl

group (-OH), the carboxyl group (-COOH), or the amine group ($-NH_2$) by a plasma-based technique [6]. Effects of these three different functionalizations on MWNT dispersion were examined while the processing techniques and procedures of the CE-MWNT nanocomposites were developed.

Use of a catalyst and coupling agents were examined separately to explore their ability to improve the phase separation that Cheng *et al*. [7] encountered (and mentioned in the previous Chapter). Details will be provided later in this chapter.

The as-received MWNTs entangle and agglomerate in bundles as shown by sample SEM images in Figures 3.1 and 3.2. The size of the as-received MWNT aggregates and those sonicated in acetone (0.1g/L) for 30 minutes using a bath-type ultrasonicator are shown in Table 3.2 [4].

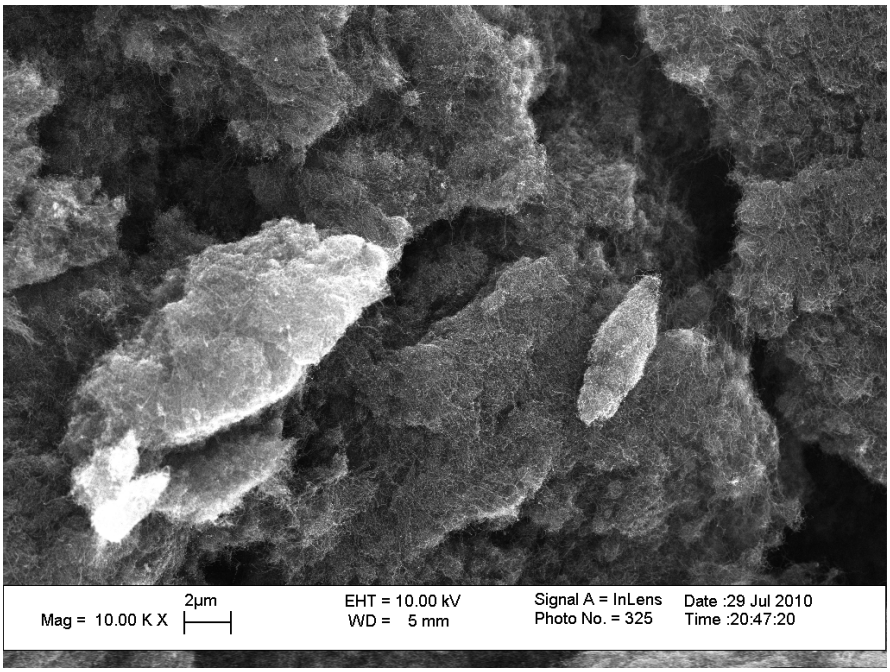

Figure 3.1. SEM micrograph of as-received (MWNT-5, C100 MWNT) showing the micron-scale aggregates of carbon multiwall nanotubes (lower magnification) [4].

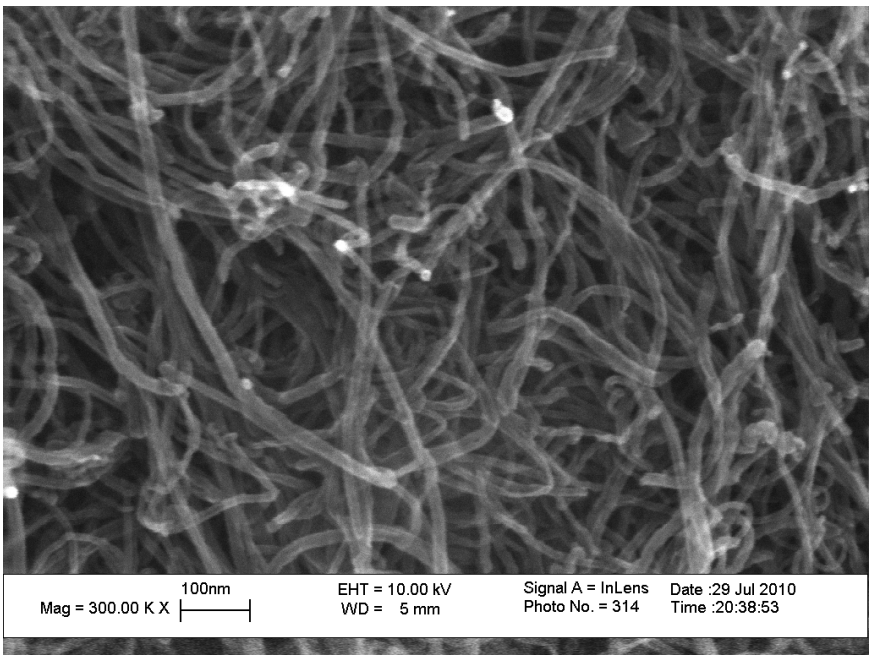

Figure 3.2. SEM micrograph of as-received (MWNT-5, C100 MWNT) showing entanglement of carbon multiwall nanotubes within aggregates (higher magnification) [4].

Table 3.2 Average MWNT Aggregate Size As-received and after Sonicaton in Acetone (0.1g/L) for 30 Minutes using a Bath-type Ultrasonicator [4]

Nanomaterial	**Aggregate Size As-Received**	**Aggregate Size After Sonication**
MWNT-1	250 μm	150 μm
MWNT-2	250 μm	150 μm
MWNT-3	200 μm	100 μm
MWNT-4	200 μm	100 μm
MWNT-5	500 μm	10 μm
MWNT-6	500 μm	10 μm
MWNT-7	100 μm	5 μm

Selection of MWNTs

When selecting the MWNTs for this study, a few aspects were taken into consideration, namely, (1) the properties of the MWNTs, (2) the compatibility of MWNTs with the CE resin, and (3) the cost of the MWNTs.

Thermal Stability Characterization of MWNTs

Thermogravimetric analysis was conducted on all seven as-received nanotubes, MWNT-1 to MWNT-7. Specimens were tested at heating rate of 10ºC/min in both an air and nitrogen (N_2) atmospheres. Figure 3.3 shows the TGA data of the seven MWNTs materials tested under a heating rate of 10ºC/min in an air atmosphere. The thermal stability of these carbon-based nanomaterials shows significant differences. Table 3.3 lists the decomposition temperatures (T_d) of the MWNTs at 10% and 50% mass loss: $T_{10\%}$ and $T_{50\%,}$ respectively.

Clearly MWNT-1 has the best thermal stability with $T_{10\%}$ and $T_{50\%}$ of 610°C and 655°C, respectively. MWNT-2, MWNT-3, and MWNT-4 that are functionalized versions of MWNT-1 have an average $T_{10\%}$ and $T_{50\%}$ of 608ºC and 653ºC, respectively, which are very close to MWNT-1. MWNT-5 has $T_{10\%}$ and $T_{50\%}$ of 552°C and 607°C, respectively. MWNT-6 has $T_{10\%}$ and $T_{50\%}$ of 528°C and 600°C, respectively. MWNT-7 has the worst thermal stability amongst this group of carbon-based nanomaterials examined, with $T_{10\%}$ and $T_{50\%}$ of 523°C and 580°C, respectively.

Figure 3.4 shows the TGA data of the seven MWNTs tested under a heating rate of 10°C/min in an inert (nitrogen) atmosphere. The thermal stability of these carbon-based nanomaterials also shows a significant difference. However, the degradation of MWNTs occurs at higher temperature comparing to the TGA conducted in air, where MWNTs are oxidized as temperature increases and decompose at lower temperature. Table 3.4 shows the decomposition temperatures of the MWNTs nanomaterials at 10% and 50% mass loss under nitrogen environment at 10°C/min. Under nitrogen environment

MWNT-6 has a $T_{10\%}$ of 891°C. The functionalization of MWNT-1 shows differences in thermal stability with $T_{10\%}$ of ranges from 814 to 833°C. MWNT-5 has the worst thermal stability amongst this group of carbon-based nanomaterials.

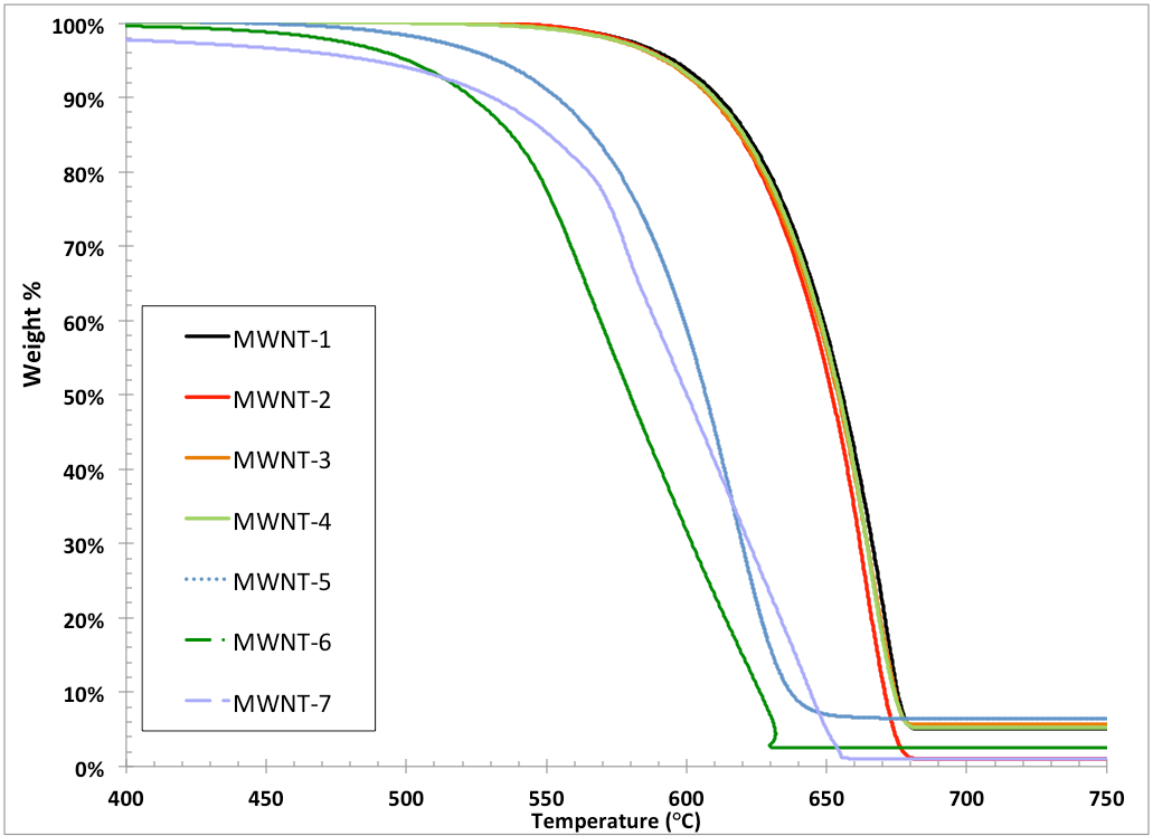

Figure 3.3. Thermogravimetric analysis of MWNTs at heating rate of 10°C/min in air. (*Number of samples per MWNT type, N = 1)*.

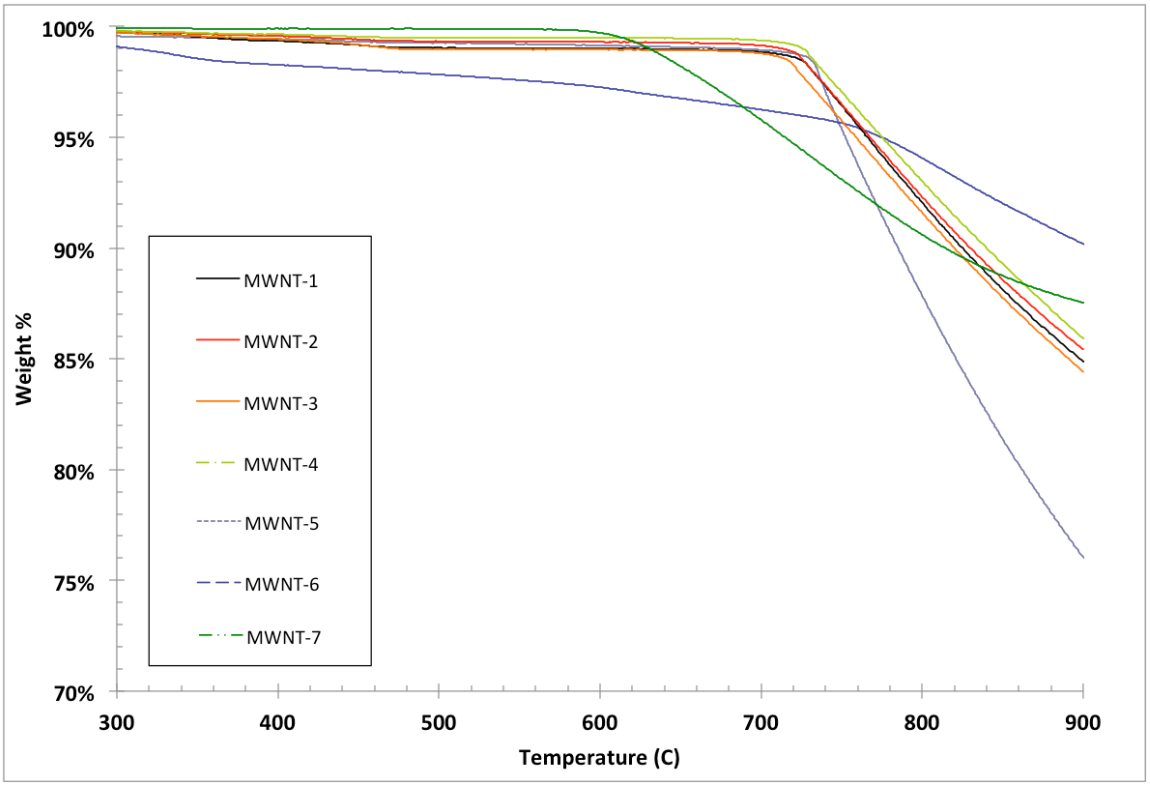

Figure 3.4. Thermogravimetric analysis of MWNTs at heating rate of 10°C/min in nitrogen *(Number of samples per MWNT type, N = 1)*.

Table 3.3 Decomposition Temperatures of MWNTs in Air (Heated at 10°C/min)

MWNTs		**$T_{10\%}$ at 10% Mass Loss (^{o}C)**	**$T_{50\%}$ at 50% Mass Loss (^{o}C)**
MWNT-1	CM-95-neat	610	655
MWNT-2	CM-95-OH	608	652
MWNT-3	CM-95-COOH	607	654
MWNT-4	CM-95-NH2	609	654
MWNT-5	C100	552	607
MWNT-6	C 150 P	528	600
MWNT-7	Cheap tube-COOH	523	580

Number of samples per MWNT type, N = 1

Table 3.4 Decomposition Temperatures of MWNTs in Nitrogen (Heated at 10°C/min)

MWNTs		$T_{10\%}$ at 10% Mass Loss (^{o}C)	$T_{50\%}$ at 50% Mass Loss (^{o}C)
MWNT-1	CM-95-neat	819	N/A
MWNT-2	CM-95-OH	823	N/A
MWNT-3	CM-95-COOH	814	N/A
MWNT-4	CM-95-NH2	833	N/A
MWNT-5	C100	782	N/A
MWNT-6	C 150 P	891	N/A
MWNT-7	Cheap tube-COOH	802	N/A

Number of samples per MWNT type, N = 1

It has been shown previously that there are significant differences in terms of thermal stability between these carbon-based nanomaterials when they are exposed to air or nitrogen. This may be due to numerous factors, such as how they were manufactured, the surface morphology are vastly different, the tube diameters, the number of walls of these tubes, the tube lengths, and cluster sizes. Further studies are needed to understand this phenomenon. Moreover, functionalization of MWNT did not affect the thermal stability of MWNTs. The difference between the decomposition temperatures (both $T_{10\%}$ and $T_{50\%}$) of neat MWNT (MWNT-1) and *f*-MWNTs (MWNT-2, MWNT-3, and MWNT-4) in air and in nitrogen is < 1% and 2%, respectively.

Compatibility of MWNTs with CE Resin

As mentioned earlier, the neat MWNT most compatible with the CE resin among the four types of MWNTs (besides MWNT-7, since no neat MWNT of this type of nanotubes was obtained) is preferred in this study. It can also be functionalized with the three different functional groups to potentially further improve the dispersion of MWNTs as well as the properties of the resulting nanocomposites. The four types of MWNTs

were mixed into the CE resin using ultrasonication for one hour at room temperature (25ºC).

It was found that MWNT-1 and MWNT-5 were more easily dispersed than the MWNT-6 and MWNT-7. After one hour of ultrasonication, relatively large aggregates of MWNT-6 and MWNT-7 were still observed while no clusters of MWNT-1 and MWNT-5 were observed by naked eyes. That said, the relative dispersibility of the as-received MWNT-1 and MWNT-5 into the PT-15 CE resin was similar.

Both MWNT-1 and MWNT-5 were functionalized with the three functional groups mentioned above using the plasma technique. Some preliminary work, as will be shown in the preliminary results section, was done using the neat MWNT-1 nanotubes.

Cost of MWNTs

While the cost of MWNT-5 and MWNT-6 are similar, MWNT-1 is about ten times more expensive. The cost of MWNT-7 is intermediate between that of MWNT-5/6 and MWNT-1. Considering scaling up for future industrial production, the lower cost MWNT is preferred.

Choice of MWNT

Despite the relatively good compatibility with the CE resin and the excellent thermal stability, MWNT-1 was not chosen for this study due to its extremely high cost. Due to its similarly good compatibility with the CE resin and lower cost, MWNT-5 was deemed to be the best candidate for this research. As a result, it was selected for further investigation.

PROCESSING AND SPECIMENS PREPARATION

As mentioned earlier, the as-received MWNTs entangled with each other in large clusters. Since the properties of the polymer nanocomposites are affected by the aggregate size, MWNTs need to be adequately dispersed into the polymer resin. While different techniques can be used, they do not necessarily achieve the same degree of dispersion. In other words, different processing techniques will influence the properties of the resulting polymer nanocomposites. Therefore, one of the objectives of this study is to directly compare a few commonly used processing techniques.

Cure of Cyanate Ester and Cyanate Ester-MWNT Nanocomposites

Using the vendor recommended cure cycle, Cheng *et al*. [7] observed phase separation of carbon nanotubes from the PT-15 cyanate ester resin upon cure, as reproduced and illustrated in Figure 3.5. Cheng modified the cure cycle to attain a uniform temperature distribution and to avoid temperature overshoot that results in an accelerated, self-catalytic exothermic cyclotrimerization, causing the resin to burn instead of cure. He used a long cure cycle with slow heating rate illustrated in Figure 3.6 [7].

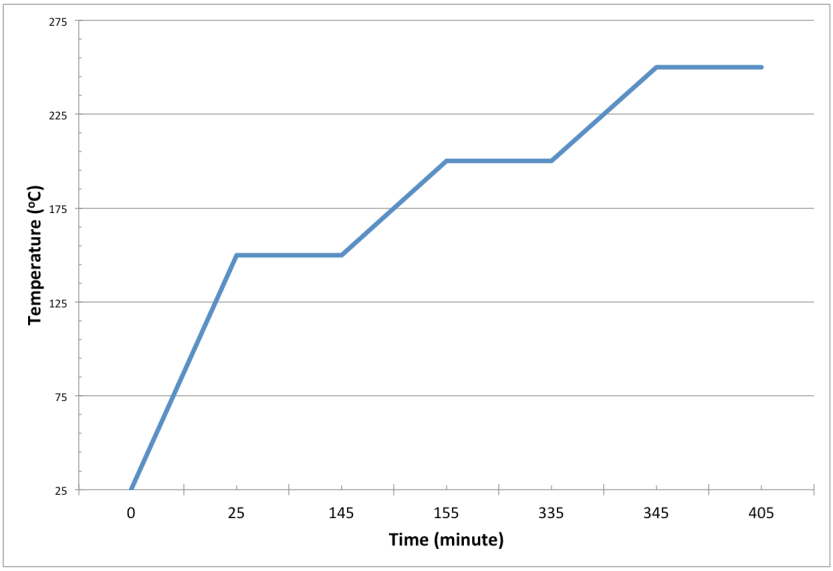

Figure 3.5. Vendor recommended curing cycle for PT-15 cyanate ester.

Unfortunately, phase separation was observed in this study's CE-MWNT nanocomposites when Cheng's modified cure cycle was used. Mirroring Cheng's results, this phenomenon also occurs when the manufacturer recommended cure cycle (150°C for 2 hours and 200°C for 3 hours) for the neat cyanate ester was used. Further examination of the cure procedures for the CE-MWNT nanocomposites revealed that the phase separation occurs when the uncured CE-MWNT nanocomposite is heated at or above 100°C for as little as 30 minutes.

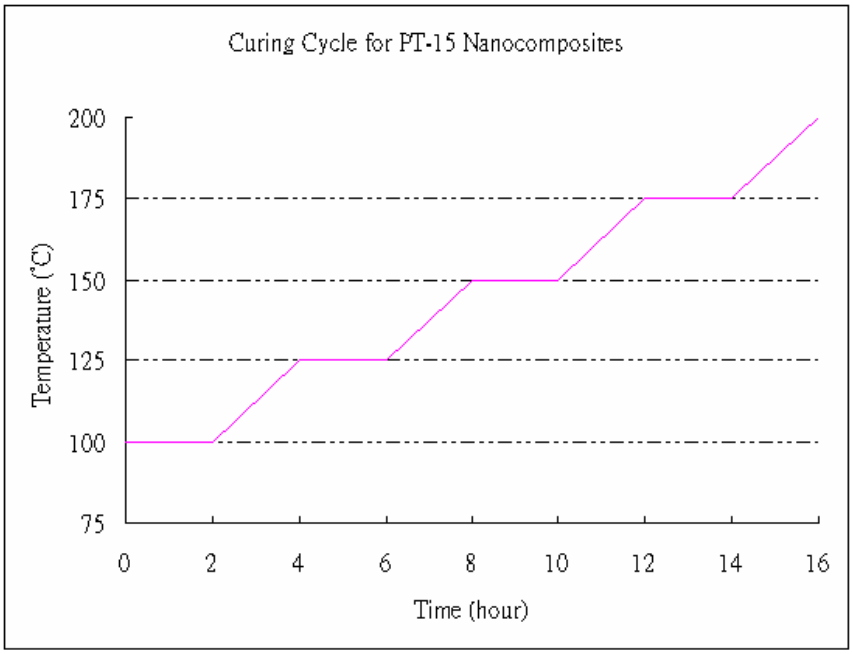

Figure 3.6. Curing cycle for PT-15 cyanate ester nanocomposites used by Cheng *et al*. [6] that resulted in phase separation.

Phase separation may be due to the fact that the cyanate ester resin is slightly polar while the multiwall carbon nanotubes are non-polar. When the temperature of the nanocomposite is raised to (or above) 100°C for 30 minutes, the resin viscosity drops several orders of magnitude. Meanwhile, MWNTs have both greater free energy (due to the higher temperature) and more mobility (due to the lower resin viscosity). As a result, the MWNTs can spontaneously rearrange themselves within the resin so as to reduce their energy state. As the same time, the polar resin seeks to minimize its contact with the non-polar MWNTs. As a result, the non-polar nanotubes move toward each other resulting in re-aggregation of MWNTs and thus phase separation shown in Figure 3.7.

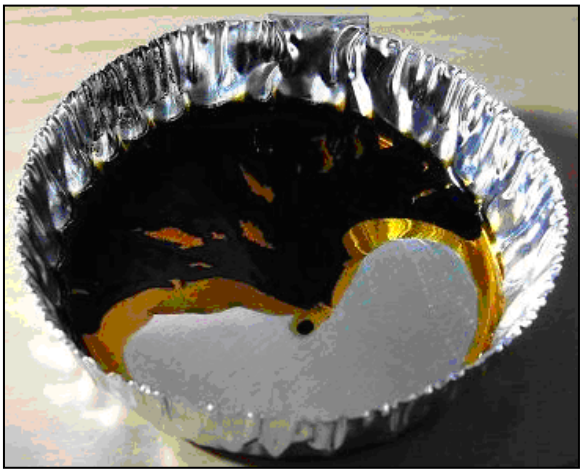

Figure 3.7. Phase separation of carbon nanotubes from PT-15 cyanate ester resin cured using the manufacturer's recommended cure cycle (Figure 3.5) as shown by Cheng *et al*. [7].

MWNT Functionalization

To reduce the phase separation, Cheng *et al*. [7] recommended functionalizing the nanotubes with polar functional groups to increase the compatibility of nanotubes with the cyanate ester resin. In fact, Wang *et al*. [13] showed that functionalization of MWNTs with carboxylic acid (-COOH) group alleviated the phase separation. Fabrication of the cyanate ester nanocomposites with functionalized MWNTs is discussed in the preliminary results section in this chapter.

Another approach to avoid the phase separation problem is to cure the nanocomposites below 100°C by the addition of Fe(III) acetylacetonate—a catalyst for the cyanate cyclotrimerization—as recommended by the CE resin manufacturer. Table 3.5 shows the results of curing study of cyanate ester using this catalyst. Parameters examined include: catalyst quantity, cure temperature, ramp rate, and time.

Since the cyclotrimerization is an exothermic reaction, it can be easily overheated when the catalyst is incorporated. A "fast" cure will result in charring of the materials and

smoke release, so a slow heating rate is needed. As shown in Table 3.5, the greater the amount of catalyst, the lower the cure temperature and the shorter the cure time are. However, since the viscosity of the cyanate ester resin increases substantially after the addition of MWNTs and the degassing procedure involving heating up the nanocomposites to 70-80°C, the cure temperature needs to be above 70-80°C. In other words, the cure temperature needs to fall in between 80°C and 100°C. According to the results shown in Table 3.5, the preferred cure condition can be achieved by using 200-250ppm of the Fe(III) catalyst. Figure 3.8 shows the cure cycle of CE-MWNT nanocomposites with 200ppm and 250ppm Fe(III) catalyst.

Table 3.5 Cure Conditions of CE-MWNT Nanocomposites with Fe(III) Catalyst Developed in this Study with Vendor Guidelines

Amount of Fe(III) Catalyst (ppm)	Cure Temperature (°C)	Cure Time (min.)	Heating Rate (°C/min)
400	70	30	1
350	70	40	1
300	75	45	1
250	90	35	1
200	90	50	1
150	100	40	1
100	120	30	1

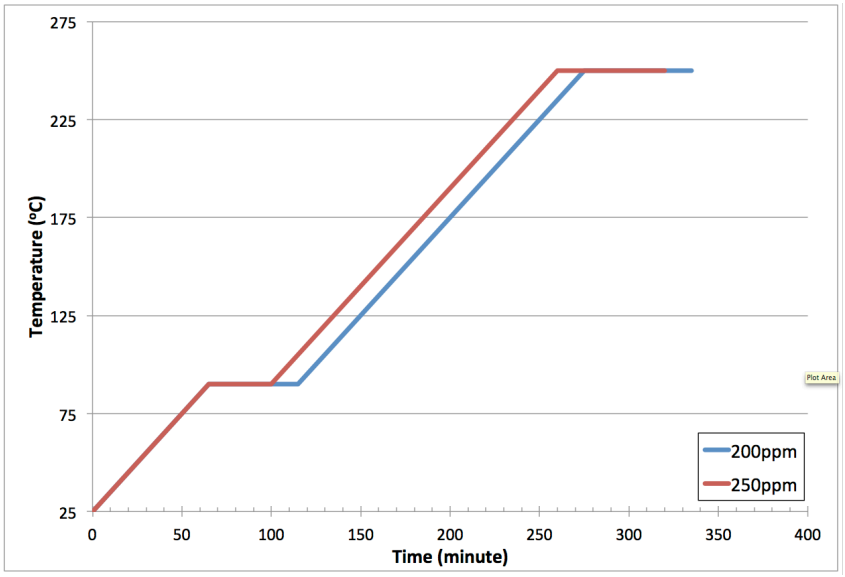

Figure 3.8. Curing cycle for PT-15 cyanate ester nanocomposites with 200ppm and 250ppm Fe(III) catalyst. Developed for and used in this study.

CE-MWNT Coupling Agent

A coupling agent—or surfactant that has both polar and non-polar groups on the same molecule—may enhance the interfacial adhesion between the polymer resin and the nanotubes, and possibly resolve the phase separation problem. Two zirconate coupling agents, namely Ken-React® KZ-TPP (CA1; Zirconium IV 2-ethyl, 2-propenolatomethyl 1,3-propanediolato, cyclo-di-2, 2-(bus 2-propenolatomethyl) butanolato pyrophosphate-O, O) [14] and NZ97 (CA2; Zirconium IV (OC-6-22)-Tris(3-aminophenolato-O)2,2-bis(2-propenyloxy)methyl-1-butanolato-O,O',O'') [15], were examined. Surprisingly, these two coupling agents also lower the cure temperature of the cyanate ester nanocomposites.

When the second coupling agent candidate (CA2) was mixed with the cyanate ester, distinct small particles of the coupling agent were visible in the mixed CE-CA2. This was true for all weight loadings (2, 3, 4 wt%) examined. On the other hand, CA1 blended uniformly with the cyanate ester resin using the same mixing technique. This suggested that CA2 is not as compatible with the cyanate ester resin as CA1.

The addition of the coupling agent CA1 affected the properties of the resulting polymer/polymer nanocomposites. Notably, the glass transition temperature and the mechanical properties of the cyanate ester are lowered by the addition of CA1 and will be shown in Chapter 4.

Although the cure temperature was above 100°C, the cured CE-MWNT nanocomposites did not show phase separation, suggesting that the coupling agents did enhance the compatibility of the cyanate ester resin and the nanotubes. Table 3.6 shows the cure conditions of the cyanate ester nanocomposites with the coupling agents. Figure 3.9 shows the cure cycle of CE-MWNT nanocomposites with 3 wt% CA1 or CA2.

Table 3.6 Cure Conditions of CE-MWNT Nanocomposites with Coupling Agents. Developed in this Study with Vendor Guidelines

Amount of Coupling Agent (wt%)	Cure Temperature (°C)	Cure Time (min.)	Heating Rate (°C/min)
CA1			
1	150	100	3
2	150	90	3
3	150	85	3
4	150	80	3
5	150	80	3
CA2			
2	120	75	3
3	120	65	3
4	120	60	3

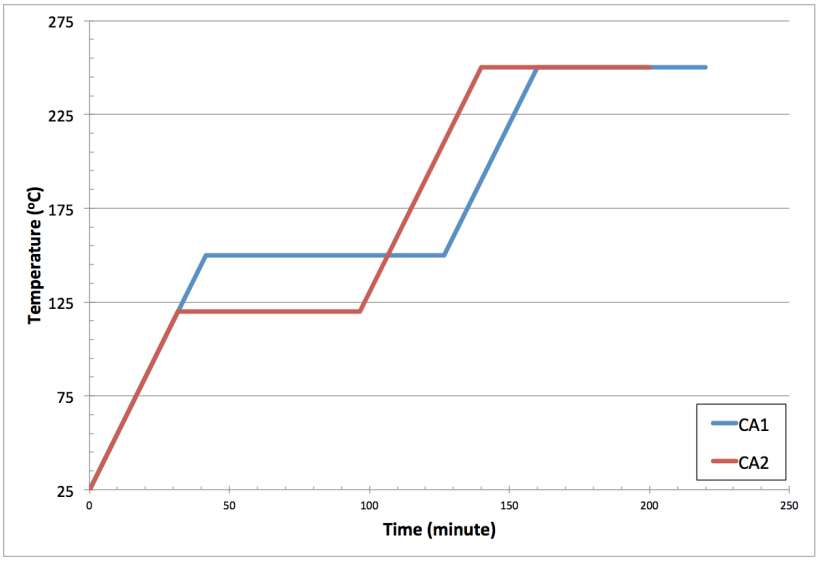

Figure 3.9. Curing cycle for PT-15 cyanate ester nanocomposites with 3 wt% CA1 and 3 wt% CA2. Developed for and used in this study.

Processing Techniques

Several processing techniques were used in this study: (a) Ultrasonication, (b) Stand mixer, (c) Planetary centrifugal vacuum mixer, (d) High shear colloid mixer, and (e) Three-roll mill (or calendaring). A brief discussion of each processing technique is given in this section.

Ultrasonication

There are two types of commonly used ultrasonicators, namely the bath-type and the horn-type. Horn-type ultrasonicator imparts a greater amount of energy and can be used to disperse nanotubes. However, it is known that nanotubes will be broken and shortened in the process, thus lowering the aspect ratio of the nanotubes. On the other hand, the bath-type ultrasonicator—although imparting a lesser amount of energy—could also disperse nanotubes into polymer resin with less fracture of nanotubes. Therefore, a Branson 1510 bath-type ultrasonicator (40W) was used in this study (Figure 3.10). Each type of MWNT was added into the molten CE resin and sonicated for two hours.

Figure 3.10. Branson 1510 bath-type ultrasonicator [16].

Stand Mixer

Although it is a low speed mechanical mixer, a stand mixer has the potential to disperse nanotubes into polymer resin. When the large clusters of nanotubes start to break down and nanotubes are partially dispersed, the viscosity of the mixture begins to increase. Since the gap between the mixing blade and the container is small (<0.1mm), it may be able to generate enough shear force with the viscous mixture to de-bundle the nanotubes. Breville Scraper Mix Pro BEM800XL Stand Mixer (Figure 3.11) was used in this study. MWNTs were added into molten CE resin and mixed for two hours. Air bubbles were entrained into the mixtures during the process, so a degassing procedure in a vacuum furnace was needed after mixing.

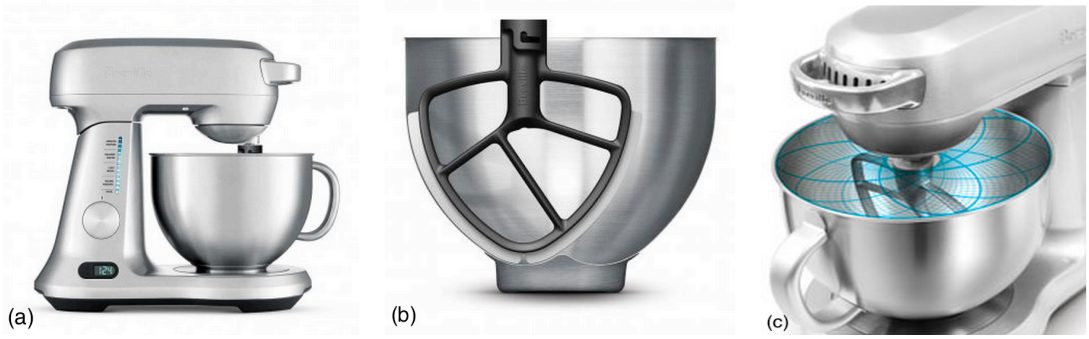

Figure 3.11. Breville Scraper Mix Pro BEM800XL Stand Mixer. (a) Mixing unit, (b) Cross section of mixing blade and bowl, and (c) Mixing motion [17].

Planetary Centrifugal Vacuum Mixer

The mixing chamber of the planetary centrifugal mixer revolves around the axis of the instrument anticlockwise while it rotates around the axis of the mixing chamber clockwise at the same time (as shown in Figure 3.12). It can mix liquid with liquid or liquid with solid. THINKY ARV-310 was used in this study. Zirconia grinding media (3 mm diameter) was added to assist in breaking down the MWNT clusters in the CE resin. The maximum revolution speed of 2,000rpm was used with vacuum to make sure the resulting mixture was free of air bubbles. Mixing time was 30min.

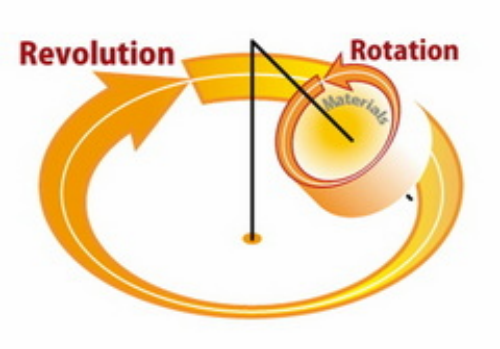

Figure 3.12. Mixing principle of the planetary centrifugal mixer [18].

High Shear Colloid Mixer

The IKA colloid mixer is a Labor-Pilot 2000/4 module. It is designed in the same way as the larger production machines of the 2000 series, and all elements can be transferred to larger machines. This enables an optimum scale-up to production plants. Figure 3.13 shows the recycling batch setup for the IKA colloid mixer. It has four main components: power supply/motor, casing and recycling pipes, hopper/collector, and mixing head. The mixing tools all perform under a rotor-stator pair mechanism. For the purpose of this study, the MK and DR modules have been fitted for material dispersion. The MK module mixing tool resembles an attrition miller, and the pair is shown on

Figures 3.14 and 3.15, while the DR module is a three-stage high shear dispersing module and is shown in Figure 3.15. A high-speed rotor with narrow teeth rotates in a stator. This results in very high shearing energies between the rotor and the stator. The internal mixing chamber has a volume of about 150mL for the MK module and 75mL for the DR module. Together with the pipes and valves, the total internal volume for circulation is 325-400mL. For purposes of synthesis, the minimum batch volume is set at 0.5L. The upper temperature tolerance of the system is listed at 120°C; although for viscous polymers, it is prudent to retain the processing temperature below 90°C to ensure that the system does not polymerize. As suggested by Cheng *et al*. [7], the operating speed of the mixer was 5000-7900rpm, depending on the viscosity of the polymer/nanotubes mixture, in order to keep the materials circulating within the mixer. The mixing time was 30min. High content of air was suspended in the viscous system during mixing and therefore a degassing procedure in vacuum furnace was needed.

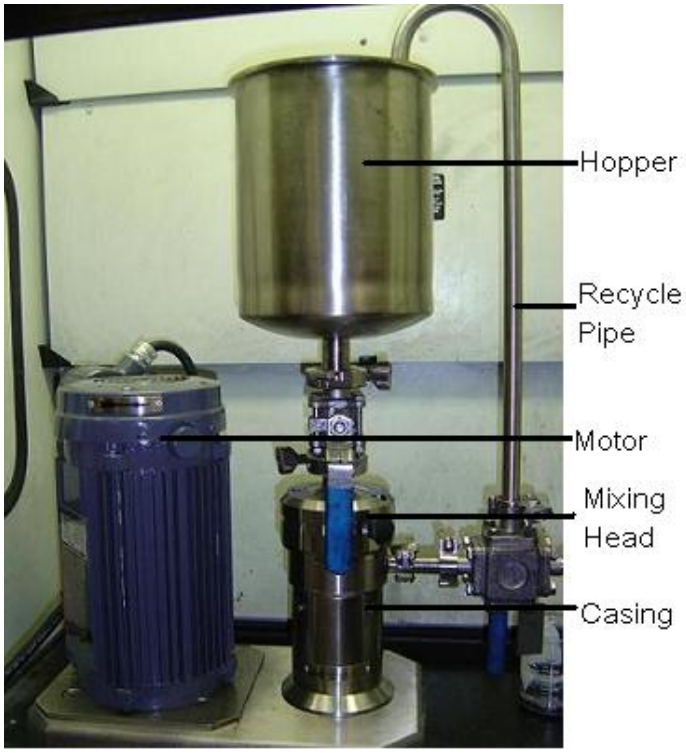

Figure 3.13. Experimental setup of IKA colloid mixer with MK module [7].

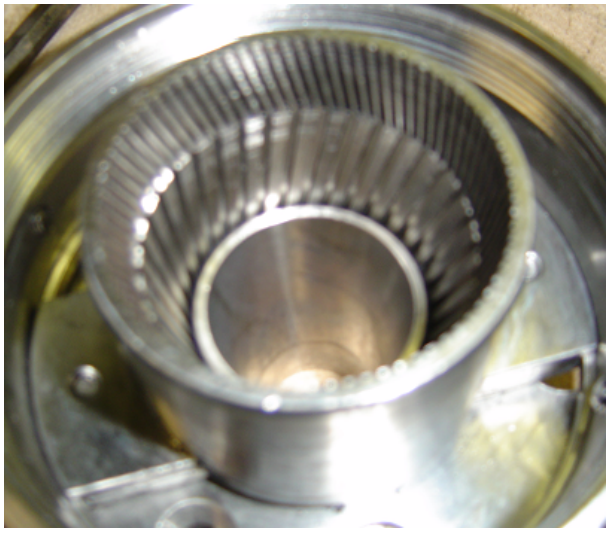

Figure 3.14. Mixing head stator of MK module (from underside up) [7].

Figure 3.15. Mixing head rotor of MK module on pump housing and collector plate [7].

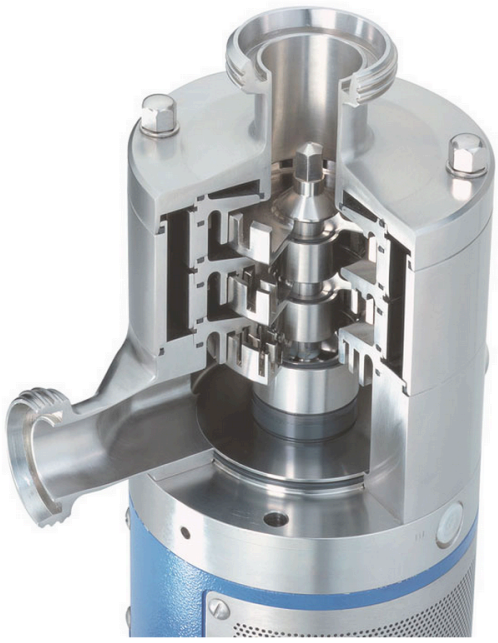

Figure 3.16. Mixing head rotor of DR module on pump housing and collector plate [19].

Three-Roll Mill

The gaps between rollers of the three-roll mill (Exakt 80E) used in this study were electronically adjustable [20]. Figure 3.17 shows pictures of the three-roll mill and how it works. The three-roll mill provides high shear force that can de-bundle the nanotubes in the polymer resin. Multiwall carbon nanotubes were mixed into molten cyanate ester, stirred by hands, and was poured to the feeder of the machine. Initially the gaps between rollers were set to tens of microns—smaller than the average aggregate size of the nanotubes—in order to break down the clusters. The product coming out from the mill was collected and manually fed back to the feeder after the gaps between rollers were decreased. The procedure was repeated until the gaps reached 1μm and then five additional passes of the mixtures in the mill were performed. Since the gaps between rollers were small, the product was essentially free of air bubbles after milling.

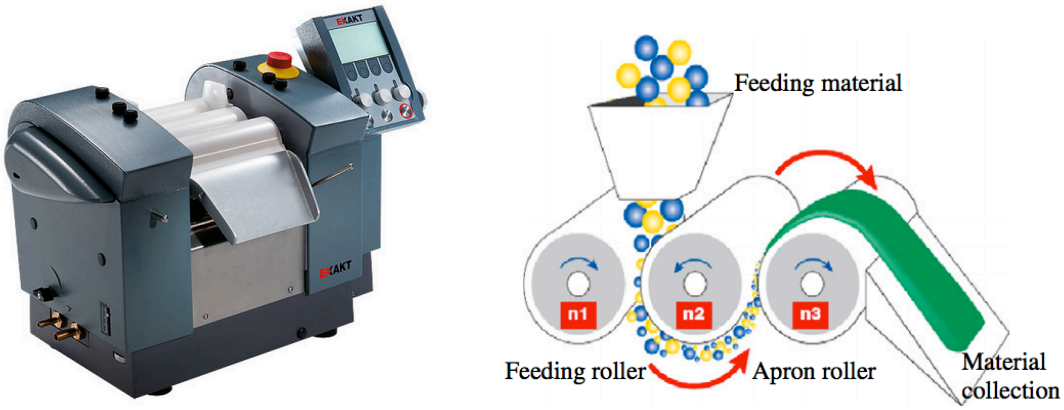

Figure 3.17. Pictures showing (left) Exakt 80E three-roll mill [20] and (right) how a three-roll mill works [21].

CHARACTERIZATION METHODS

Degree of Functionalization on MWNTs

The degree of MWNT functionalization was studied using FT-IR/ATR and XPS, since the quantity of functional groups attached to MWNTs will affect the interactions or adhesions between the CE and MWNTs, as well as dispersion of MWNTs.

Dispersion of MWNTs and Morphological Microstructures Analysis

Degree of nanoparticles dispersion affects the properties, such as thermal stability, flammability, and mechanical properties, etc., of the polymer nanocomposites [22]. Best dispersion is achieved when individual nanoparticles are separated from the micron-size aggregates of the nanoparticles and uniformly distributed in the polymer matrix. On the other hand, the dispersion is considered poor when the nanoparticles stay as the form of aggregates in the resin. However, depending on the targeting property enhancement, best dispersion of nanoparticles in the polymer matrix is not always desired. For instance, well dispersed MWNTs in the resin may not form a connecting network in the polymer matrix to improve the electrical conductivity of the resulting nanocomposites. This is discussed in more details in Chapter 4. Scanning transmission electron microscopy (STEM; Hitachi

S5500), and transmission electron microscopy (TEM; FEI Tecnai) were be used to examine the MWNT dispersion in the CE resin. Cured CE or CE-MWNT nanocomposites specimens were cut by ultramicrotome (Leica Ultracut UTC) using diamond knife into sections of 1mm (l) x 1mm (w) x 70±5nm (t) and placed on copper grids. Topographical images of these thin sections were obtained using secondary electron (SE) signals and an accelerating voltage of 30kV by the S5500 STEM. TEM images of the same thin-section samples were obtained using phase contrast and an accelerating voltage of 80kV by the Tecnai TEM. Since the same set of specimens was used for both STEM and TEM imaging, no coating was applied to the specimen surfaces so that transmission electron signals could be used in TEM. STEM images are used to measure the MWNT aggregate sizes while the TEM images are used to characterize the de-bundling of the MWNTs.

Scanning electron microscopy (SEM; FEI Quanta 650) was used to examine the cross section of carbon fiber-reinforced CE-MWNT nanocomposites. The cross sections of specimens cut by waterjet cutter and tested/fractured tensile bars were coated with Ag/Pd and examined using secondary electron signals with an accelerating voltage of 5kV.

Finally, as there is no generally accepted definition or method to assess the degree of MWNT dispersion in polymer matrices, novel metrics are introduced in order to describe and document the effects of resin modifiers and processing on MWNT dispersion. In fact, characterization of nanoparticle dispersion continues to challenge the research community.

Thermal Stability Testing

Thermogravimetric analysis with simultaneous differential scanning calorimetry (Mettler Toledo TGA/DSC1) was used to examine the thermal stability of the CE-

MWNT nanocomposites when they were heated to 900°C in air or nitrogen. This instrument is equipped with micro and ultra-micro balances providing ultra-microgram resolution (~1.0μg) over the whole measurement range (from 25 to 1600°C). The standard heating rates of 5°C/min, 10°C/min, and 20°C/min were used, so that kinetics calculation for activation energy can be performed using the isoconversion technique [23] in the future.

Dynamic Mechanical Thermal Analysis

Complex modulus and glass transition temperature of the CE-MWNT nanocomposites were measured using the TA Instrument Q800 dynamic mechanical thermal analyzer (DMTA) to examine the effects of different weight loadings of MWNTs with various mixing techniques on the PNC. The DMTA were performed from room temperature (25°C) to 350°C. Specimens of 2mm thick were tested in three-point bending mode.

Flammability Testing

Flammability properties, such as heat release rate, were measured using the Govmark MCC-2 microscale combustion calorimeter according to ASTM D 7309 [24].

Electrical Conductivity

Electrical conductivity/resistivity were calculated from the voltage drop measured by the Hioki Super Megohmmeter and plate sample electrode. Plate specimens of 1mm thick were used in the electrical volume resistivity measurement.

Mechanical Properties

Waterjet cutter (WARD*Jet*'s Z-45 Gantry Waterjet) was used to cut dogbone and straight specimens from 8" x 10" x 0.125" panel carbon fiber-reinforced CE and CE-MWNT composites for mechanical properties characterization. Using the MTS Servo Hydraulic Test System, which has a capacity of 22kips, static tension and bending tests were performed.

RESULTS

Sample Preparation

The cyanate ester resin was blended with MWNT-1, as well as the corresponding three functionalized MWNTs (*f*-MWNTs), MWNT-2, MWNT-3, and MWNT-4. In each case, 0.5 wt% of nanotubes were mixed with CE resin using the IKA high shear mixer with the MK module. All CE-MWNT nanocomposites were cured to 200°C without the catalyst.

MWNT Dispersion

Although MWNT aggregates were not visible to the naked eye prior to curing, TEM images (illustrated in Figure 3.18) reveal large aggregates of MWNTs in the cured CE resin. High resolution SEM images showed large aggregates of MWNT-2 in the CE resin (illustrated in Figure 3.19) but smaller aggregates and more individual nanotubes of MWNT-3 and MWNT-4 were observed in the CE resin (Figures 3.20 and 3.21). Overall, MWNT-4 (with the $-NH_2$ functionalization) has the best degree of dispersion in the CE resin among the three *f*-MWNTs. This observation has yet to be confirmed by TEM imaging. However, these preliminary results may indicate that the high shear mixing alone was insufficient to achieve acceptable dispersion of MWNTs.

Figure 3.18. Illustrative TEM image of fracture surface of CE-0.5%MWNT-1 nanocomposites (length bar: 0.2µm).

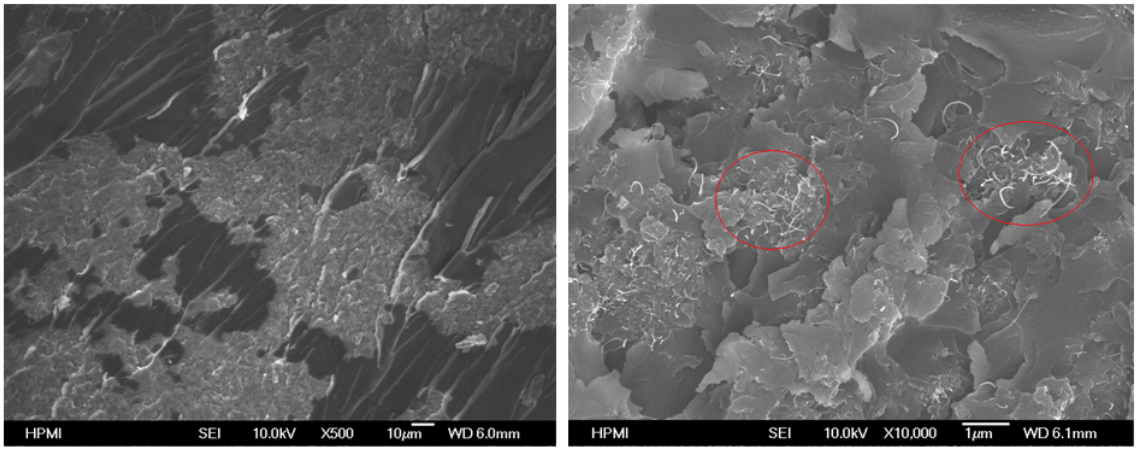

Figure 3.19. SEM images of fracture surface of CE-0.5%MWNT-2 nanocomposites in progressive magnification (length bar: 10µm left, 1µm right). Resin rich area is darker than nanotube area. MWNT dispersion is poor. The regions circled in red illustrate aggregates of MWNTs.

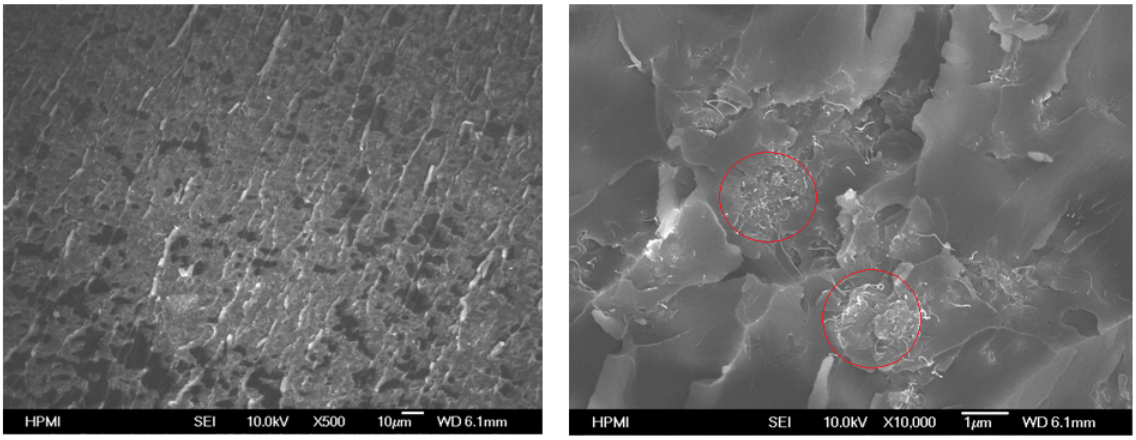

Figure 3.20. SEM images of fracture surface of CE-0.5%MWNT-3 nanocomposites in progressive magnification (length bar: 10μm left, 1μm right). Resin rich area is smaller than nanotube area. MWNT-3 distribution is better than that of MWNT-2. The regions circled in red illustrate aggregates of MWNTs.

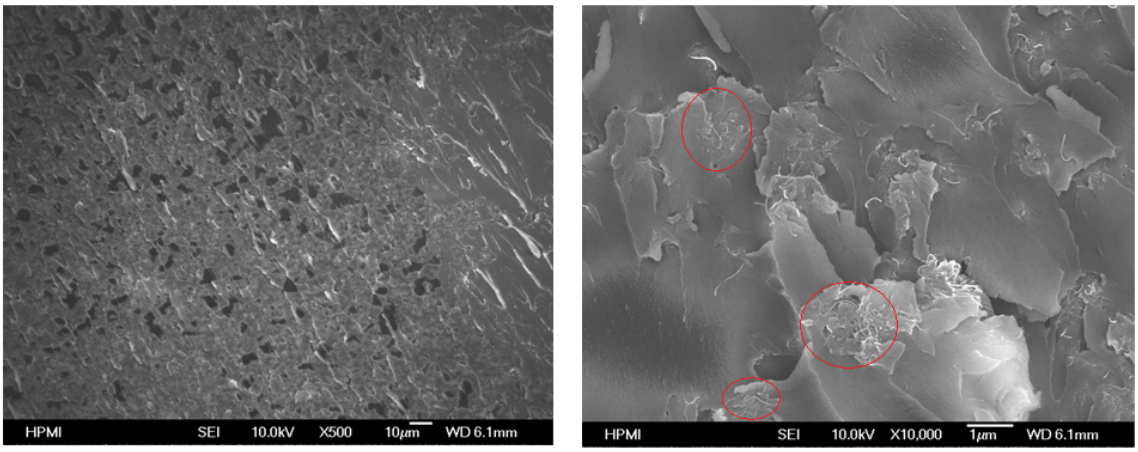

Figure 3.21. SEM images of fracture surface of CE-0.5%MWNT-4 nanocomposites in progressive magnification (length bar: 10μm left, 1μm right). While resin rich areas are observed, MWNT-N4 has smaller nanotube aggregation and more individual MWNTs. The regions circled in red illustrate aggregates of MWNTs.

Thermal Stability

TGA data (Figures 3.22 and 3.23; Table 3.7) showed that MWNTs did not enhance the decomposition temperature at 10% mass loss and only increased the decomposition temperature a few degrees at 50% mass loss. In general, none of the

MWNTs improve the thermal stability of the CE resin. This may be due to poor or mediocre MWNT dispersion or impurities, such as metal catalyst in the CE resin [25-26].

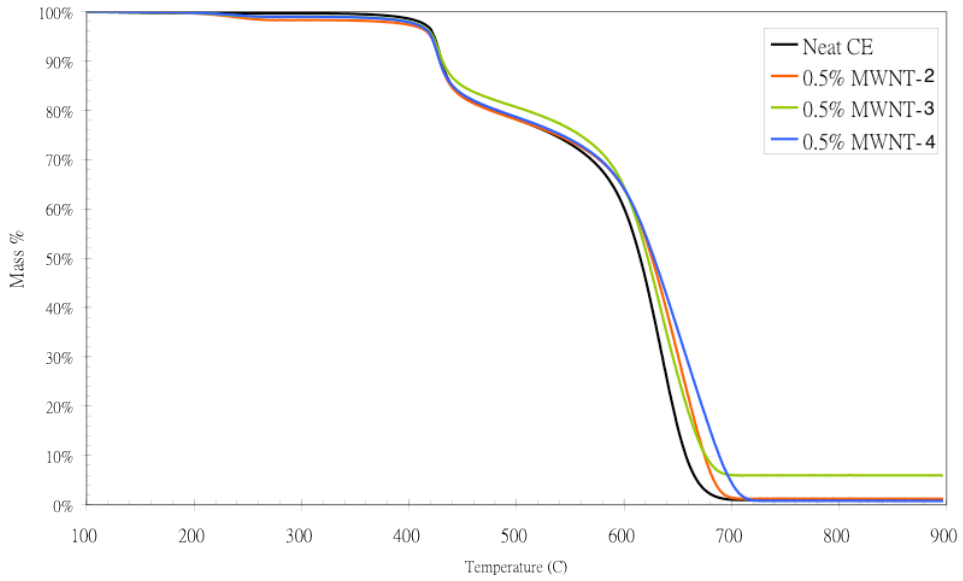

Figure 3.22. Thermogravimetric analysis of CE-MWNT nanocomposites at 10°C/min in air (*Number of samples per CE or CE-MWNT type, N = 1)*.

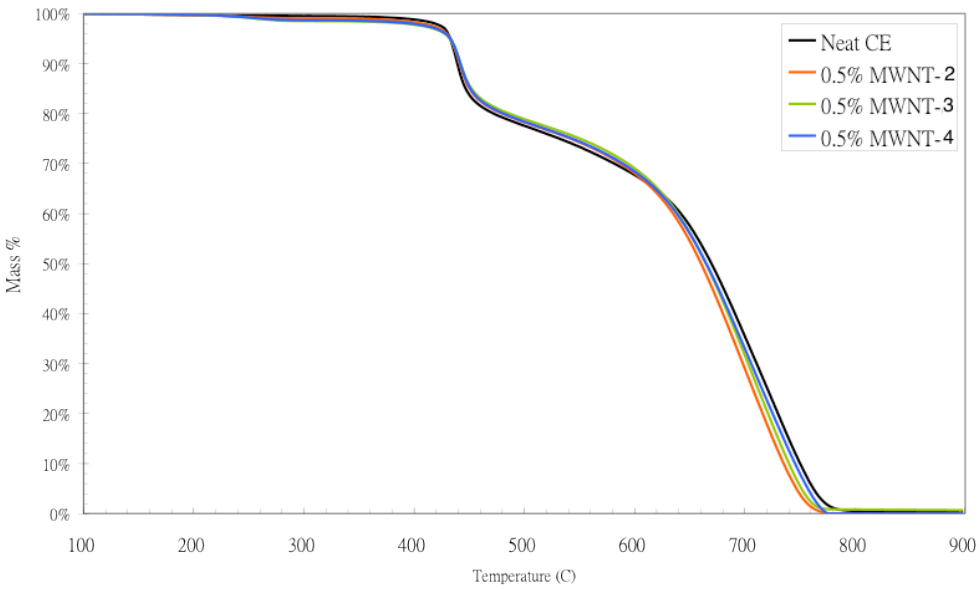

Figure 3.23. Thermogravimetric analysis of CE-MWNT nanocomposites at 20°C/min in air *(Number of samples per CE or CE-MWNT type, N = 1)*.

Table 3.7 Decomposition Temperatures of CE-MWNT Nanocomposites in Air

	10°C/min		20°C/min	
	$T_{10\%}$ (°C)	$T_{50\%}$ (°C)	$T_{10\%}$ (°C)	$T_{50\%}$ (°C)
Neat CE	430	615	439	669
CE-MWNT-2	428	625	441	659
CE-MWNT-3	430	621	442	664
CE-MWNT-4	428	627	441	664

Number of samples per CE or CE-MWNT type, N = 1

MWNT: Degree of Functionalization

MWNT-1 was functionalized with –OH, –COOH, and –NH2 groups using a plasma technique in Korea [6] to create MWNT-2, MWNT-3 and MWNT-4, respectively. FT-IR/ATR was used to analyze the degree of functionalization of each *f*-MWNT. However, this method was unable to detect any functional groups, which may be due to very low degree of functionalizations on each sample. Wepasnick claimed that, while FT-IR was not able to detect functional groups in their samples, XPS was able to do so [27]. As a result, x-ray photoelectron spectroscopy (XPS) and electron energy loss spectroscopy (EELS) were performed on the three *f*-MWNT types [Courtesy Zsolt E. HORVATH; 28].

f-MWNT samples were glued by indium onto a copper sample holder being fixed in the vacuum system. The XPS and EELS measurements were performed in a KRTATOS ES-300 system equipped with Al K_α X-ray source and an electron beam gun in 100-1000eV energy. A hemispherical analyzer of 100cm diameter was used for the measurement of electron energy distribution of XPS and EELS investigations. Energy resolution of the X-ray and electron energy distribution measurement was 1eV and 0.5eV, respectively. The investigation of the different samples was carried out under identical conditions in all respects. The Indium 3d peak was used as a reference for the energy scale of core level measurements. The energy scale of electron energy loss was

determined by the energy of elastically reflected electrons. Using the Shirley model, the background of the core level peaks and electron energy loss peaks was determined [29].

In case of the O1s and C1s peaks (Figures 3.24 and 3.25) the differences between the peak shapes were distinct, illustrating that different chemical states of the corresponding elements were present in the samples in diverse composition. The interpretation of the results is difficult due to the complex, highly porous character of the samples. In addition to the oxygen-containing functional groups, the O1s peak shape was influenced by the presence of atmospheric O_2, CO, and water molecules adsorbed on the high area surface and the In-oxide coverage of the exposed indium surface. On the other hand, the C1s peak was influenced by the carbon in the MWNTs, as well as inevitable organic contaminations from the air and vacuum oil. Further, more detailed analysis (e.g. decomposition of the peaks by fitting) of the samples can give more valid information, but the investigation of the O1s and C1s XPS peaks did not seem to be a generally applicable technique for the study of these *f*-MWNTs. That said, the presence of the N1s peak in case of the $–NH_2$ functionalized sample (Figure 3.26) could be interpreted as the sign of the functional groups, since this peak was absent in the spectra of the other samples.

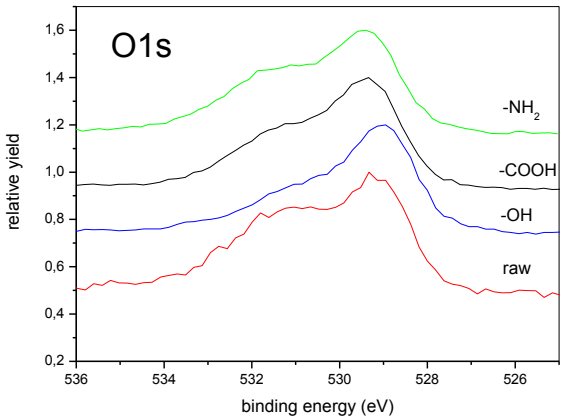

Figure 3.24. XPS Oxygen (O1s) peak of the raw (MWNT-1) and functionalized MWNT (MWNT-2, MWNT-3, MWNT-4) samples [28].

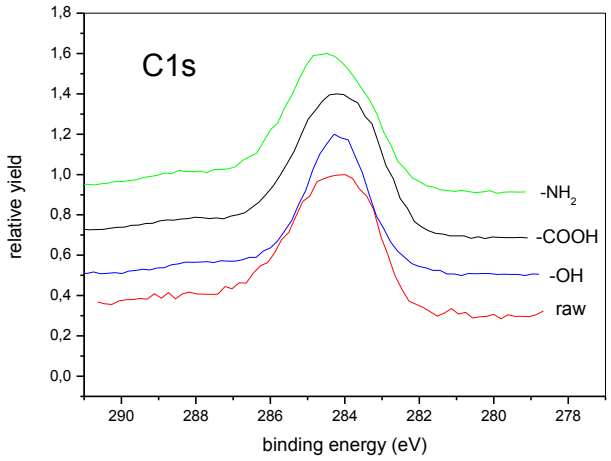

Figure 3.25. XPS Carbon (C1s) peak of the raw (MWNT-1) and functionalized MWNT (MWNT-2, MWNT-3, MWNT-4) samples [28].

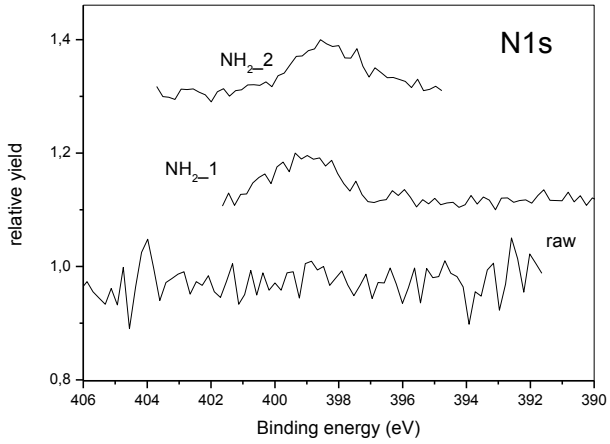

Figure 3.26. XPS Nitrogen (N1s) peak of the raw (MWNT-1) and–NH_2-functionalized (MWNT-4) samples [28].

A part of the EELS spectra of the samples is presented in Figure 3.27. Electron energy loss peak at about 6 eV can be interpreted either as a π-π* transition or π plasmon modes. Both are characteristic for graphite and graphitic carbon structures like MWNT.

In case of the neat or raw MWNT material, a well-defined peak was observed at 6.2 eV. For the -NH_2 functionalized MWNT sample (MWNT-4) the peak was less pronounced, while in case of the -COOH and -OH functionalized samples, MWNT-3 and MWNT-2, respectively, it was very weak. The relative intensity of the peak is in correlation with the degree of graphitic character of the surface. Functional groups attached to the outer wall of MWNTs act as defects breaking the graphitic character of the electronic state. Consequently, the decrease of peak intensity qualitatively correlates with the degree of functionalization. The determination of any quantitative dependence needs further study on standard samples and those with different degrees of functionalization.

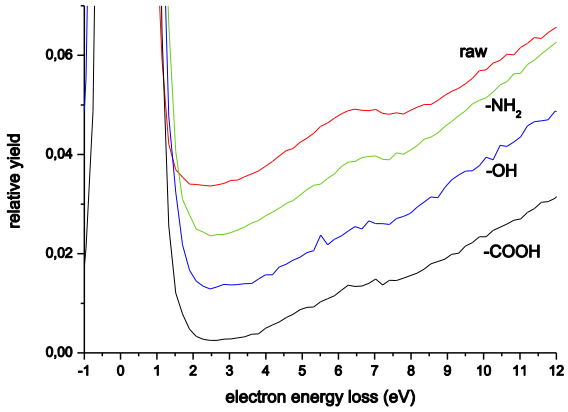

Figure 3.27. A part of the Electron Energy Loss spectra of the raw (MWNT-1) and functionalized MWNT (MWNT-2, MWNT-3, MWNT-4) samples [28].

Due to the quantitative uncertainty in the degree of functionalization on the MWNTs, the research, thus the rest of this dissertation, focused on the processing and characterizations of the CE with neat MWNT-5. Additional study is underway to further quantify the degree of functionalization on carbon nanotubes.

SUMMARY

Materials selection, processing techniques, characterization methods, and some preliminary results were introduced in this chapter. The PT-15 CE was selected because of the low viscosity in its molten states that provides advantage of larger processing flexibility. Selection of MWNTs were based on the considerations of the balance among the properties of MWNTs, the compatibility of the MWNTs with the CE resin, and the cost of the MWNTs. MWNT-5 was selected due to its relatively good compatibility with CE and its lower cost. Processing instruments used in this study were ultrasonicator, three-roll mill, stand mixer, high shear mixer, and planetary centrifugal mixer, while characterization methods include SEM, STEM, TEM, DMA, MCC, TGA, and electrical resistivity measurement.

Phase separation of MWNTs from the CE resin was avoided by adding a FE(III) catalyst to lower the cure temperature of CE-MWNT nanocomposite, or by incorporating a coupling agent, which also lowered the cure temperature of the CE-MWNT nanocomposites, to increase the affinity between CE and MWNTs. Cure cycles of CE with the Fe(III) catalyst and with the coupling agent, respectively, were developed.

REFERENCES

1. Lonza Primaset® PT-15 Technical Data Sheet, Lonza Inc., Fair Lawn, NJ.
2. F. Abali, K. Shivakumar, N. Hamidi, and R. Sadler, "An RTM Densification Method of Manufacturing Carbon-Carbon Composites Using PT-30 Resin," *Carbon*, 41(5): 893, 2003.
3. R. E. Myers, US Patent # 07/447751, 1992.
4. J. H. Koo, S. C. Lao, *et al*., "Morphology and Thermal Characterization of Carbon-based Nanomaterials," *Proc. SAMPE 2011 ISSE*, SAMPE, Covina (2011).
5. S. Ghose, K. A. Watson, H. A. Elliott, D. C. Working, J. M. Criss, K. L. Dudley, E. J. Siochi, and J. W. Connell, "Fabrication and Characterization of High Temperature Resin/Carbon Nanofiller Composites," *Proc. Multifunctional Nanocomposites 2006*, Sept 20-22, Honolulu, HI, 2006.
6. J. Lee, Agency of Defense Development, Daejon, South Korea.
7. J. Cheng, S. Lao, J. Yong, J. H. Koo, P. Ferreira, L. Pilato, G. Wissler, and Z. P. Luo, "Cyanate Ester-Buckytubes Nanocomposites: Processing and Characterization," *Proc. SAMPE 2007 ISSE*, SAMPE, Covina, CA (2007).
8. ILjin Nanotech Co., Ltd., Seoul, South Korea (www.iljin.co.kr).
9. The CM-95 neat MWNT was functionalized with hydroxy (-OH), carboxyl (-COOH), and amine ($-NH_2$) groups using plasma technology supplied by Dr. Lee of Agency for Defense Development (ADD).
10. Arkema, Lacq, France (www.graphistrength.fr).
11. Bayer MaterialScience (www.baytubes.com).
12. Cheap Tubes Inc., Brattleboro, VT (www.cheaptubes.com).
13. G. Wang, Z. Tan, X. Liu, V. Samuilov, and M. Dudley, "Preparation and Electrical Properties oft he MWNT/Polymer Nanocomposite Fibers," *Proc. MRS 2006 Fall Meeting*, Boston, MA, 693 (2006).
14. Plastics News Online Directory, Ken-React® Coupling Agents (V) (http://www.plasticsnewsdirectory.com/).
15. ChemBlink, Zicronate Coupling Agent Ken-React® NZ 97 (http://www.chemblink.com/products/111083-78-4.htm).
16. Emerson Industrial Automation, Branson 1510 (http://www.bransonic.com/).
17. Breville USA (http://www.brevilleusa.com/stand-mixer.html).
18. THINKY USA Inc. (http://www.thinkymixer.net/commentary/jiten-kouten.html).

19. IKA, Inc. (http://www.ikaprocess.com/Products/Inline-disperser-dispersing-machine-high-shear-cph-6/DISPAX-REACTOR-DR-csb-DR/#).

20. Exakt Technologies, Inc. (http://www.exaktusa.com/products/exakt_E.html)

21. P.-C. Ma, N. A. Siddiqui, G. Marom, J.-K. Kim, "Dispersion and Functionalization of Carbon Nanotubes for Polymer-based Nanocomposites: A Review," *Composites: Part A*, 41: 1345-1367, 2010.

22. J. H. Koo, *Polymer Nanocomposites: Processing, Characterization, and Applications,* McGraw-Hill, New York, 2006

23. W. K. Ho, J. H. Koo, and O. A. Ezekoye, "Kinetics and Thermophysical Properties of Polymer Nanocomposites for Solid Rocket Motor Insulation," *J. of Spacecraft and Rockets,* 46 (3): 526-544, 2009.

24. ASTM 7309, "Standard Test Method for Determining Flammability Characteristics of Plastics and Other Solid Materials Using Microscale Combustion Calorimetry."

25. S. Choi, Y. Jeong, G.-W. Lee, and D. H. Cho, "Thermal and Mechanical Properties of Polypropylene Filaments Reinforced with Multiwalled Carbon Nanotubes via Melt Compounding," *Fibers and Polymers*, 10(4): 513-518, 2009.

26. Z. Li, S. J. Wilkins, K. S. Moon, and C. P. Wong, "Carbon Nanotube/Polymer Nanocomposites: Improved or Reduced Thermal Stabilities?" *Materials Science Forum*, 722: 77-86, 2012.

27. K. A. Wepasnick, B. A. Smith, K. E. Schrote, H. K. Wilson, S. R. Diegelmann, and D. H. Fairbrother, "Surface and Structural Characterization of Multi-walled Carbon Nanotubes Following Different Oxidative Treatments," *Carbon*, 49: 24-36, 2011.

28. XPS analysis conducted and data provided by Zsolt E. HORVATH, Hungarian Academy of Sciences, Jul 2011.

29. D. A. Shirley, "High-Resolution X-Ray Photoemission Spectrum of the Valence Bands of Gold," *Phys. Rev. B.*, 5: 4709-4714, 1972.

Chapter 4

Characterization of CE-MWNT-5 Polymer Nanocomposites

Morphology, MWNT dispersion, thermal stability, flammability properties, mechanical properties, and electrical resistivity of the CE-MWNT-5 polymer nanocomposites were characterized. Specimens of 64 mm x 64 mm x 1 mm were fabricated for the electrical conductivity measurement, while specimens of 36 mm x 12 mm x 2 mm were used in the dynamic mechanical analysis (DMA). Electron microscopy specimens were sectioned from the DMA bar, while small (5 – 10 mg) pieces were cut from the remaining bar for thermogravimetric analysis (TGA) and microscale combustion calorimetry (MCC).

CE-MWNT-5 Polymer Nanocomposites

Cyanate ester and 0.5 wt% MWNT-5 (neat and functionalized) nanotubes were mixed using various methods, then cured with the Fe(III) catalyst or coupling agents (see Table 4.1).

Scanning transmission electron microscope (STEM) was used to examine the dispersion of the MWNT-5 nanotubes in several sample nanocomposites. Representative samples were cut into thin, 70nm-thick sections using an ultramicrotome (Leica Ultracut UTC) with diamond knife. The maximum accelerating voltage of the microscope is 30keV—too low for obtaining transmission images of the 70nm-thick samples. As a result, SEM images of the section surfaces were obtained using the secondary electron signals. These sections were further examined using transmission electron microscopy (TEM) and distribution of nanotubes spacing was assessed.

Table 4.1 CE-0.5%MWNT-5 Polymer Nanocomposite Test Matrix

Sample		Processing Technique
MWNT	**Fe^{3+} or CA**	
MWNT-5	200ppm Fe^{3+}	Ultrasonication
MWNT-5	200ppm Fe^{3+}	Planetary
MWNT-5	200ppm Fe^{3+}	Stand mixer
MWNT-5	200ppm Fe^{3+}	Three-roll mill
MWNT-5	200ppm Fe^{3+}	High shear (MK)
MWNT-5-OH	200ppm Fe^{3+}	Stand mixer
MWNT-5-NH_2	200ppm Fe^{3+}	Stand mixer
MWNT-5	3% CA1	Stand mixer
MWNT-5	3% CA1	High shear (MK)
MWNT-5	3% CA1	High shear (DR)

MORPHOLOGY OF THE CE-MWNT-5 POLYMER NANOCOMPOSITES

Images from Scanning Transmission Electron Microscopy

Figures 4.1 thru 4.7 are representative SEM images. The maximum accelerating voltage of the SEM (30kV) and secondary electrons were used when obtaining images. Visual observation reveals that the sample processed by the three-roll mill has the best dispersion of MWNTs, as it had most de-bundled MWNTs and the smallest aggregates (smaller than 500nm). Large aggregates of MWNTs (>7μm) were observed in samples processed by ultrasonication and planetary centrifugal mixer. Smaller aggregates (~5μm) are observed in the sample processed by the stand mixer, albeit smaller aggregates are observed in all samples. Furthermore, neither the functionalizations of the MWNTs nor the addition of coupling agent improved the dispersion of MWNTs in CE using the stand mixer. In fact, a very large aggregate of 30μm is observed in the CE-MWNT-5-NH_2 sample.

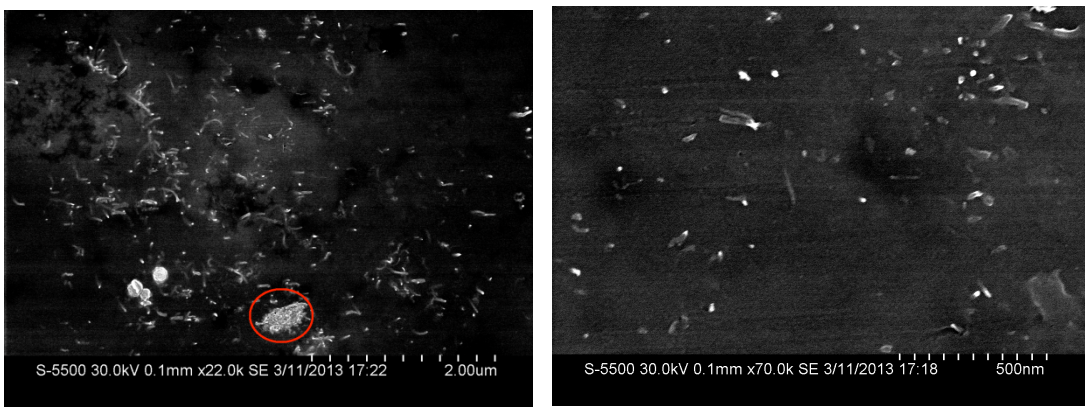

Figure 4.1. SEM images (in progressive magnification) of the surface of a thin section of CE-MWNT-5 polymer nanocomposite, processed by three-roll mill with roller gaps of 5μm. Regions circled in red denote MWNT aggregates (length bar: 2μm left, 500nm right).

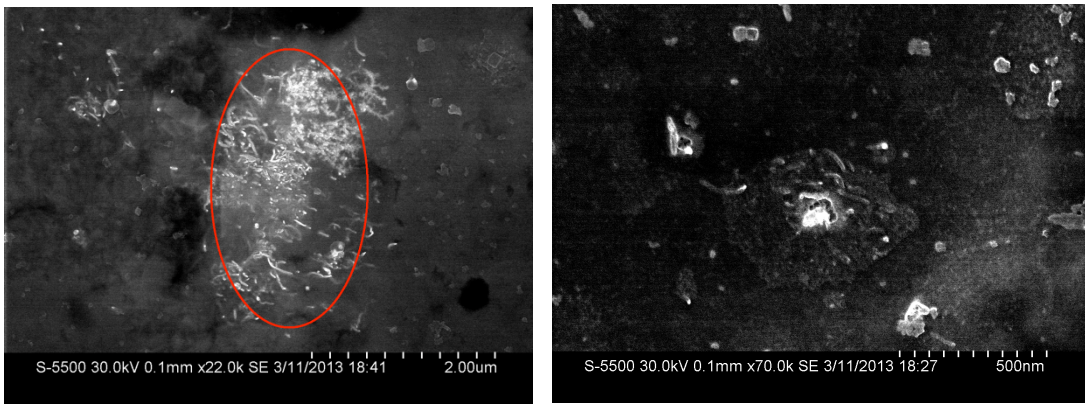

Figure 4.2. SEM images (in progressive magnification) of the surface of a thin section of CE-MWNT-5 polymer nanocomposite, processed by planetary centrifugal mixers with grinding media for 30 minutes. Regions circled in red denote MWNT aggregates (length bar: 2μm left, 500nm right).

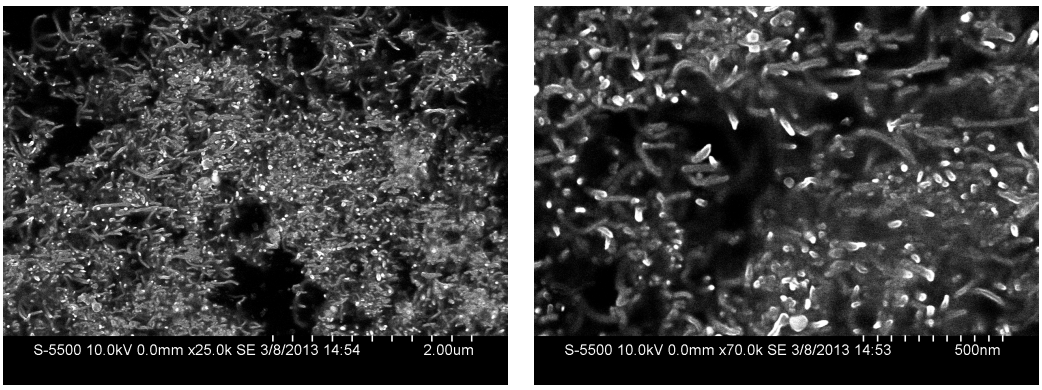

Figure 4.3. SEM images (in progressive magnification) of the surface of a thin section of CE-MWNT-5 polymer nanocomposite, processed by ultrasonicator for 2 hours. Large (>7μm) MWNT aggregates were observed (length bar: 2μm left, 500nm right).

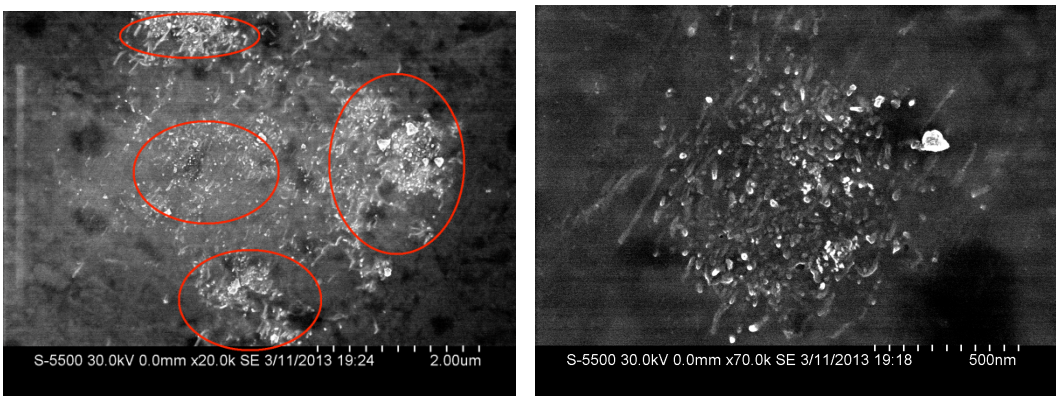

Figure 4.4. SEM images (in progressive magnification) of the surface of a thin section of CE-MWNT-5 polymer nanocomposite, processed by stand mixer for 2 hours. Regions circled in red denote MWNT aggregates (length bar: 2μm left, 500nm right).

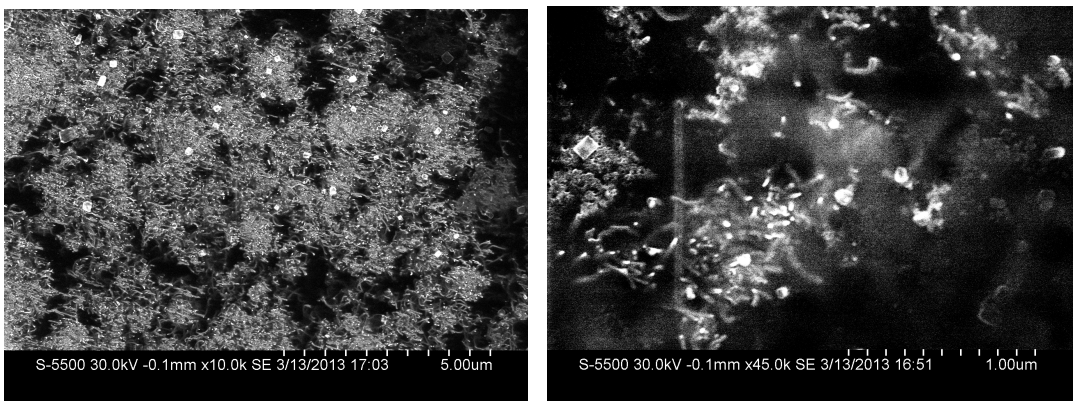

Figure 4.5. SEM images (in progressive magnification) of the surface of a thin section of CE-MWNT-5-NH_2 polymer nanocomposite, processed by stand mixer for 2 hours. Large MWNT aggregates were observed (length bar: 5µm left, 1µm right).

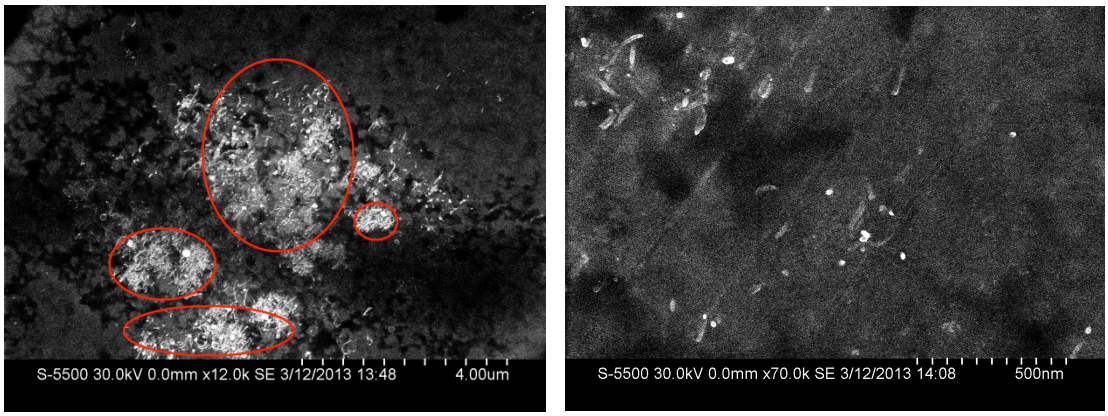

Figure 4.6. SEM images (in progressive magnification) of the surface of a thin section of CE-MWNT-5-OH polymer nanocomposite, processed by stand mixer for 2 hours. Regions circled in red illustrate MWNT aggregates (length bar: 4µm left, 500nm right).

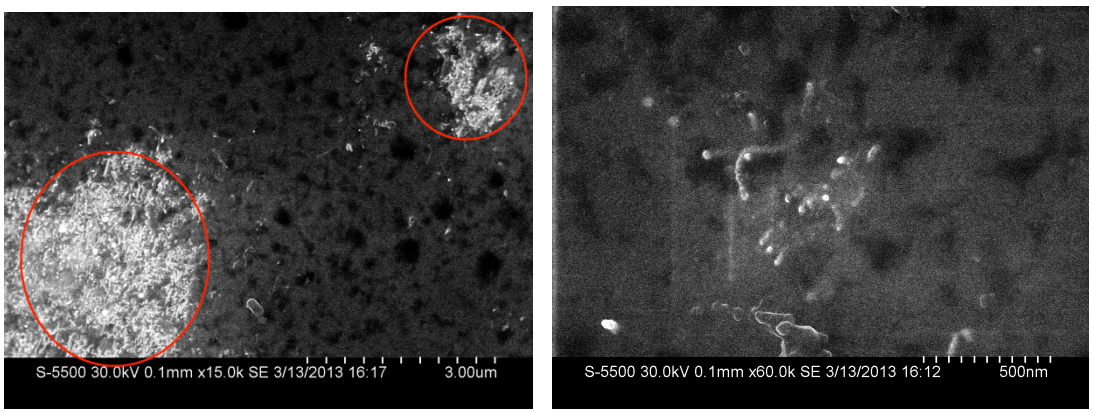

Figure 4.7. SEM images (in progressive magnification) of the surface of a thin section of CE-MWNT-5 + 3%CA-1 polymer nanocomposite, processed by stand mixer for 2 hours. Regions circled in red illustrate MWNT aggregates (length bar: 3μm left, 500nm right).

Since electron probe diameter is smaller with higher accelerating voltage in SEM, images of higher resolution can be obtained at higher accelerating voltage [1]. However, unnecessary signals, such as backscattered electrons, are generated from within the specimen with higher accelerating voltage as the beam penetration and diffusion area become deeper and larger, respectively, These extra signals reduce the image contrast and surface structures.

As a result, a set of SEM images of the same location of the specimens were obtained at different accelerating voltages to ensure no MWNTs on the specimen surface were ignored due to high accelerating voltage (Figures 4.8-14). Figure 4.8 shows a SEM images obtained using an accelerating voltage of 30kV. On the right, it shows a MWNT aggregate of ~1μm in diameter, while on the left a MWNT-absent / pure resin area. When the accelerating voltage is lowered progressively (30, 25, 20, 15, 10, 5, 3 kV), no additional MWNTs were observed in the pure resin area. This suggests that the higher accelerating voltage does not affect the fineness of surface structure in this study nor the visibility of MWNTs. Notably, when the accelerating voltage decreases, the resolution is lowered and it is more difficult to obtain a clear focus.

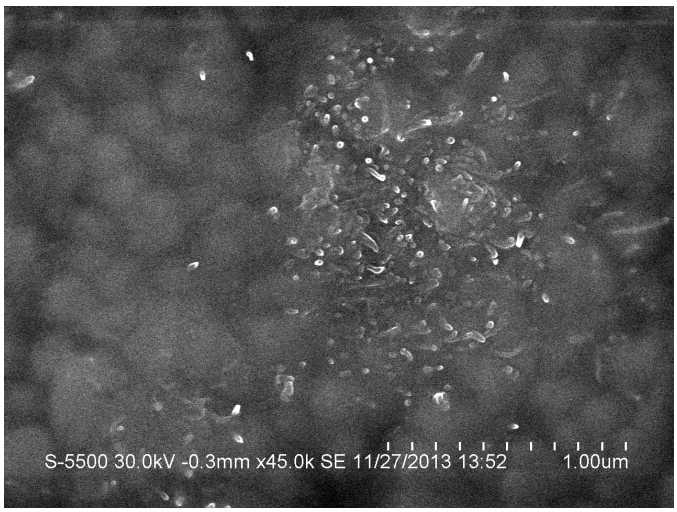

Figure 4.8. SEM images (accelerating voltage = 30kV) of the surface of a thin section of CE-MWNT-5 polymer nanocomposite, processed by three-roll mill with roller gaps of 5μm. On the left, a relatively MWNT-free, resin-rich area, while on the right, a MWNT aggregate (length bar: 1μm).

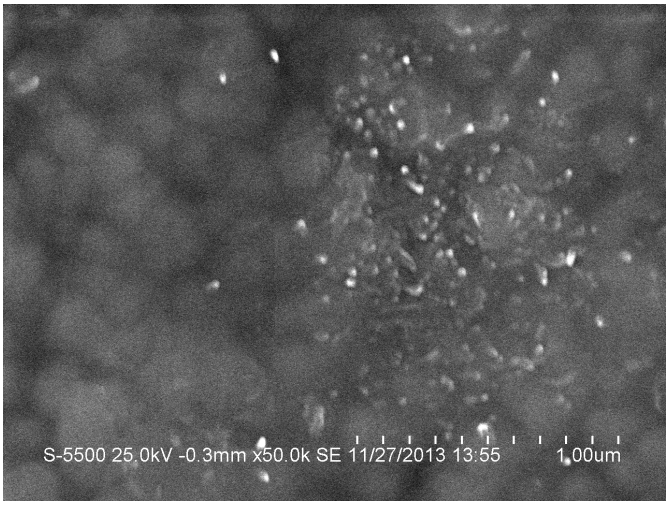

Figure 4.9. SEM images (accelerating voltage = 25kV) of the surface of a thin section of CE-MWNT-5 polymer nanocomposite, processed by three-roll mill with roller gaps of 5μm. On the left, a relatively MWNT-free, resin-rich area, while on the right, a MWNT aggregate (length bar: 1μm).

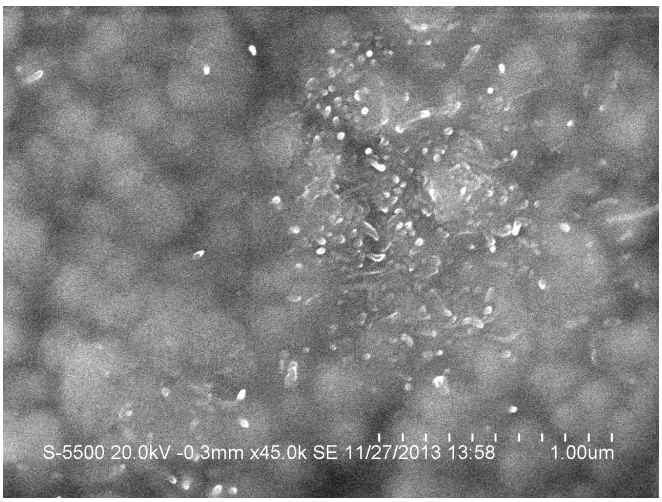

Figure 4.10. SEM images (accelerating voltage = 20kV) of the surface of a thin section of CE-MWNT-5 polymer nanocomposite, processed by three-roll mill with roller gaps of 5μm. On the left, a relatively MWNT-free, resin-rich area, while on the right, a MWNT aggregate (length bar: 1μm).

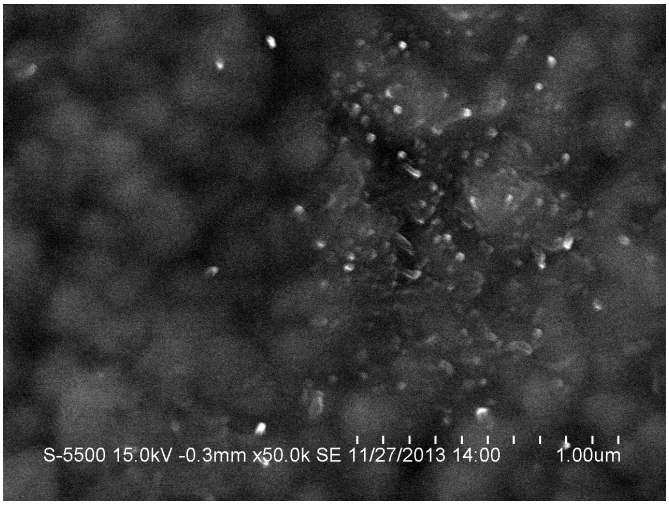

Figure 4.11. SEM images (accelerating voltage = 15kV) of the surface of a thin section of CE-MWNT-5 polymer nanocomposite, processed by three-roll mill with roller gaps of 5μm. On the left, a relatively MWNT-free, resin-rich area, while on the right, a MWNT aggregate (length bar: 1μm).

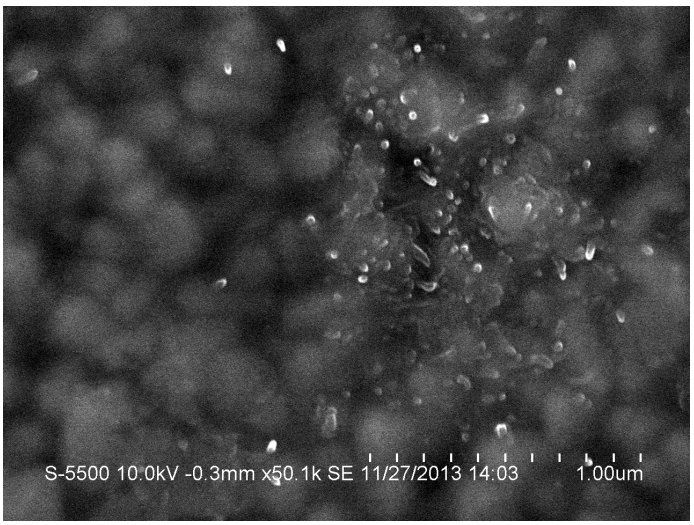

Figure 4.12. SEM images (accelerating voltage = 10kV) of the surface of a thin section of CE-MWNT-5 polymer nanocomposite, processed by three-roll mill with roller gaps of 5μm. On the left, a relatively MWNT-free, resin-rich area, while on the right, a MWNT aggregate (length bar: 1μm).

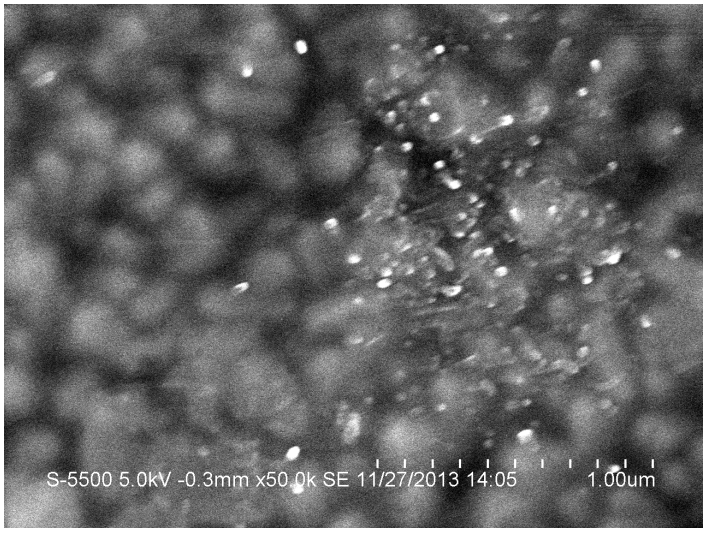

Figure 4.13. SEM images (accelerating voltage = 5kV) of the surface of a thin section of CE-MWNT-5 polymer nanocomposite, processed by three-roll mill with roller gaps of 5μm. On the left, a relatively MWNT-free, resin-rich area, while on the right, a MWNT aggregate (length bar: 1μm).

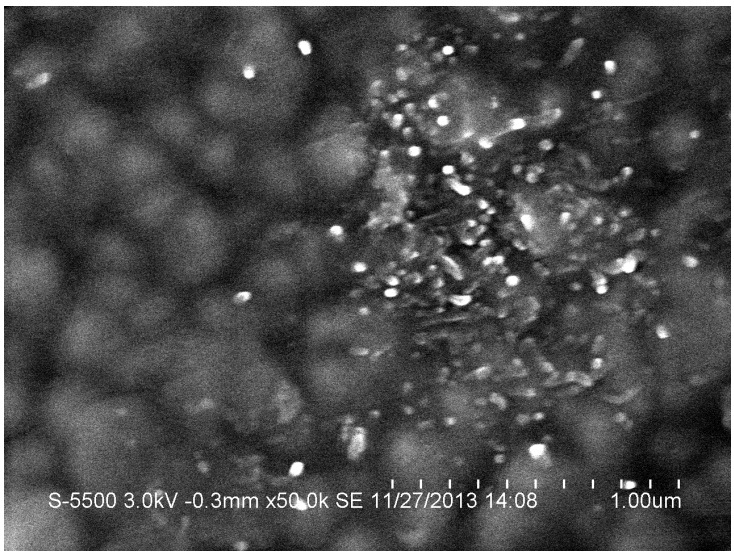

Figure 4.14. SEM images (accelerating voltage = 3kV) of the surface of a thin section of CE-MWNT-5 polymer nanocomposite, processed by three-roll mill with roller gaps of 5μm. On the left, a relatively MWNT-free, resin-rich area, while on the right, a MWNT aggregate (length bar: 1μm).

Images from Transmission Electron Microscopy

Samples were examined using TEM in higher magnification and using the transmission electron signals. Figures 4.15 thru 4.23 show representative TEM images. In the samples processed by three-roll mill, the MWNTs are more de-bundled than those processed by stand mixer and ultrasonication with the one processed by the planetary centrifugal mixer being intermediate. However, despite being more de-bundled, the MWNTs are not more uniformly distributed in the matrix. Both MWNT aggregates and individual MWNTs are observed in samples processed by the high shear mixer.

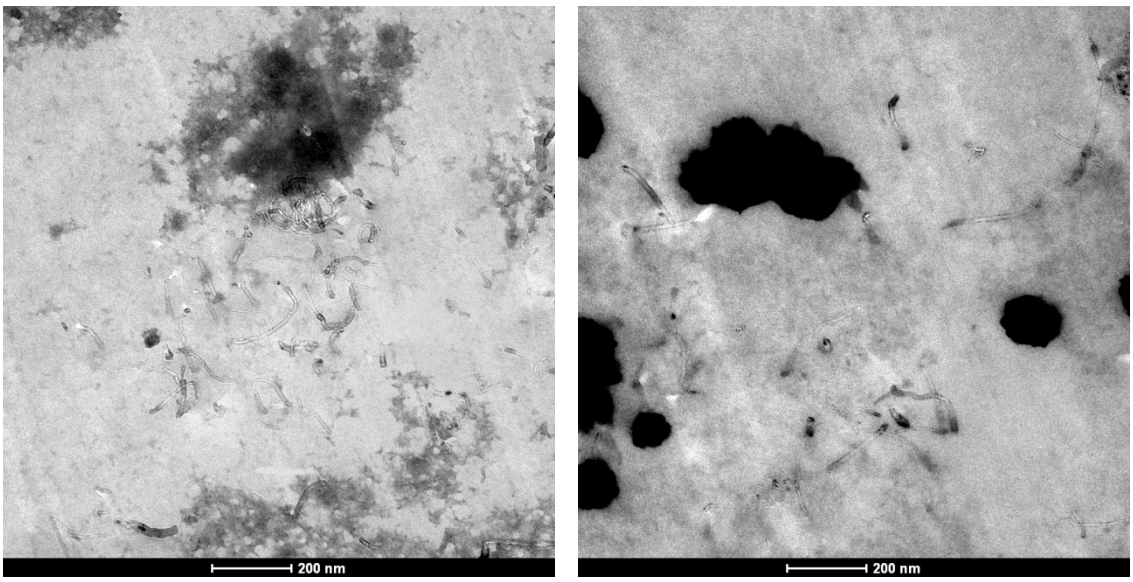

Figure 4.15. TEM images of the surface of a thin section of CE-MWNT-5 polymer nanocomposite, processed by three-roll mill with roller gaps of 5μm (length bar: 200nm).

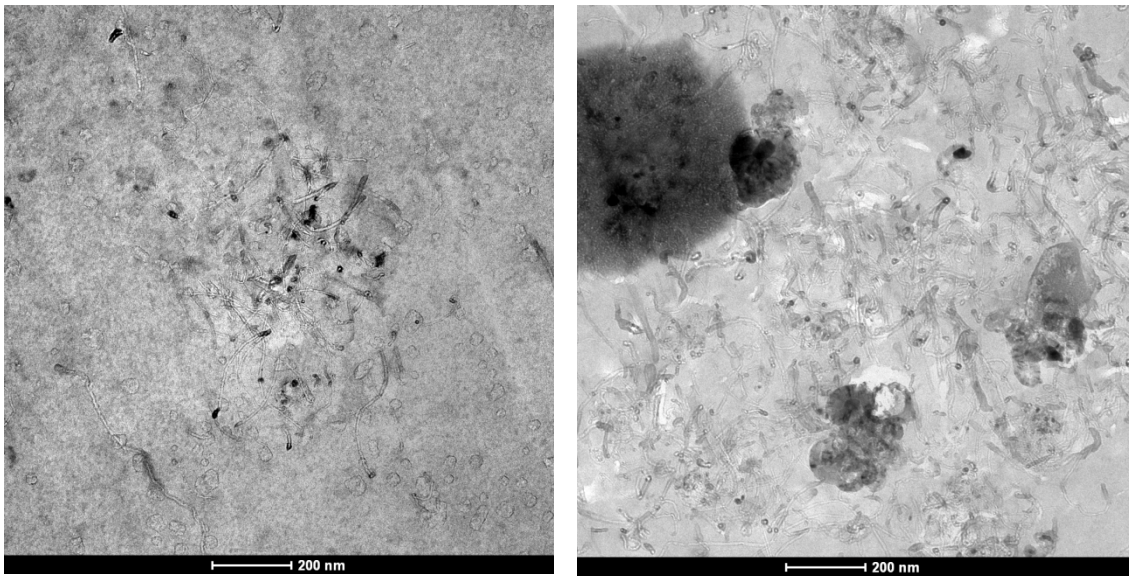

Figure 4.16. TEM images of the surface of a thin section of CE-MWNT-5 polymer nanocomposite, processed by planetary centrifugal mixers with grinding media for 30 minutes (length bar: 200nm).

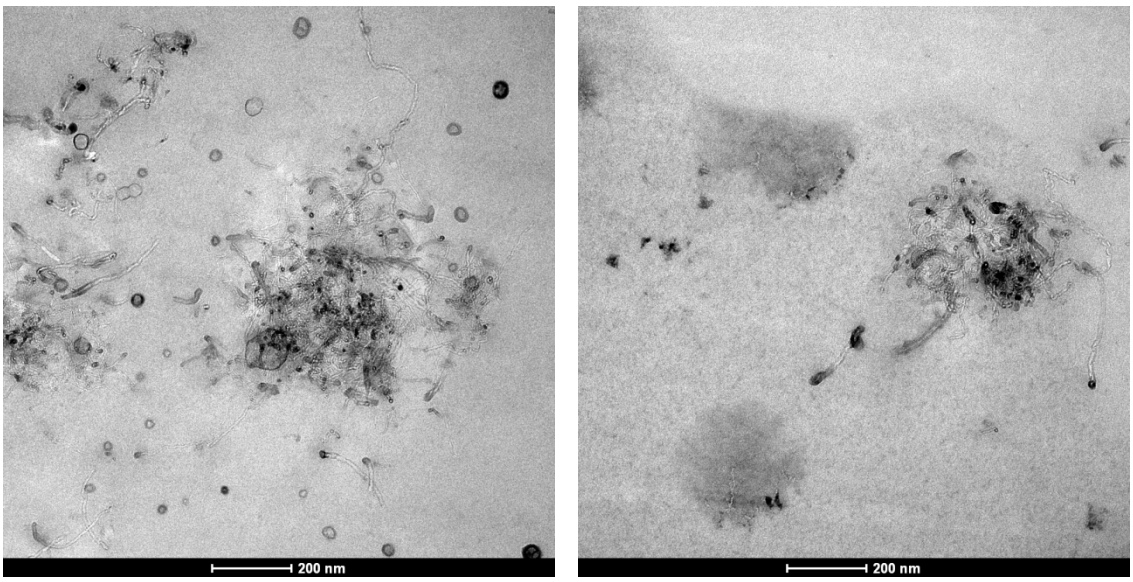

Figure 4.17. TEM images of the surface of a thin section of CE-MWNT-5 polymer nanocomposite, processed by ultrasonicator for 2 hours (length bar: 200nm).

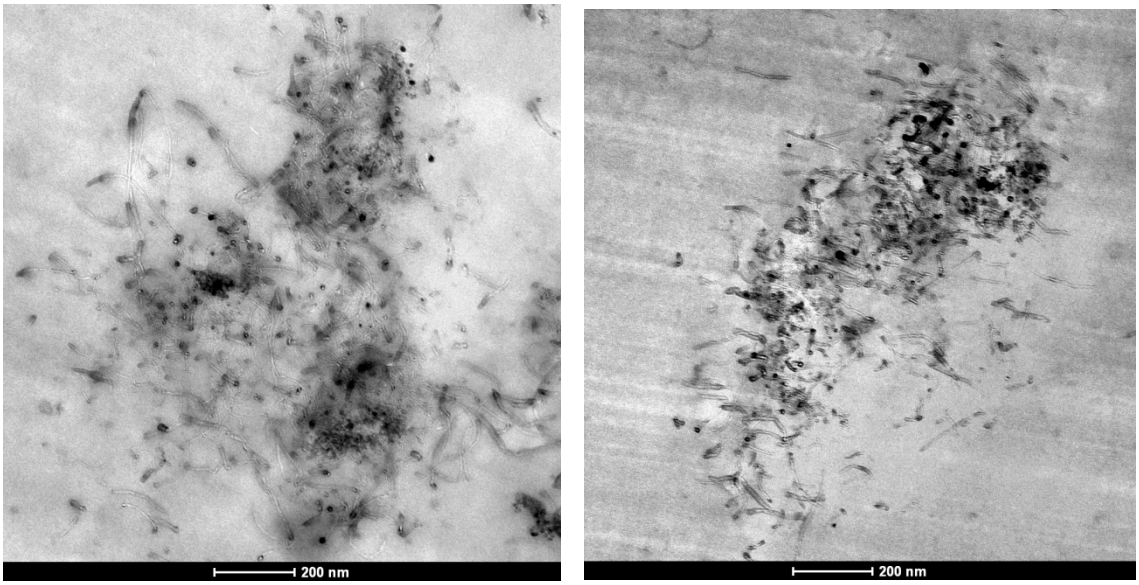

Figure 4.18. TEM images of the surface of a thin section of CE-MWNT-5 polymer nanocomposite, processed by stand mixer for 2 hours (length bar: 200nm).

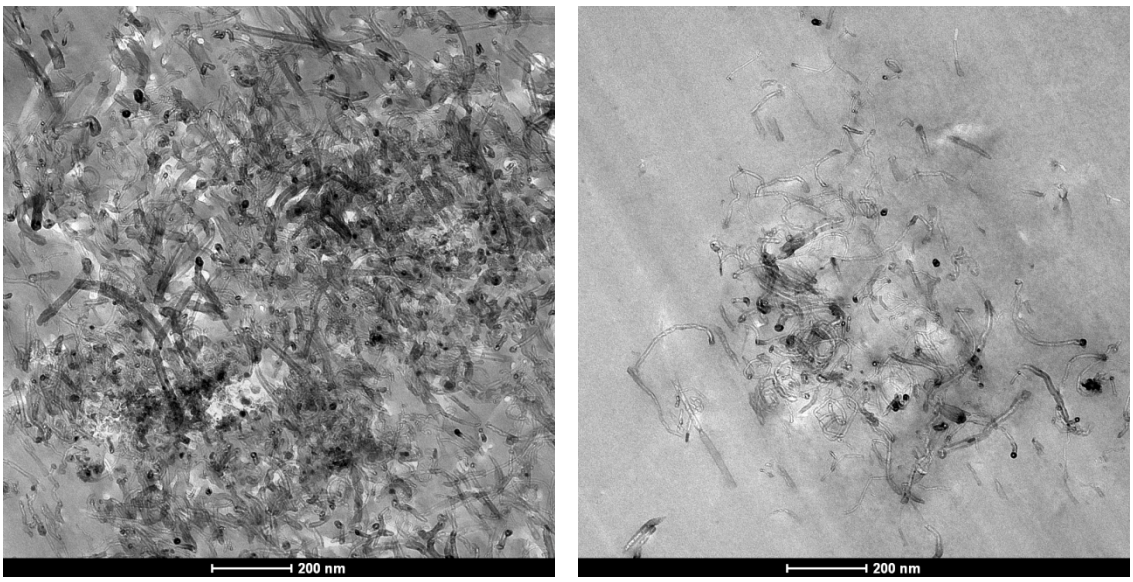

Figure 4.19. TEM images of the surface of a thin section of CE-MWNT-5-NH_2 polymer nanocomposite, processed by stand mixer for 2 hours (length bar: 200nm).

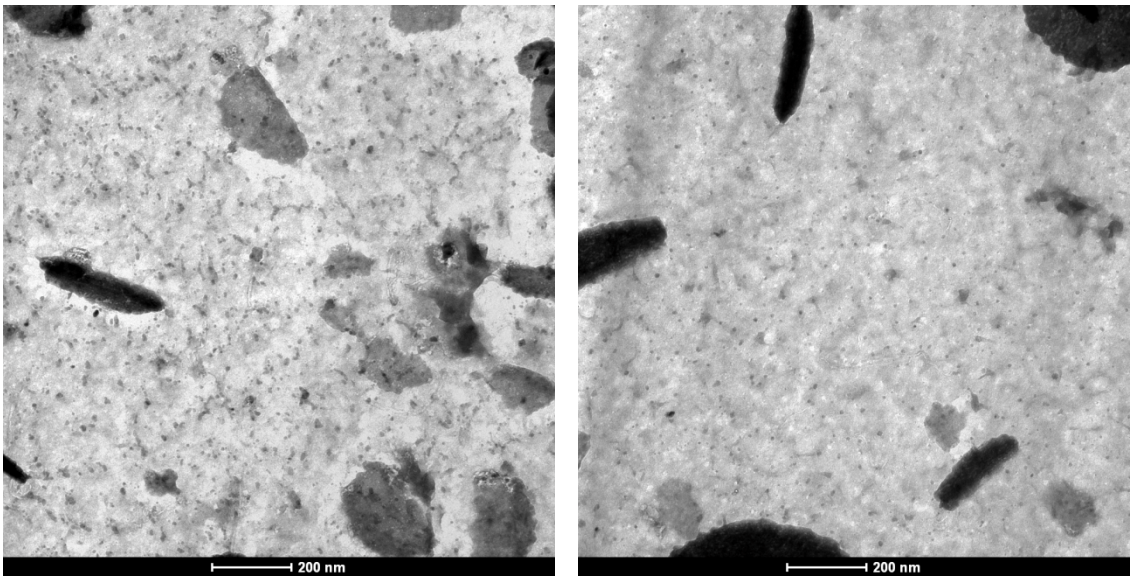

Figure 4.20. TEM images of the surface of a thin section of CE-MWNT-5-OH polymer nanocomposite, processed by stand mixer for 2 hours (length bar: 200nm).

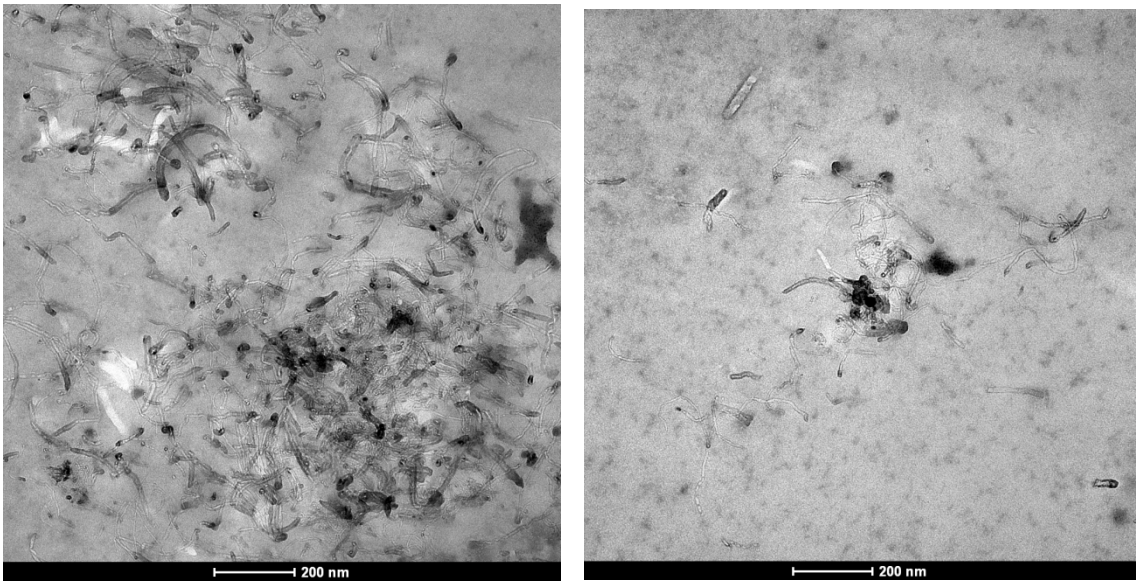

Figure 4.21. TEM images of the surface of a thin section of CE-MWNT-5 + 1% CA-1 polymer nanocomposite, processed by stand mixer for 2 hours (length bar: 200nm).

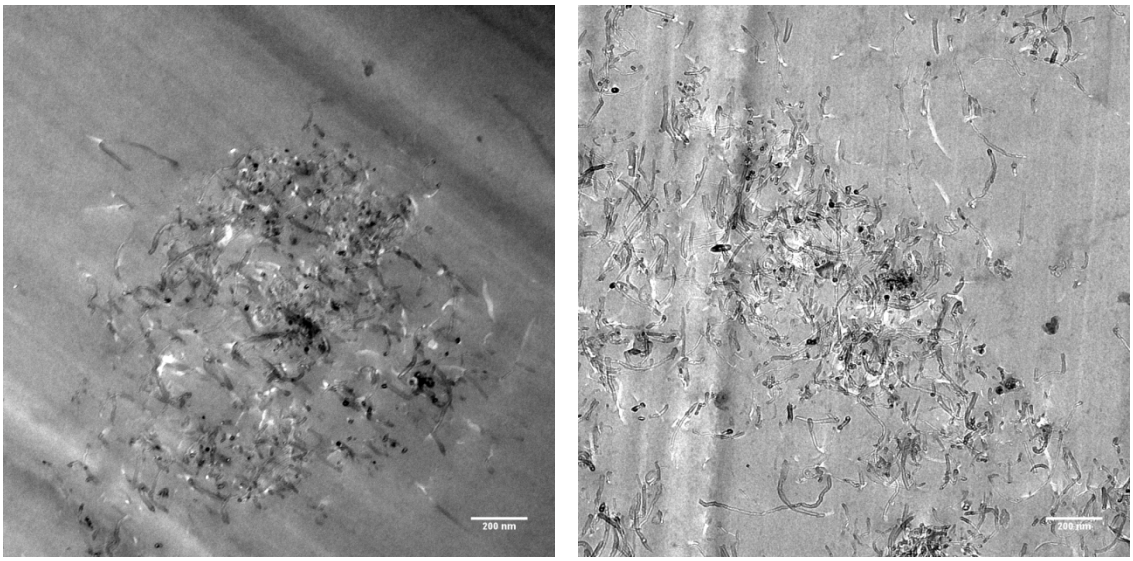

Figure 4.22. TEM images of the surface of a thin section of CE-MWNT-5 polymer nanocomposite, processed by high shear mixer with MK module for 1 hour (length bar: 200nm).

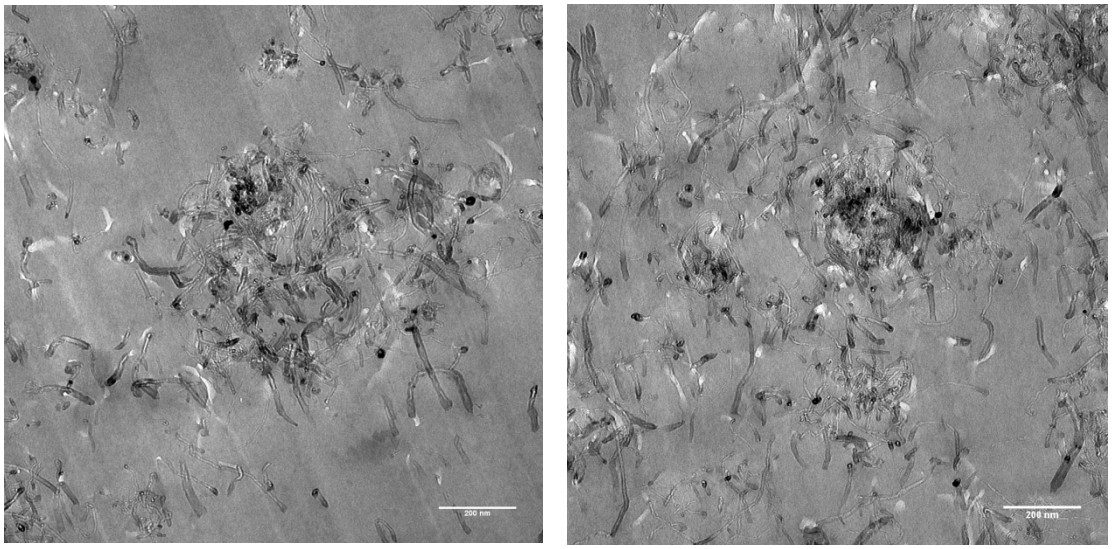

Figure 4.23. TEM images of the surface of a thin section of CE-MWNT-5 polymer nanocomposite, processed by high shear mixer with DR module for 1 hour (length bar: 200nm).

Quantification of MWNT Dispersion

Quality of nanoparticle dispersion has been assessed by visual observation—with the aid of SEM and TEM—for some time. The determination of the dispersion quality is usually based on the size of aggregates or how separated or de-bundled the nanoparticles are. Subjective judgment is usually involved in this visual assessment, which can lead to inconsistent results. This also makes comparison of nanoparticle dispersion difficult to conduct. In recent years, methods to quantify nanoparticle dispersion have been developed [2-8]. However, as commented by Haslam *et al*. [7], existing methods with different levels of sophistication for quantifying carbon nanotubes dispersion are limited by their accuracy, complexity of implementation, and scalability. Also, some of these methods fail to take dispersion and agglomeration into account separately. More importantly, the quantitative technique should be simple, non-subjective and be implementable in engineering practice.

Luo and Koo [8] proposed to measure the free-path spacing between particles and agglomeration to quantify the dispersion. The dispersion grade is higher when the spacing between particles is more uniform. The analysis in this section is based on Luo and Koo's method with modification and simplification. Note that development of nanoparticle quantification is not within the scope in this study. Also, since microscopy images were obtained in an earlier stage of the study, before effort was made in quantifying nanoparticles dispersion, results may be affected by a lack of an objective and systematic way in acquiring images.

In this method, random lines are placed on microscopy images intercepting nanoparticles. Free-path spacing is measured between surfaces of nanoparticles tracing along these lines. The spacing is counted as zero if two particles attach together on the line. Figure 4.24 shows an illustration of how the free-path spacing is measured [8]. In real practice, in order to avoid subjective placement of lines on the images, a grid of horizontal and vertical lines are set prior to the quantification process. Then the same grid is placed on every TEM images used in the quantification analysis.

Distributions of free-path spacing of different CE-MWNT polymer nanocomposite samples are shown from Figures 4.25 to 4.34. For measurements ≤100nm, free-path spacing is grouped in 5nm-bins between 0 and 100nm, while for those greater than 100nm it is grouped in 100nm-bins between 100 and 400nm. These bin sizes were chosen because (1) the average diameter of MWNT-5 is 10-15nm [9], and (2) spacing of 100nm or longer approaches the size of aggregates.

All distributions are bimodal. The first peak reflects the distribution inside the aggregates with shorter spacing, while the second one indicates the distribution of those aggregates with larger spacing. It is consistent in all cases that the peak of the first mode appears at 10nm or below. Also taking the average diameter of MWNT-5 into account, the spacing of less than 10nm indicates nanotubes that are connected with each other or in very close proximity, which is not preferred in good and uniform dispersion of

nanoparticles. Therefore, the distribution of the free-path spacing, as well as the average of it, between 10 and 100nm should reflect how de-bundled the aggregates in the resin matrix are. The frequency of the second mode indicates the distance between aggregates or the size of the pure resin area. Therefore, in order to achieve the best dispersion (most uniform distribution) of MWNTs, processing techniques should minimize the first mode between 0 and 10nm (breaking apart the connecting/entangling MWNTs in aggregates) and the second mode beyond 100nm (reducing pure resin areas). These distribution essentially quantifies how de-bundled or separated the MWNTs are. Note that TEM images rather than SEM images should be used for this purpose since only the MWNTs on/close to the surface of the specimens are observed from the SEM images using the secondary electron signals. Therefore, MWNTs in larger depth may be veiled and not be taken into consideration for the dispersion quantification using SEM images. On the contrary, TEM images obtained using transmission electron signals can reveal MWNTs through the whole depth (70μm) of the specimens. Figure 4.35 show a SEM image and a TEM image of the same location of a specimen. They show that different amounts of MWNTs are observed on the same spots, as shown in circled area (a), (b), and (c). Therefore, quantification of de-bundling should be based on TEM images. However, SEM images are still useful since a much larger area of the specimens can be seen in SEM than in TEM. Aggregate sizes can be better estimated/measured using SEM images. Table 4.2 shows the distribution frequency and average spacing of MWNTs measured from TEM images while Table 4.3 shows aggregates sizes/diameters measured from the aggregates observed on the SEM images.

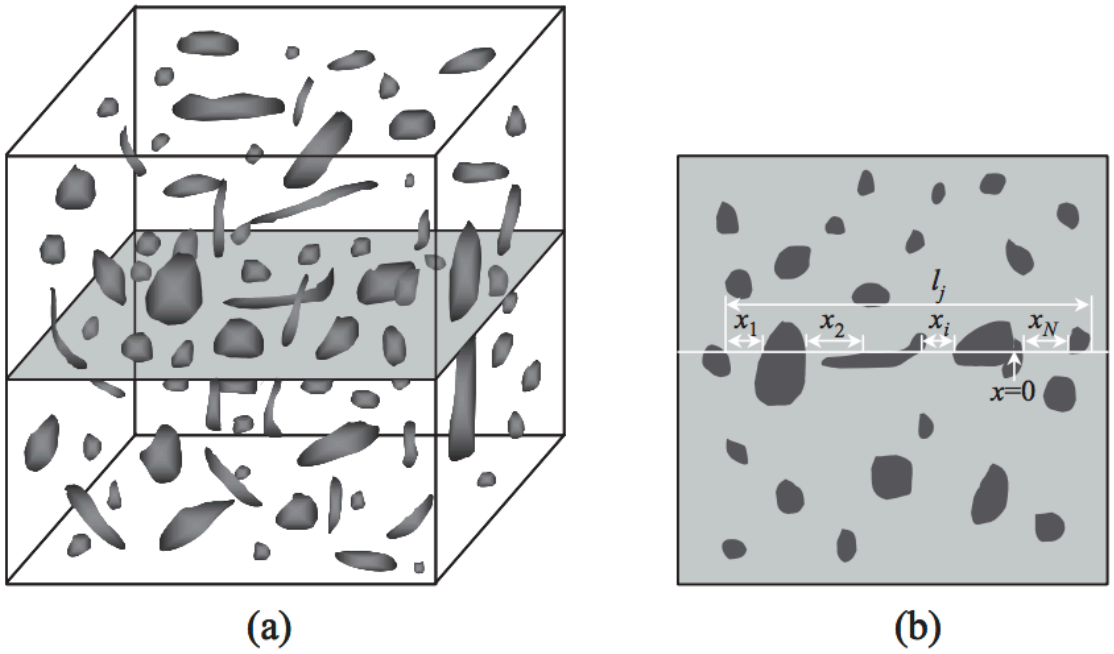

Figure 4.24. Method of measuring the free-path spacing suggested by Luo and Koo [8]. (a) Irregular particles (dark) in a solid matrix; (b) Free-path spacing x between particles surfaces as seen on a two-dimensional cross section of the solid specimen.

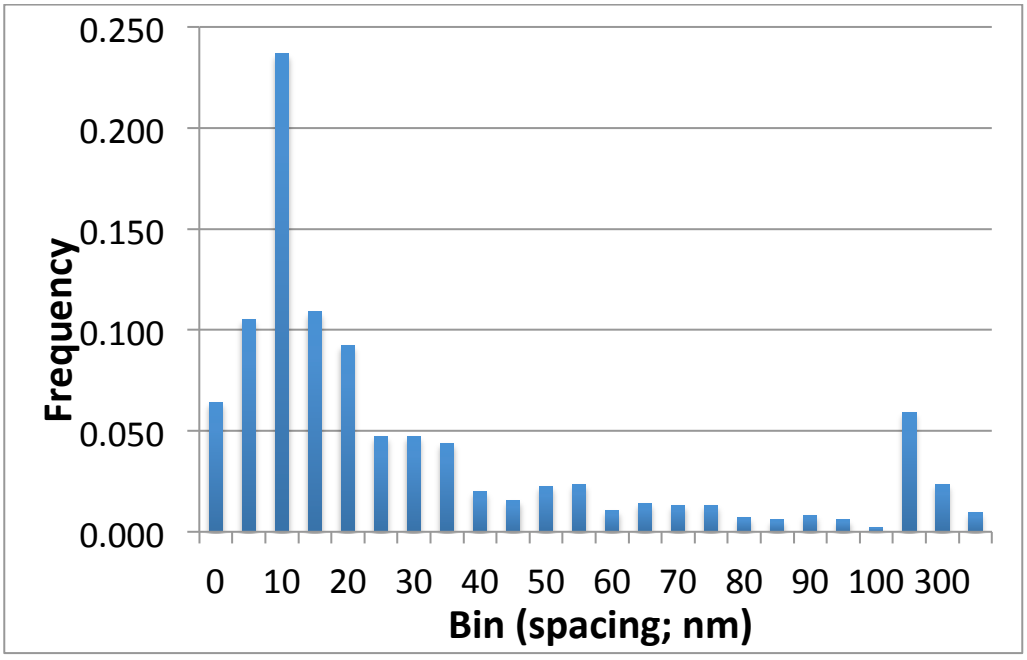

Figure 4.25. Distribution of MWNT spacing of CE-MWNT-5 processed by ultrasonication. Data collected from TEM images (*Total number of MWNT spacing readings* N=1000).

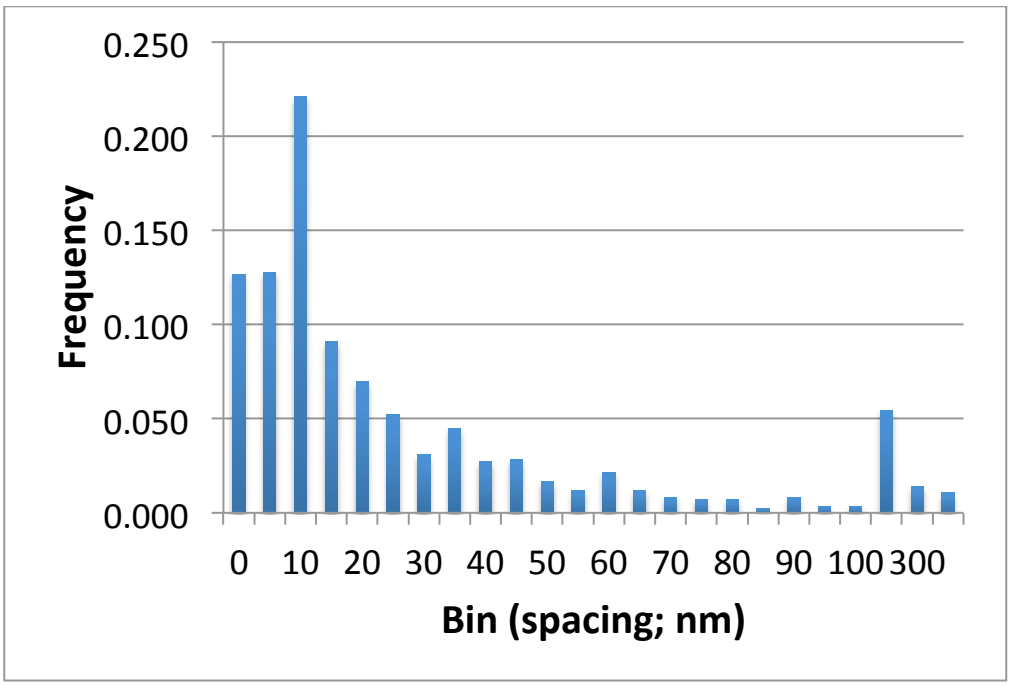

Figure 4.26. Distribution of MWNT spacing of CE-MWNT-5 processed by stand mixer. Data collected from TEM images (*Total number of MWNT spacing readings* N=1000)

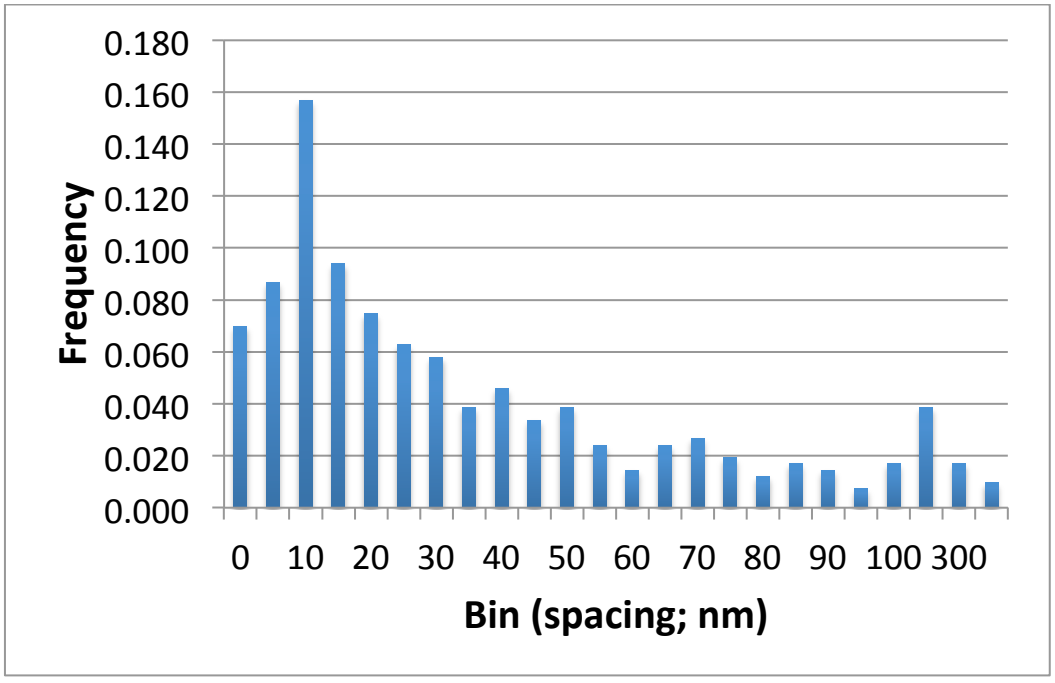

Figure 4.27. Distribution of MWNT spacing of CE-MWNT-5-OH processed by stand mixer. Data collected from TEM images (*Total number of MWNT spacing readings* N=1000).

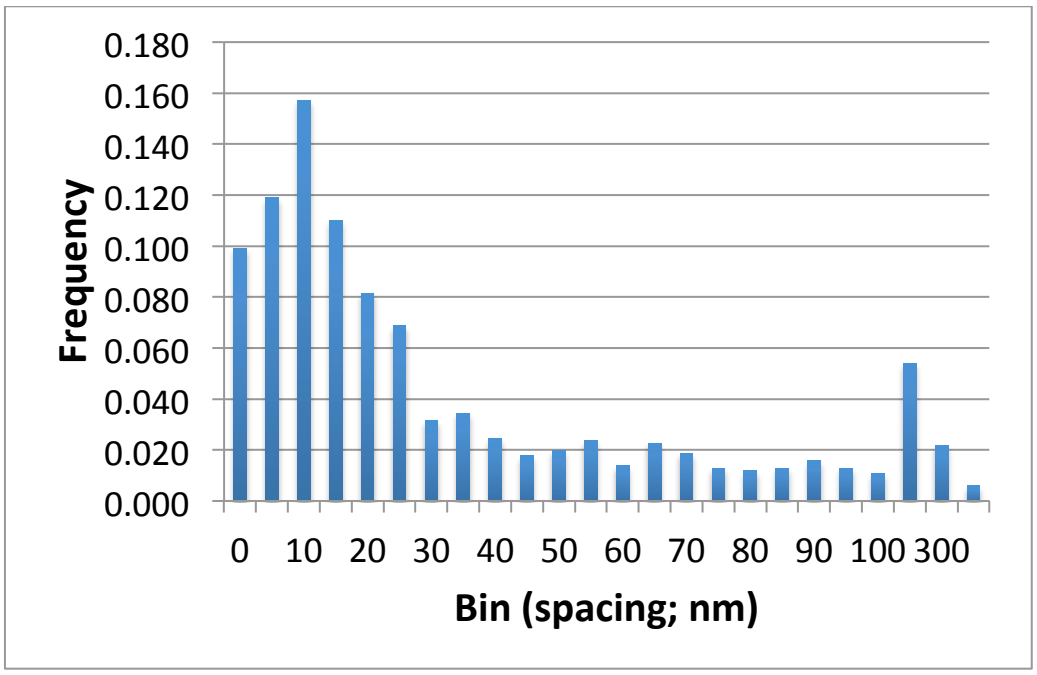

Figure 4.28. Distribution of MWNT spacing of CE-MWNT-5-NH2 processed by stand mixer. Data collected from TEM images (*Total number of MWNT spacing readings* N=800).

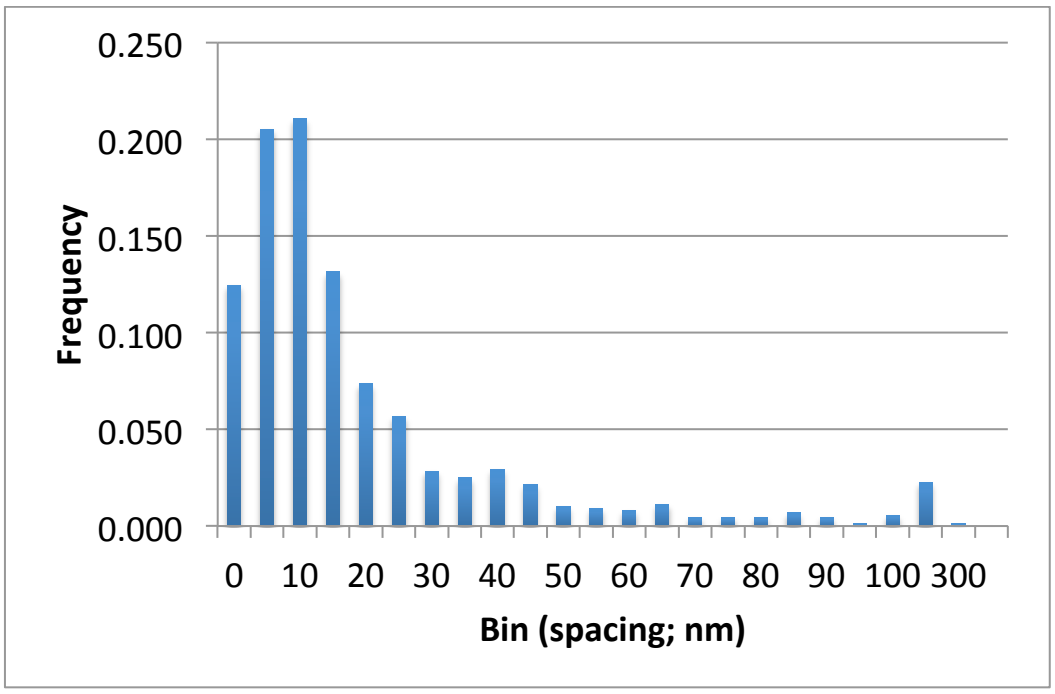

Figure 4.29. Distribution of MWNT spacing of CE-MWNT-5 processed by centrifugal and planetary mixer. Data collected from TEM images (*Total number of MWNT spacing readings* N=1000).

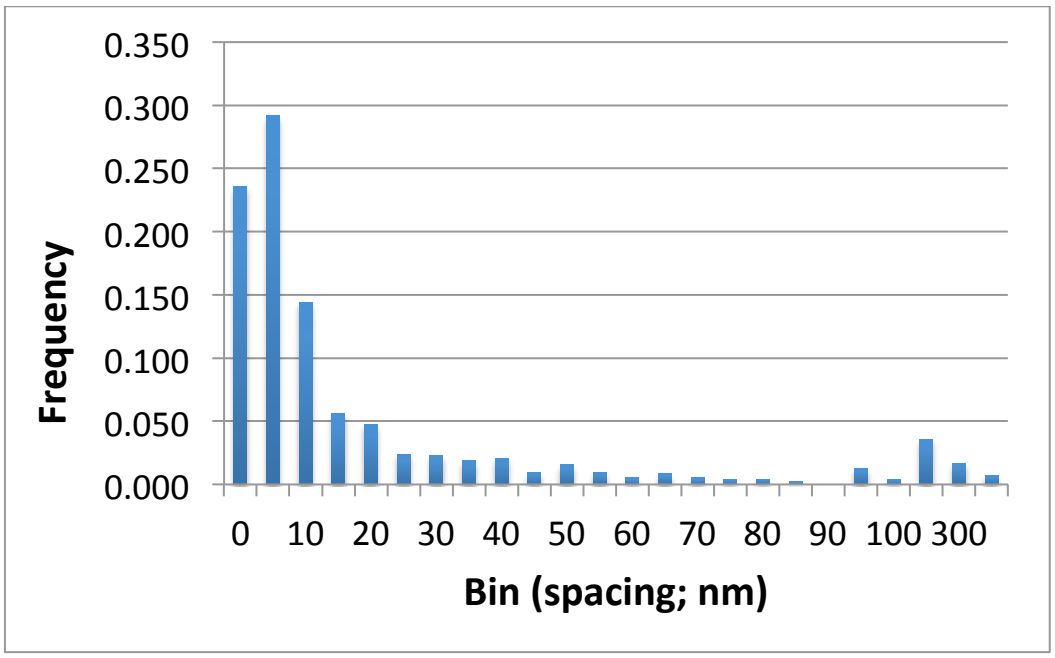

Figure 4.30. Distribution of MWNT spacing of CE-MWNT-5 processed by high shear colloid mill with MK module. Data collected from TEM images (*Total number of MWNT spacing readings* N=900).

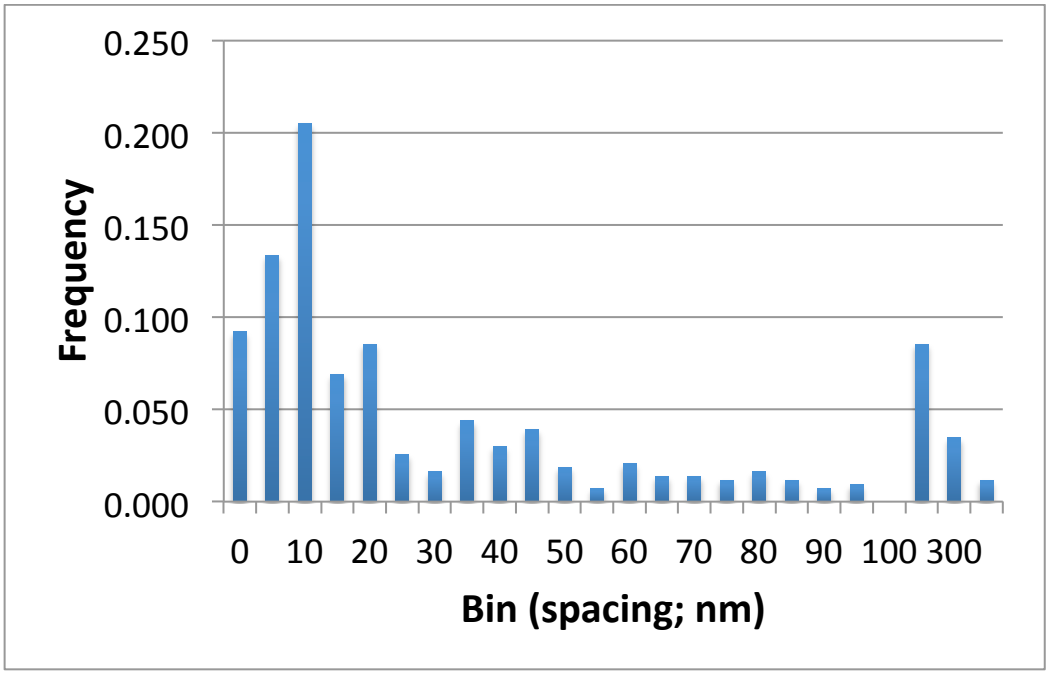

Figure 4.31. Distribution of MWNT spacing of CE-MWNT-5 processed by three-roll mill. Data collected from TEM images (*Total number of MWNT spacing readings* N=1000).

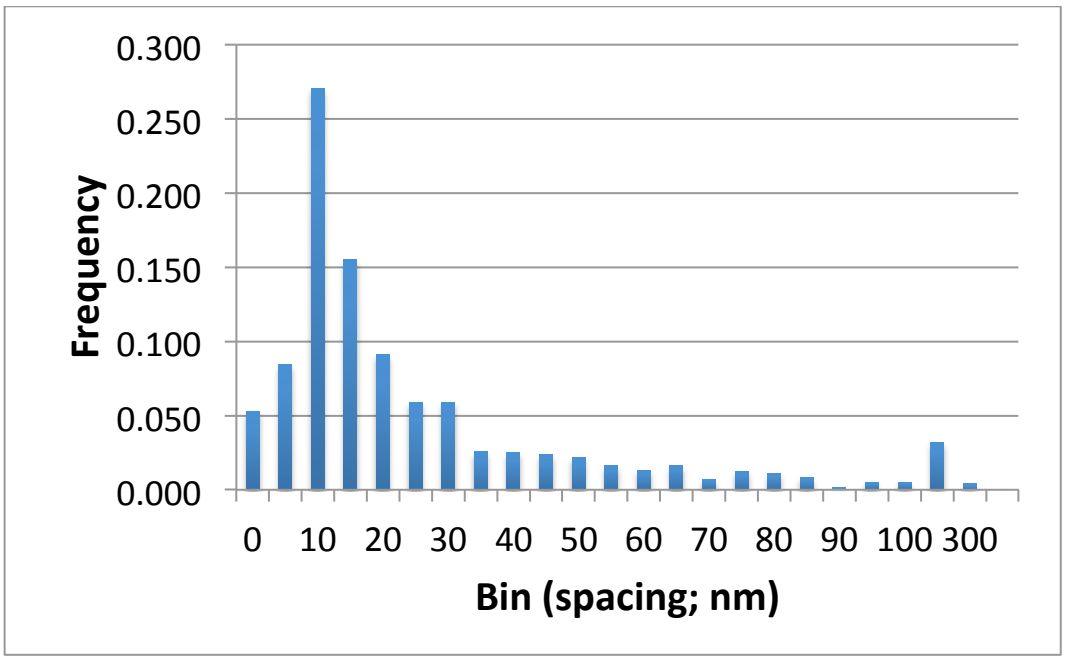

Figure 4.32. Distribution of MWNT spacing of CE-MWNT-5 + 3wt%CA1 processed by stand mixer. Data collected from TEM images (*Total number of MWNT spacing readings* N=1000).

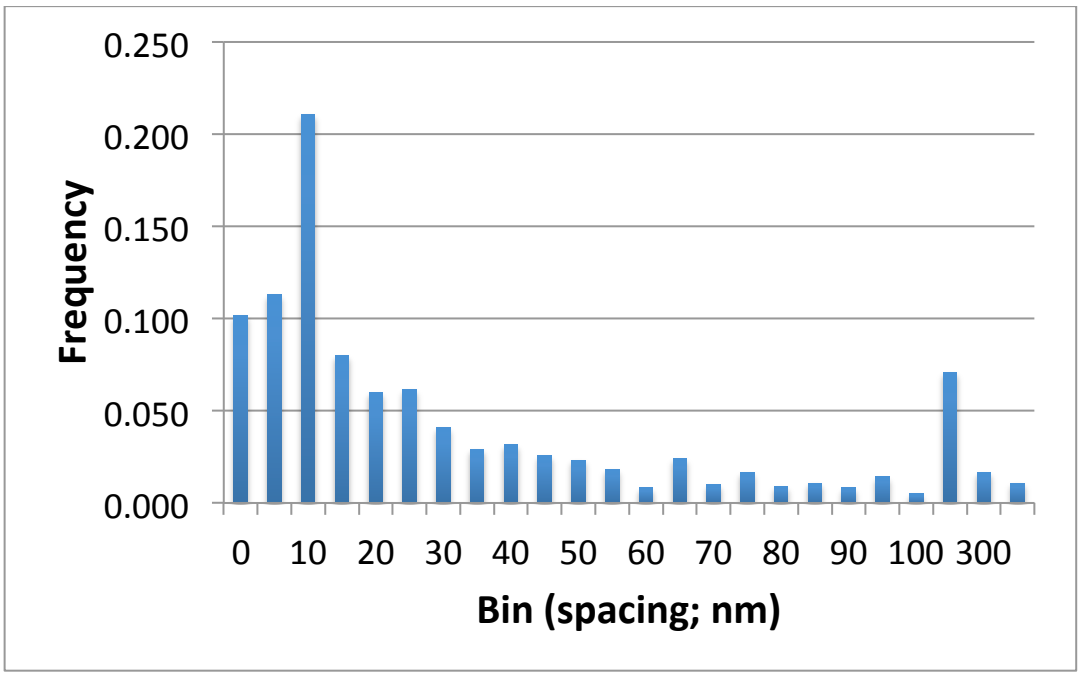

Figure 4.33. Distribution of MWNT spacing of CE-MWNT-5 + 3wt%CA1 processed by high shear colloid mill with MK module. Data collected from TEM images (*Total number of MWNT spacing readings* N=1000).

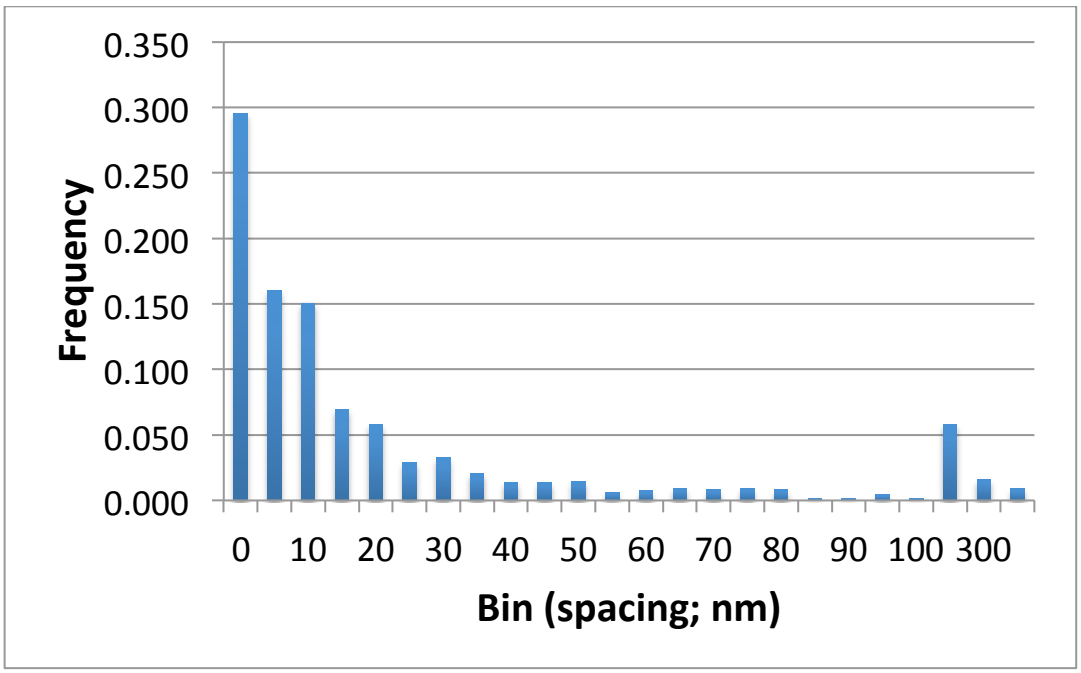

Figure 4.34. Distribution of MWNT spacing of CE-MWNT-5 + 3wt%CA1 processed by high shear colloid mill with DR module. Data collected from TEM images (*Total number of MWNT spacing readings* N=900).

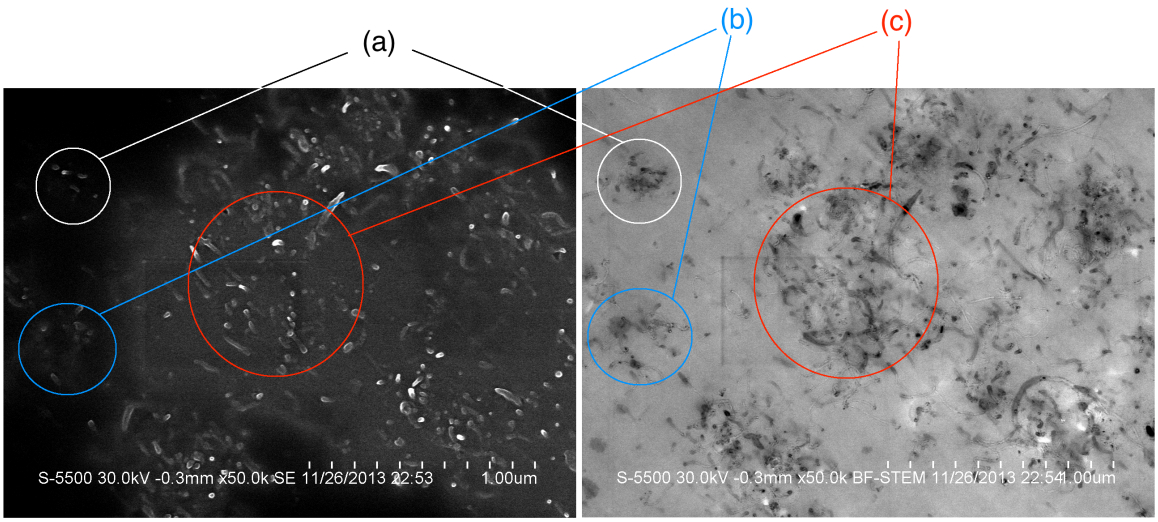

Figure 4.35. SEM (left) and TEM (right) images of same location of CE-MWNT-5 processed by ultrasonication. On the SEM image, only MWNTs on/close to the surface are observed while on the TEM image, MWNTs through the whole depth of the specimen are observed. Examples are shown as circled area (a), (b), and (c) (length bar: 1μm).

Table 4.2 MWNT Free-Path Spacing Distribution in CE-0.5%MWNT-5 Polymer Nanocomposites. Data collected from TEM images.

Sample		Processing Technique	MWNT Spacing Distribution Frequency (%)		$\bar{x}$ (σ) MWNT Spacing for data between 10-100nm
MWNT	Fe^{3+} or CA		(0-10nm)	(10-100nm)	
MWNT-5	200ppm Fe^{3+}	Ultrasonication	41	50	32 (21)
MWNT-5	200ppm Fe^{3+}	Planetary	54	44	29 (20)
MWNT-5	200ppm Fe^{3+}	Stand mixer	48	45	33 (21)
MWNT-5	200ppm Fe^{3+}	Three-roll mill	43	44	37 (20)
MWNT-5	200ppm Fe^{3+}	High shear (MK)	67	27	34 (23)
MWNT-5-OH	200ppm Fe^{3+}	Stand mixer	31	62	37 (24)
MWNT-5-NH_2	200ppm Fe^{3+}	Stand mixer	38	54	35 (25)
MWNT-5	3% CA1	Stand mixer	41	55	30 (21)
MWNT-5	3% CA1	High shear (MK)	43	48	37 (24)
MWNT-5	3% CA1	High shear (DR)	61	31	32 (21)

Number of MWNT spacing readings per sample type, N = 800-1000

Table 4.3 MWNT Aggregates Sizes in CE-0.5%MWNT-5 Polymer Nanocomposites. Data collected from SEM images.

Sample		Processing Technique	MWNT Aggregate Sizes (nm)			
MWNT	Fe^{3+} or CA		$\bar{x}$	σ	Min	Max
MWNT-5	200ppm Fe^{3+}	Ultrasonication	1,100	2,100	83	9,800
MWNT-5	200ppm Fe^{3+}	Planetary	1,200	1,200	160	7,200
MWNT-5	200ppm Fe^{3+}	Stand mixer	1,100	860	160	4,900
MWNT-5	200ppm Fe^{3+}	Three-roll mill	290	190	68	1,200
MWNT-5	200ppm Fe^{3+}	High shear (MK)	1,100	900	95	3,900
MWNT-5-OH	200ppm Fe^{3+}	Stand mixer	1,100	700	31	3,400
MWNT-5-NH_2	200ppm Fe^{3+}	Stand mixer	950	1,000	140	4,900
MWNT-5	3% CA1	Stand mixer	970	780	110	3,900
MWNT-5	3% CA1	High shear (MK)	1,300	780	86	4,100
MWNT-5	3% CA1	High shear (DR)	1,400	840	180	4,300

Number of aggregate size readings per sample type, N = 50-100

Degree of Debundling

Based on the MWNT spacing distribution frequency and the average spacing within the aggregates of CE-0.5%MWNT-5 processed by different techniques between 10 and 100nm, it shows that the aggregates processed by ultrasonication are the most de-bundled among the five processing techniques. Stand mixer, planetary mixer and three-roll mill have the similar level of de-bundling, while the high shear mixer (MK module) is the least de-bundled. When CA1 is used, the spacing distribution frequency increases, with both stand mixer and high shear mixer (MK module).

Size of Aggregates in Processed Composites

Among the five processing techniques, planetary centrifugal mixer yields the largest average aggregate size, while the three-roll mill results in the smallest. The latter could be due to the small gap size (5μm) between rollers that broke down the MWNT aggregates. Although the average aggregate sizes for the other four techniques are similar, there is a huge deviation in aggregate sizes by the ultrasonication with the largest aggregates observed over 9 μm (via SEM). This suggests that ultrasonication is able to de-bundle the MWNT aggregates better than the other techniques (as reflected in its greater MWNT spacing distribution frequency) but fails to break down the aggregates into smaller size.

Effects of MWNT Functionalization and Coupling Agents

Surprisingly, the samples with MWNT-5-OH and MWNT-5-NH_2 processed by the stand mixer have wider MWNT spacing distribution frequency than the one with neat MWNT-5. This suggests that MWNT functionalization may have some small beneficial effect on MWNT dispersion. The incorporation of CA1 increases the spacing distribution frequency and decreases the average and maximum aggregate size at the same time (as

shown in the samples processed by the stand mixer). Therefore, CA1 is beneficial to the dispersion using stand mixer.

Lingering Issues Regarding Qualifying and Quantifying MWNT Dispersion

In spite of best efforts to apply this method, there remains an inconsistency between the visual observation and the dispersion quantification based on the electron microscopy images. It could be due to the subjective judgment during image acquisition and/or visual qualitative observation. Moreover, human errors as well as resolution of the images also affect the value obtained by the quantification method. Further work may be needed for better investigation with a better and objective method in image acquisition in both lower and higher magnifications.

DYNAMIC MECHANICAL ANALYSIS

Figures 4.36 through 4.41 present results of DMA tests on CE-MWNT polymer nanocomposite samples. The measured glass transition temperatures are shown in Table 4.4, while storage moduli at different temperatures are shown in Table 4.5. It was observed that both the catalyst and coupling agents had detrimental effects on the mechanical properties and glass transition temperatures of the CE-MWNT nanocomposites. The addition of catalyst lowered the glass transition temperature of the neat CE by 16% (200ppm Fe^{3+}) and 19% (250ppm Fe^{3+}), while the KZ-TPP (CA1) and NZ97 (CA2) coupling agents decreased the glass transition temperature by 10% and 23%, respectively. The storage modulus of the CE-0.5%MWNT-5 sample processed by the planetary mixer is lower (~10%) than that of the neat CE and the sample processed by the three-roll mill, while the one processed by ultrasonication has a significantly lower (~33%) storage modulus. This observation is consistent with the degree of nanotube dispersion in the resin. However, the glass transition temperature is not affected by the

mixing methods (differences were less than 2%). Moreover, different weight loadings of well-dispersed nanotubes (as shown in Figure 4.36) do not have significant effects on either the storage modulus or glass transition temperature. The hump of CA-2 storage modulus is believed to be due to a lower polymer conversion than other samples. The storage modulus decreases initially but while it is heated in the DMA the polymer conversion results in increasing the storage modulus to its fully-cured value.

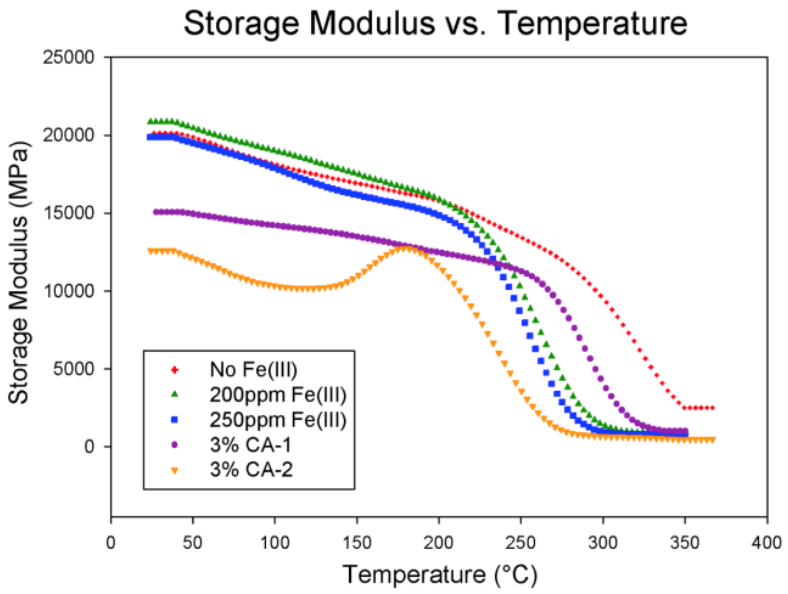

Figure 4.36. Storage moduli of CE modified with Fe^{3+} catalyst (200 or 250 ppm) or coupling agents (CA-1 or CA-2). Data for neat CE shown for comparison.

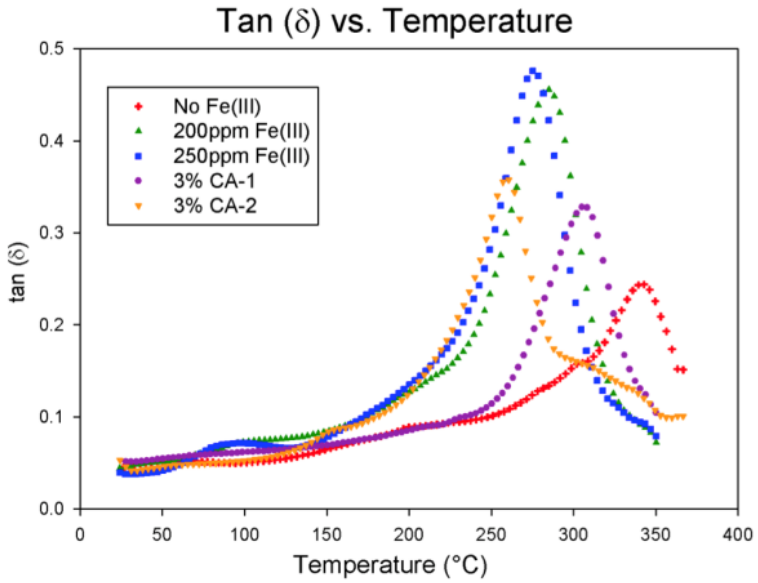

Figure 4.37. Tangent of the Phase Angle Delta (δ) of CE modified with Fe^{3+} catalyst (200 or 250 ppm) or coupling agents (CA-1 or CA-2). Data for neat CE shown for comparison.

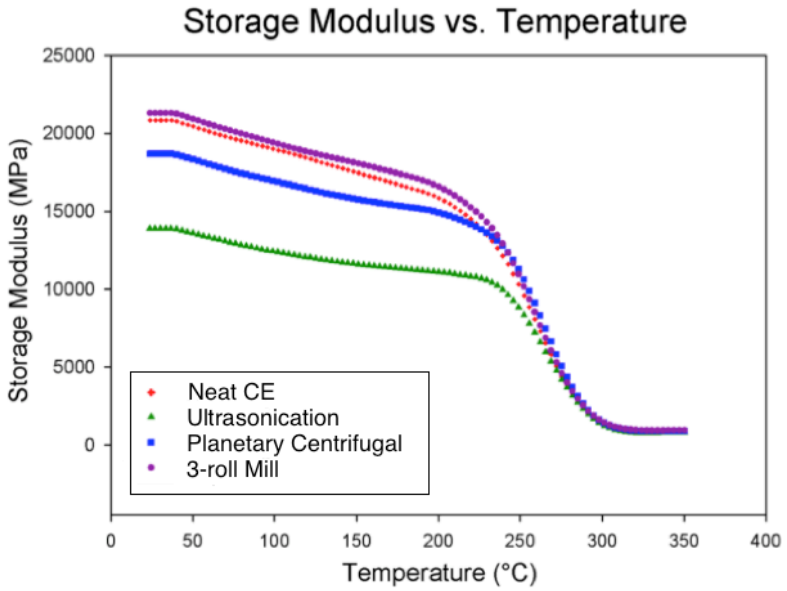

Figure 4.38. Storage moduli of CE-0.5%MWNT-5 (with 200ppm Fe^{3+} catalyst) processed by three different techniques. Data for neat CE shown for comparison.

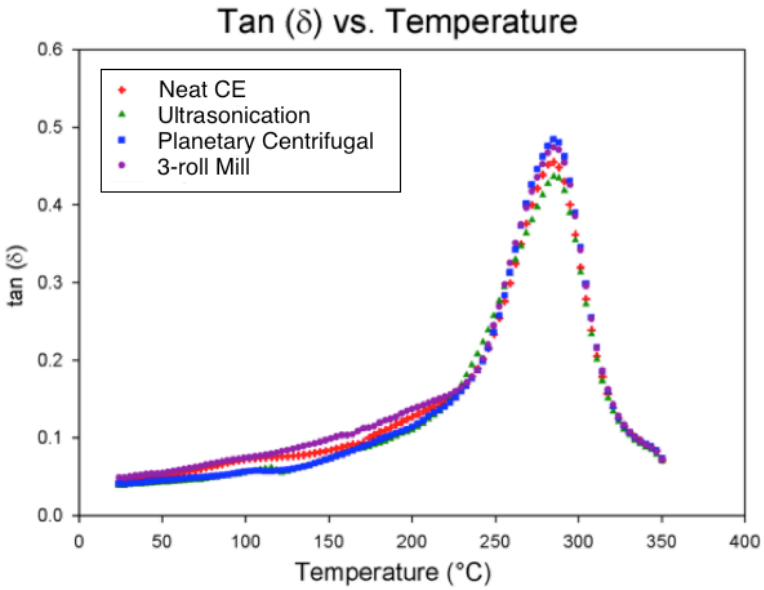

Figure 4.39. Tangent of the Phase Angle Delta (δ) of CE-0.5%MWNT-5 (with 200ppm Fe^{3+} catalyst) processed by three different techniques. Data for neat CE shown for comparison.

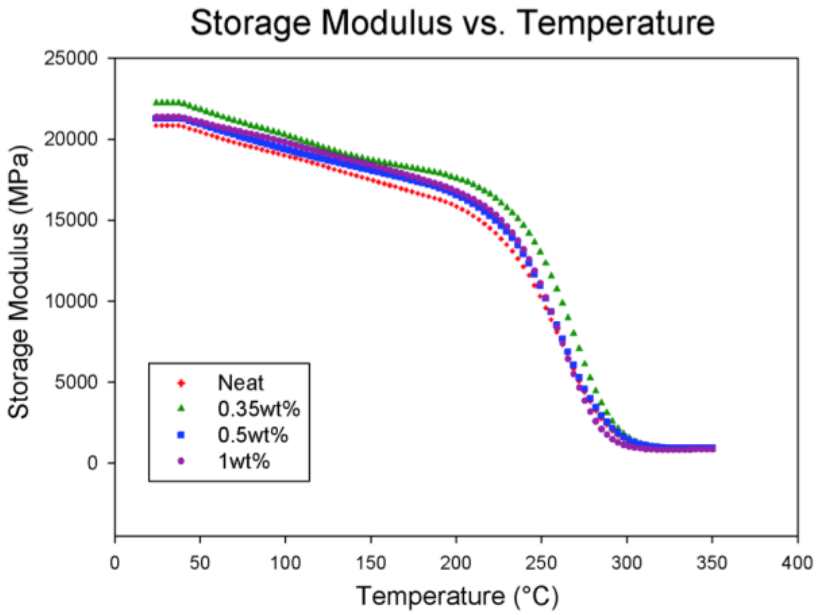

Figure 4.40. Storage moduli of CE-0.5%MWNT-5 (with 200ppm Fe^{3+} catalyst) processed by three-roll mill. Data for neat CE shown for comparison.

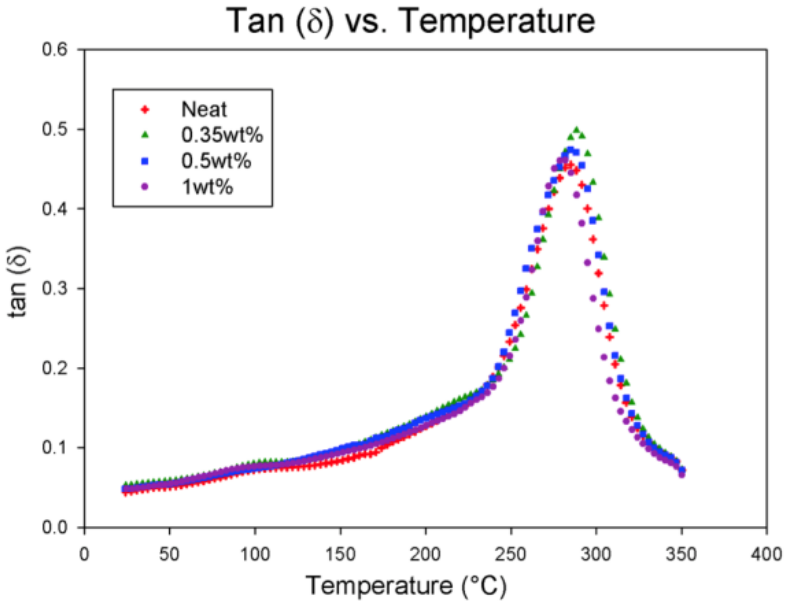

Figure 4.41. Tangent of the Phase Angle Delta (δ) of CE-0.5%MWNT-5 (with 200ppm Fe^{3+} catalyst) processed by three-roll mill. Data for neat CE shown for comparison.

Table 4.4. Glass Transition Temperatures of CE-MWNT-5 Polymer Nanocomposites

Sample				**T_g (°C)**	
MWNT-5 (wt%)	**Fe^{3+} (ppm)**	**CA (wt%)**	**Processing Technique**	**$\bar{x}$**	**σ**
0	---	---	---	339	5
0	200	---	---	284	2
0	250	---	---	276	5
0	---	CA1 (3wt%)	---	306	1
0	---	CA2 (3wt%)	---	259	2
0	200	---	---	284	2
0.5	200	---	Ultrasonication	290	2
0.5	200	---	Planetary Centrifugal	286	1
0.5	200	---	Three-roll Mill	284	2
0	200	---	---	284	2
0.35	200	---	Three-roll Mill	288	1
0.5	200	---	Three-roll Mill	284	2
1	200	---	Three-roll Mill	281	2

Number of glass transition temperature samples per nanocomposite type, N = 3

Table 4.5. Storage Modulus of CE-MWNT-5 Polymer Nanocomposites

Sample				Storage Modulus (x1000 MPa)					
MWNT-5 (wt%)	Fe^{3+} (ppm)	CA (wt%)	Processing Technique	at 50°C		at 100°C		at 200°C	
				$\bar{x}$	σ	$\bar{x}$	σ	$\bar{x}$	σ
0	---	---	---	19.9	0.7	18.1	0.6	17.3	0.6
0	200	---	---	20.9	0.5	19.5	0.6	17.0	0.5
0	250	---	---	19.5	0.6	17.9	0.5	16.9	0.6
0	---	CA1 (3wt%)	---	12.5	0.5	10.3	0.4	12.7	0.4
0	---	CA2 (3wt%)	---	15.0	0.4	14.2	0.4	13.4	0.4
0	200	---	---	20.9	0.5	19.5	0.6	17.0	0.5
0.5	200	---	Ultra-sonication	13.6	0.4	12.4	0.4	11.5	0.5
0.5	200	---	Planetary Centrifugal	18.3	0.6	16.9	0.4	15.9	0.4
0.5	200	---	Three-roll Mill	21.4	0.7	19.9	0.4	18.0	0.5
0	200	---	---	20.9	0.5	19.5	0.6	17.0	0.5
0.35	200	---	Three-roll Mill	21.8	0.6	20.2	0.6	18.2	0.5
0.5	200	---	Three-roll Mill	21.4	0.7	19.9	0.4	18.0	0.5
1	200	---	Three-roll Mill	21.4	0.5	20.0	0.8	18.0	0.6

Number of storage modulus samples per nanocomposite type, N = 3

THERMAL STABILITY

Thermogravimetric analysis (TGA) was performed on different samples. They were heated to 900°C at 10°C/min in air.

Figure 4.42 and Table 4.6 show the TGA curves and decomposition temperatures, respectively, of CE-0.5%MWNT-5 nanocomposites processed by different techniques. The decomposition temperature at 10% mass loss ($T_{10\%}$) is unaffected by the mixing techniques (less than a 2% difference), while the decomposition temperature at 50% mass loss ($T_{50\%}$) shows a slightly larger difference. The $T_{50\%}$ of the sample processed by the high shear mixer is higher than the neat CE while all the others are lower. As the

differences are small (< 5%), the effects of processing are insignificant and could be due to random error.

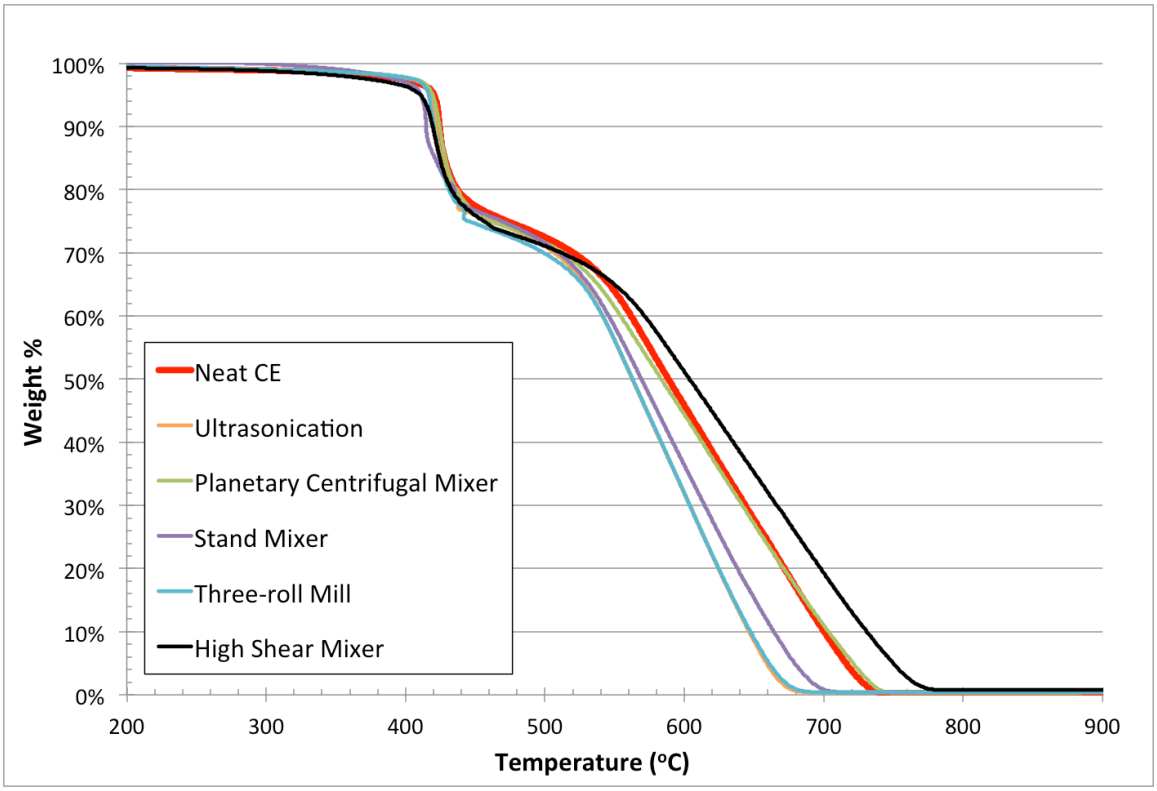

Figure 4.42. TGA of CE-0.5%MWNT-5 (with 200ppm Fe^{3+} catalyst) polymer nanocomposites processed by five different techniques. Samples were heated 10°C/min in air. Data for neat CE shown for comparison. (*Number of samples per processing technique, N = 1)*

Table 4.6 Decomposition Temperature of CE-0.5%MWNT-5 (with 200ppm Fe^{3+} catalyst) polymer nanocomposites processed by five different techniques. Samples were heated 10°C/min in air. Data for neat CE shown for comparison

Processing Technique	$T_{10\%}$ at 10% Mass Loss		$T_{50\%}$ at 50% Mass Loss	
	$T_{10\%}$ (°C)	Δ (%)	$T_{50\%}$ (°C)	Δ (%)
Neat CE	424	--	585	--
Ultrasonication	422	0	562	-4
Planetary Centrifugal	424	0	582	-1
Stand Mixer	415	-2	568	-3
Three-Roll Mill	420	-1	562	-4
High Shear Mixer	419	-1	602	3

Number of samples per processing technique, N = 1

Figure 4.43 and Table 4.7 show the TGA curve and decomposition temperatures, respectively, of CE-MWNT-5 polymer nanocomposites, with different weight loadings (0.5, 1, 1.5, and 3 wt%) of MWNTs, all processed by the stand mixer. The differences in both $T_{10\%}$ and $T_{50\%}$ for the polymer nanocomposites as comparing to that of the neat CE are small (<3%). Figure 4.44 and Table 4.8 show the TGA curve and decomposition temperatures, respectively, of CE-MWNT-5 polymer nanocomposites with different weight loadings (0.3, 0.5, and 1.5 wt%) of MWNTs processed by the three-roll mill. Similar to what is observed for stand mixer, the differences in both $T_{10\%}$ and $T_{50\%}$ as compared to that of the neat CE resin are not significant. Although, the $T_{50\%}$'s deviate slightly more from that of the neat CE resin as comparing to the stand mixer. In general, for loadings less than 3 wt%, the thermal stability of CE is unaffected by the amount of MWNT. The degree to which higher weight loadings affect the decomposition temperatures remains an open question.

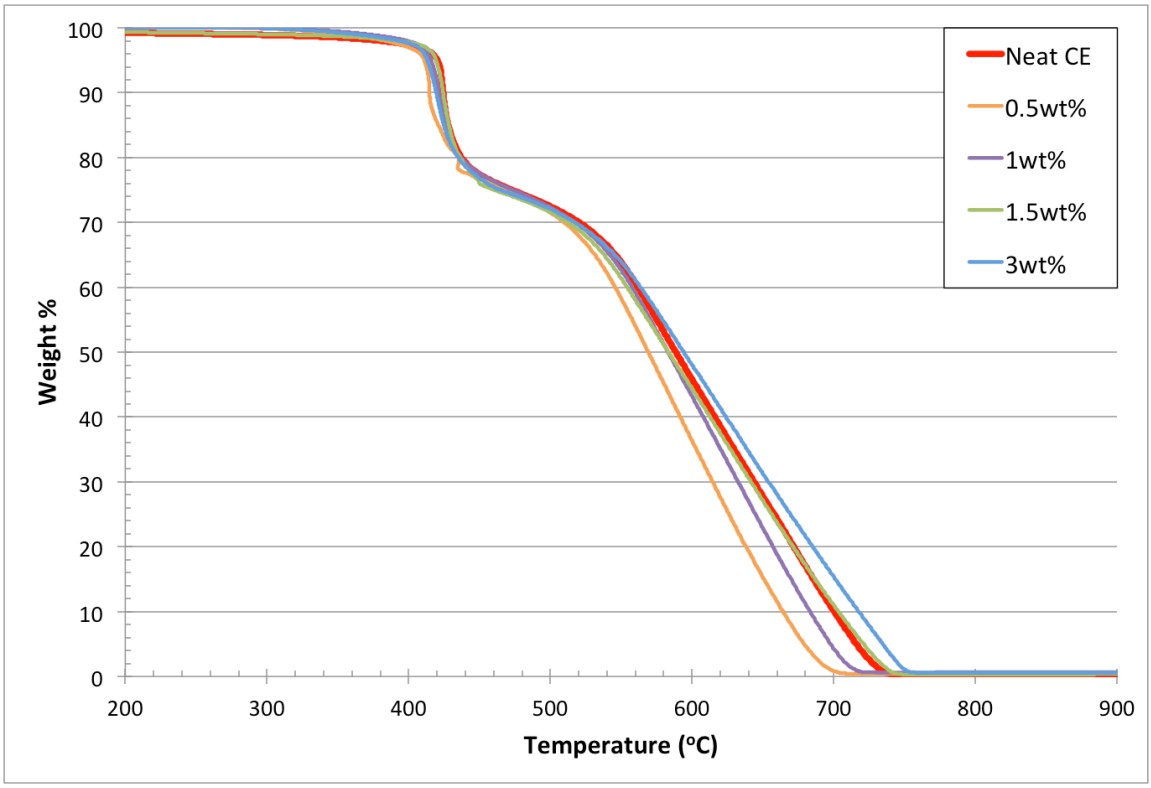

Figure 4.43. TGA of CE-MWNT-5 (with 200ppm Fe^{3+} catalyst) polymer nanocomposites processed by stand mixer. Samples were heated 10°C/min in air. Data for neat CE shown for comparison (*Number of samples per MWNT wt%, N = 1)*.

Table 4.7 Decomposition Temperature of CE-MWNT-5 (with 200ppm Fe^{3+} catalyst) polymer nanocomposites processed by stand mixer. Samples were heated 10°C/min in air. Data for neat CE shown for comparison.

MWNT (wt%)	$T_{10\%}$ at 10% Mass Loss		$T_{50\%}$ at 50% Mass Loss	
	$T_{10\%}$ (°C)	Δ (%)	$T_{50\%}$ (°C)	Δ (%)
Neat CE	424	--	585	--
0.5%	415	-2	568	-3
1%	422	0	583	0
1.5%	426	0	584	0
3%	419	-1	593	1

Number of samples per MWNT wt%, N = 1

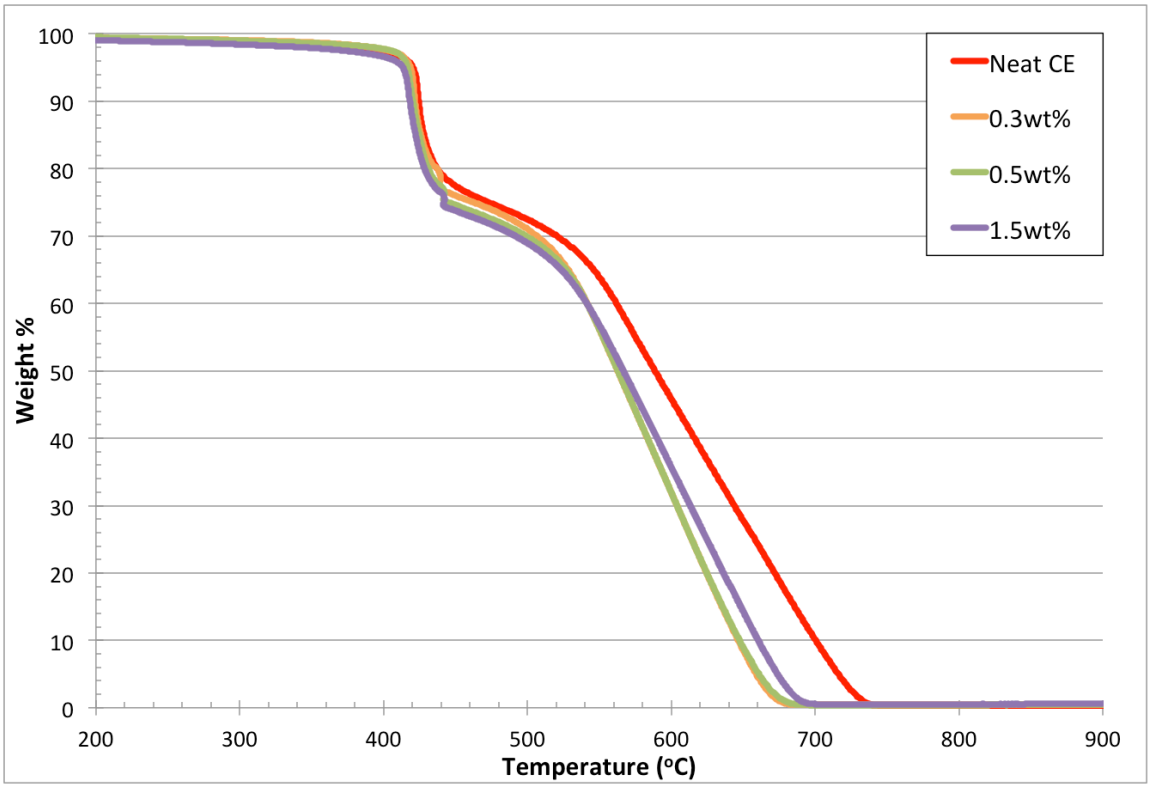

Figure 4.44. TGA of CE-MWNT-5 (with 200ppm Fe^{3+} catalyst) polymer nanocomposites processed by three-roll mill. Samples were heated 10°C/min in air. Data for neat CE shown for comparison (*Number of samples per MWNT wt%, N = 1)*.

Table 4.8 Decomposition Temperature of CE-MWNT-5 (with 200ppm Fe^{3+} catalyst) polymer nanocomposites processed by three-roll mill. Samples were heated 10°C/min in air. Data for neat CE shown for comparison.

MWNT (wt%)	$T_{10\%}$ at 10% Mass Loss		$T_{50\%}$ at 50% Mass Loss	
	$T_{10\%}$ (°C)	Δ (%)	$T_{50\%}$ (°C)	Δ (%)
Neat CE	424	--	585	--
0.3%	422	0	563	-4
0.5%	420	-1	562	-4
1.5%	418	-1	567	-3

Number of samples per MWNT wt%, N = 1

MICROSCALE COMBUSTION CALORIMETRY

The flammability properties of the CE-MWNT polymer nanocomposites were evaluated using microscale combustion calorimetry (MCC). The samples were pyrolyzed in nitrogen from 75 to 900°C. The resulting gaseous particles were combusted in air (20% oxygen) at 950°C. At the same time, the heat release rate (HRR) and peak heat release rate (PHRR) were measured. Figure 4.45 shows the HRR and PHRR of CE cured with either Fe^{3+} catalyst (200 or 250 ppm) or the coupling agent CA-1 as compared to that of neat CE, Neat CE has an excellent inherent flammability property as shown by its relatively low HRR. Moreover, neat CE's PHRR (150W/g) is low as compared to that of polyethylene (7kW/g), ABS (~3kW/g), and PEEK (~0.8kW/g) [10]. Addition of coupling agent CA-1 increases neat CE's PHRR by ~33%, while addition of the Fe^{3+} catalyst (200 or 250 ppm) doubles it. That said, even with these increases, the PHRR still relatively low as compared to other polymer materials, such as those mentioned. Interestingly, the onset temperature (~405°C) is not significantly affected by the modifiers—at least at the concentration levels tested.

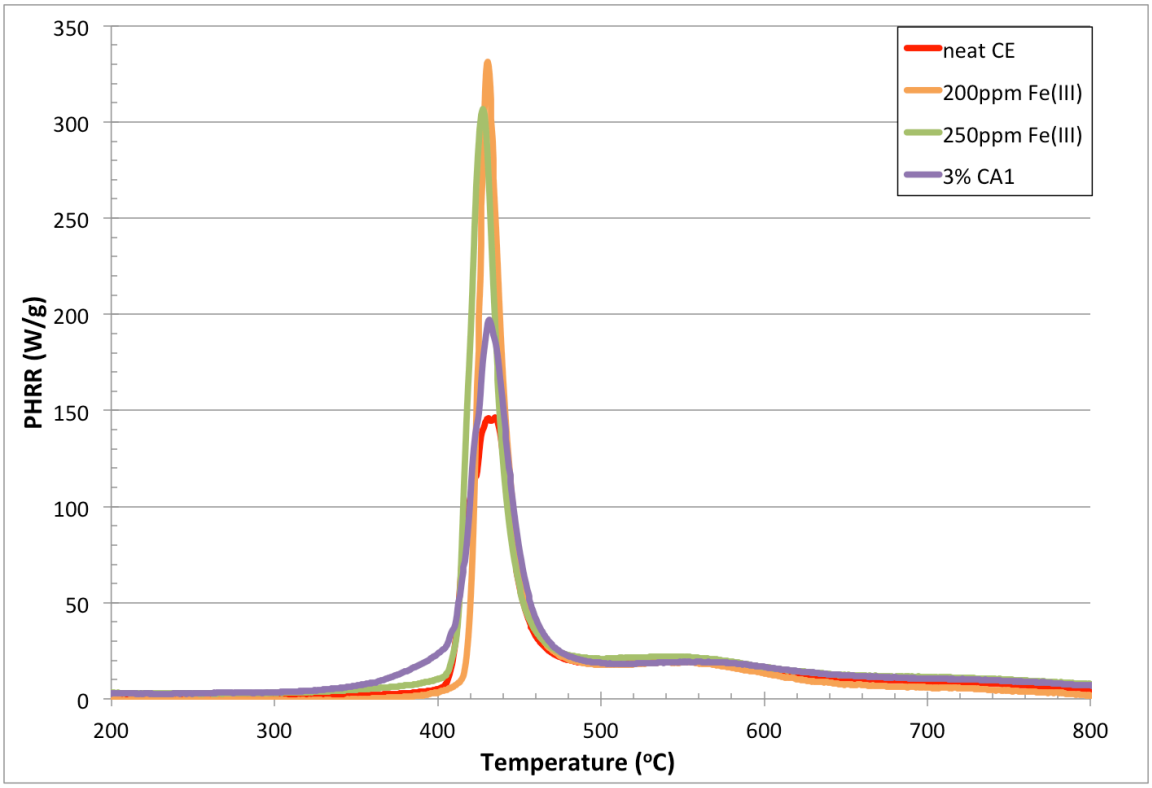

Figure 4.45. Heat Release Rates for CE modified with Fe^{3+} catalyst (200 or 250 ppm) or coupling agent (3% CA-1). Samples were heated 1°C/s in air. Data for neat CE shown for comparison (*Number of samples per resin modifier, N = 1)*.

Figure 4.46 shows the HRR of CE-MWNT nanocomposites processed by different techniques. In general, when the loading of MWNT remains at relatively low level, the PHRR is not affected significantly (<10%). Figure 4.47 shows the HRR of CE-MWNT nanocomposites with various weight loadings (0.3, 0.5, 1, and 1.5 wt%) processed by the three-roll mill and cured with the Fe^{3+} catalyst (200ppm), while Figure 4.48 shows the those processed with CA-1 by the stand mixer. There are no trends observed on the PHRR when the amount of MWNT changes by either processing methods. Note that the onset temperature remains unaffected by mixing techniques or weight loadings of MWNTs.

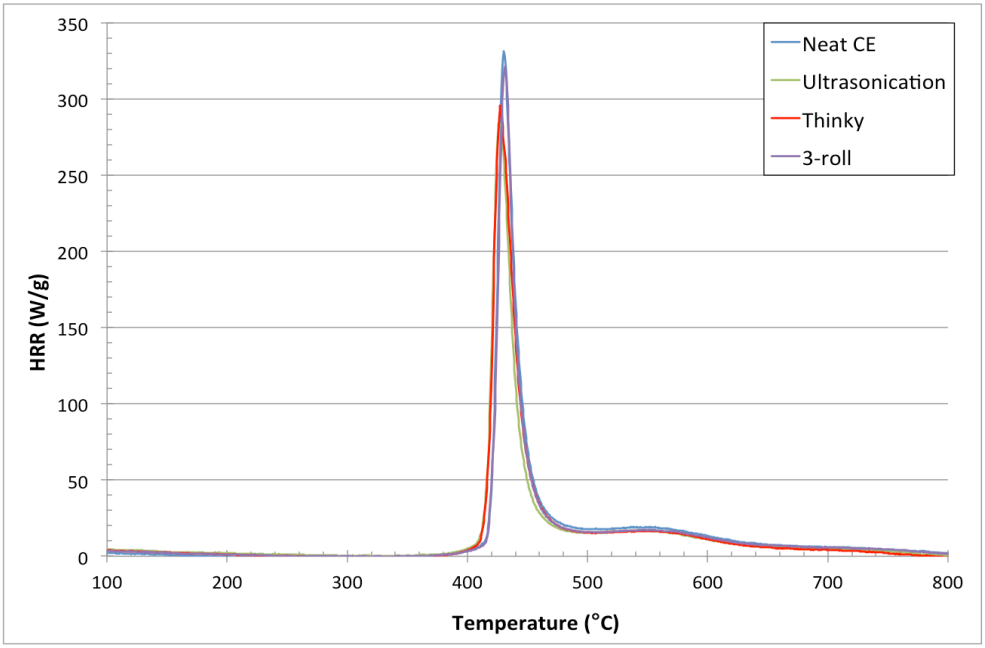

Figure 4.46. Heat Release Rates of CE-0.5%MWNT-5 (with 200ppm Fe^{3+} catalyst) polymer nanocomposites processed by three different techniques. Samples were heated 1°C/s in air. Data for neat CE shown for comparison (*Number of samples per processing technique, N = 1).*

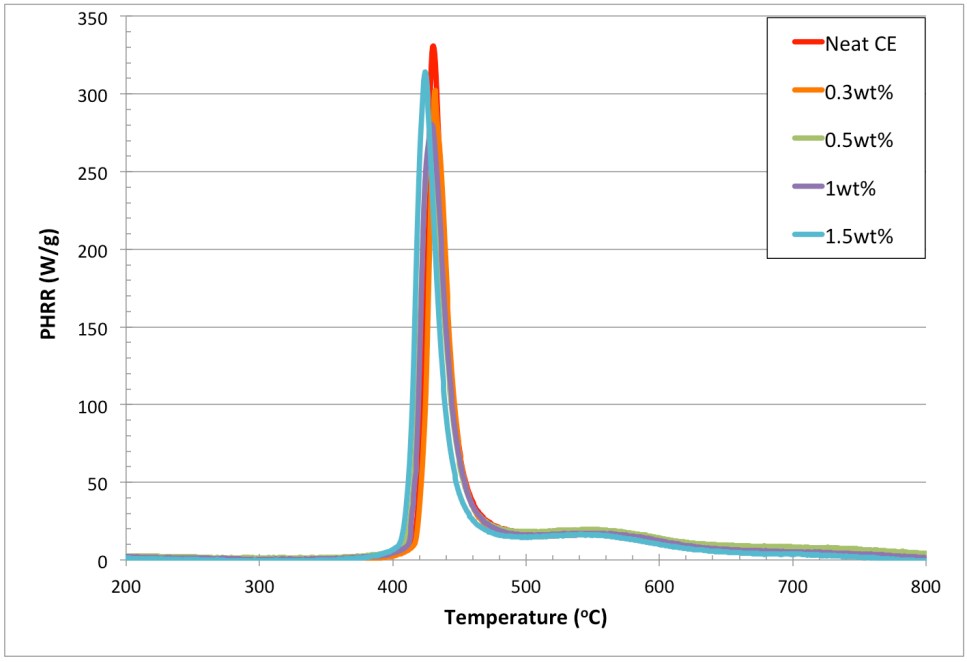

Figure 4.47. Heat Release Rates CE-MWNT-5 (with 200ppm Fe^{3+} catalyst) polymer nanocomposites processed by three-roll mill. Samples were heated 1°C/s in air. Data for neat CE shown for comparison (*Number of samples per MWNT wt%, N = 1).*

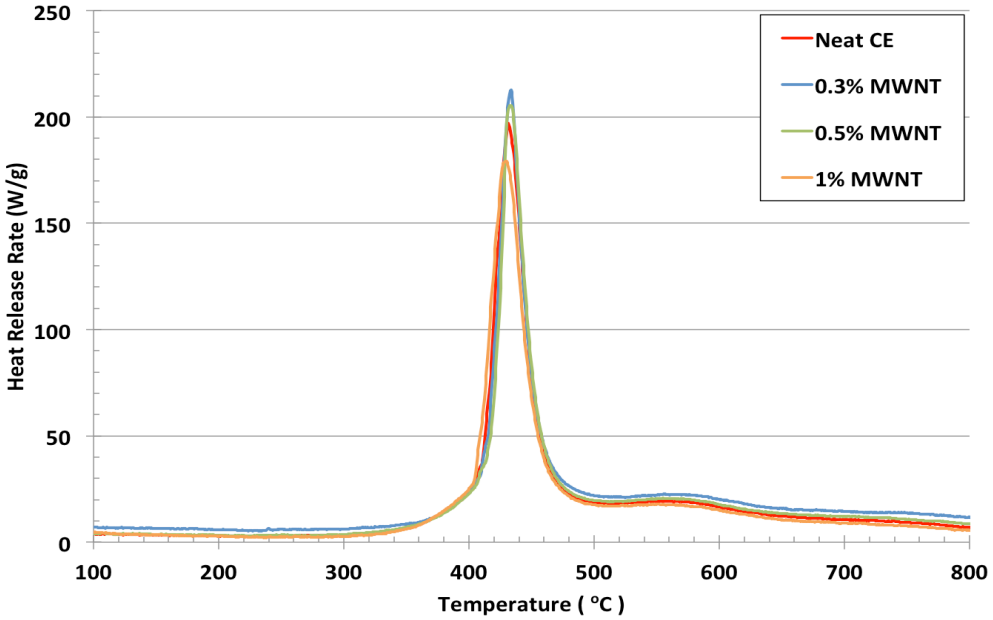

Figure 4.48. Heat Release Rates of CE-MWNT-5 (with 3% CA-1) polymer nanocomposites processed by stand mixer. Samples were heated 1°C/s in air. Data for neat CE shown for comparison (*Number of samples per MWNT wt%, N = 1)*.

ELECTRICAL RESISTIVITY

Neat MWNT-5 was mixed with CE and cured with 200ppm the Fe^{3+} catalyst or coupling agents, CA-1 and CA-2, followed by a post cure at 250°C for 2 hours [11-13]. Specimens of 1mm thick were made for the electrical resistivity measurement.

Figures 4.49 and 4.50 show that the addition via stand mixer of less than 0.5 wt% or 0.3 vol% MWNT lowers the neat CE's electrical resistivity. These measurements reveal that the percolation threshold is around 0.4 wt% or 0.24 vol% and the resistivity reaches a plateau beyond 1 wt% or 0.6 vol%. Furthermore, the electrostatic dissipation (ESD) requirement ($<10^{11}$ohm.cm) [14] is fulfilled by incorporating as little as 0.3 wt% or 0.18 vol% MWNT into the CE matrix. The resulting percolation threshold matches Hu *et al.*'s review [15], which reported other reports of percolation thresholds of 1 wt% multi- or single-wall carbon nanotubes (or below) in other resin systems. Similar

percolation threshold of 1 wt% was reported by Ma *et al*.'s review [16]. In fact, the viscosity of the polymer becomes too high to fabricate void-free polymer nanocomposites when the content of nanotubes is higher than 1 wt%. Therefore, it is crucial to use processing techniques, which can produce polymer MWNT nanocomposites with a percolation threshold below 1 wt%. Among the processing techniques used in this study, stand mixer is able to achieve that.

Interestingly, similar electrical resistivity drops were not seen in samples processed by other techniques—even at the same MWNT weight loadings. For instance, the electrical resistivity of the CE-MWNT nanocomposites is still higher than the ESD requirement at a loading of 1 wt% or 0.6 vol% (Figures 4.51-4.52), although the addition of 1.5 wt% or 0.91 vol% of MWNT lowers the electrical resistivity by about four orders of magnitudes relatively to the 1 wt% or 0.6 vol% sample. While it is likely that the percolation threshold is between 1 and 1.5 wt% of MWNTs, more data points are needed to determine to value. Although the percolation threshold is above 1 wt%, void-free polymer nanocomposites can still be fabricated since air bubbles are removed during the three-roll milling process because of the small gap distance between rollers.

Figure 4.53 compares the electrical resistivity of a CE-0.5%MWNT-5 polymer nanocomposite processed by five different techniques. The electrical resistivities of samples prepared by three-roll mill, ultrasonication, and planetary centrifugal mixer are two orders of magnitude lower than that of, neat CE, but still higher than the ESD requirement. Perplexingly, their readings are about six orders of magnitudes higher than the one processed by the stand mixer. This indicates that the MWNTs in the sample processed by the stand mixer were dispersed and de-bundled enough to form a much better conductive path for the electron to pass through the sample than the other samples, just as Ma *et al*. commented on the conducting behavior of composites consisting of conducting fillers and insulating matrices using percolation theory [16]. Figure 4.54 shows an illustration of the relationship between nanotubes dispersion and electrical

conductivity. In sample with better nanotubes dispersion as shown in Figure 4.54(a), individual de-bundled nanotubes may appear in the polymer matrix uniformly. However, they may be separated that electrons may not have a continuous conductive path to travel through the polymer matrix. On the contrary, as shown in Figure 4.54(b), connected paths may be formed in sample with lower degree of nanotubes dispersion, resulting in higher electrical conductivity.

Figure 4.55 shows that when 1 wt% of CA-1 is used instead of the Fe^{3+} catalyst (200 ppm), the electrical resistivity is the same. However, when higher weight loading (3wt%) of CA-1 is used, the electrical resistivity is two orders of magnitudes higher.

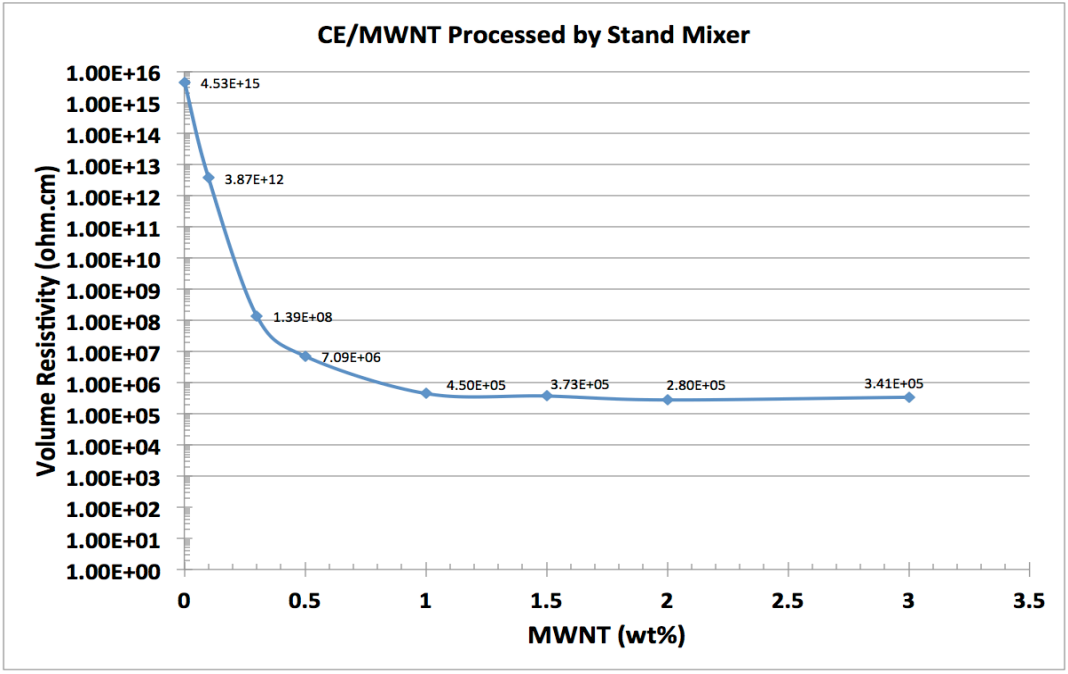

Figure 4.49. Electrical resistivity of CE-MWNT-5 (with 200ppm Fe^{3+} catalyst) polymer nanocomposites processed by stand mixer with various MWNT loadings (wt%) (*Number of samples per MWNT wt%, N = 1)*.

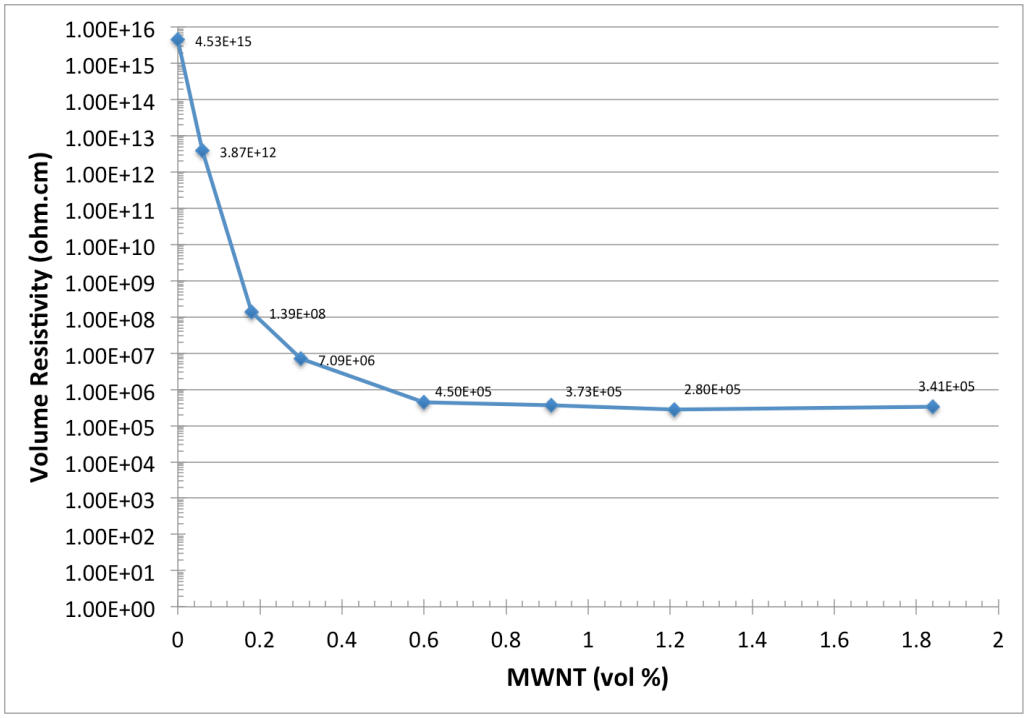

Figure 4.50. Electrical resistivity of CE-MWNT-5 (with 200ppm Fe^{3+} catalyst) polymer nanocomposites processed by stand mixer with various MWNT loadings (vol%) (*Number of samples per MWNT vol%, N = 1)*.

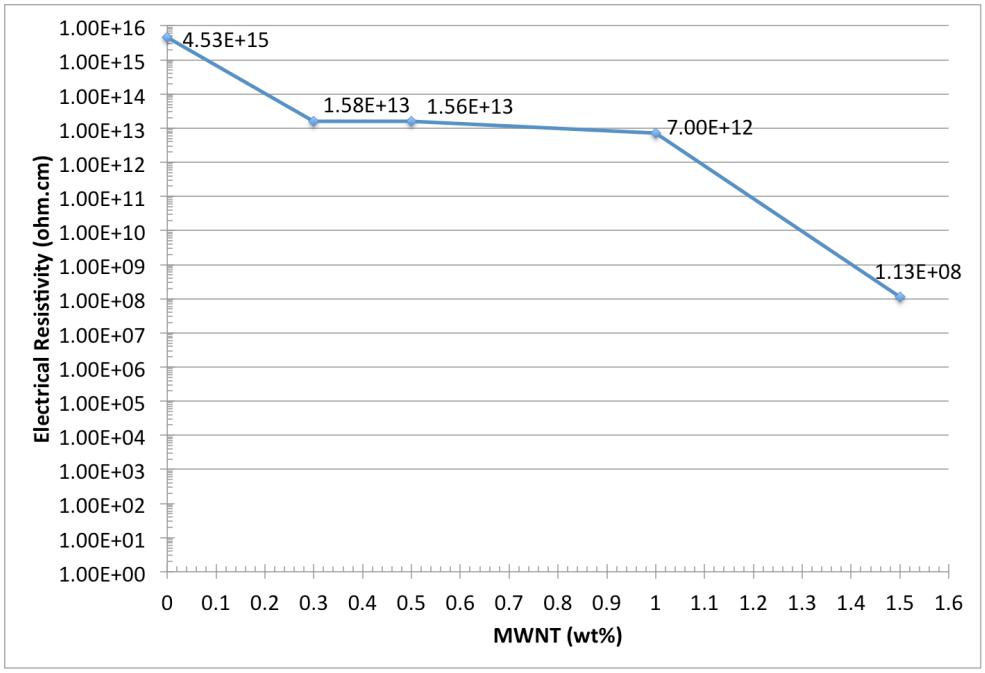

Figure 4.51. Electrical resistivity of CE-MWNT-5 (with 200ppm Fe^{3+} catalyst) polymer nanocomposites processed by three-roll mill with various MWNT loadings (wt%) (*Number of samples per MWNT wt%, N = 1)*.

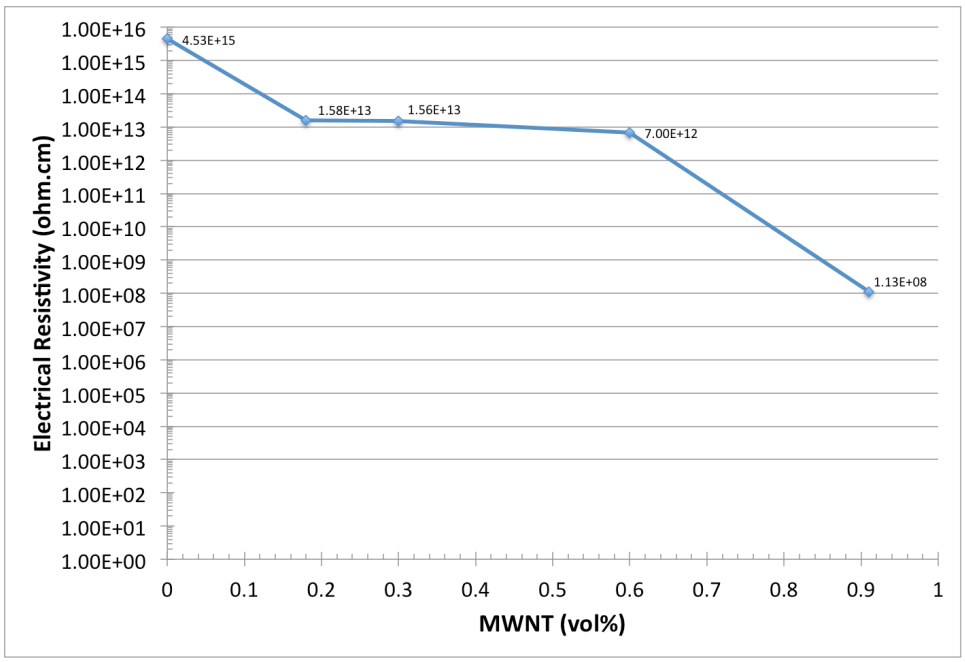

Figure 4.52. Electrical resistivity of CE-MWNT-5 (with 200ppm Fe^{3+} catalyst) polymer nanocomposites processed by three-roll mill with various MWNT loadings (vol%) (*Number of samples per MWNT vol%, N = 1)*.

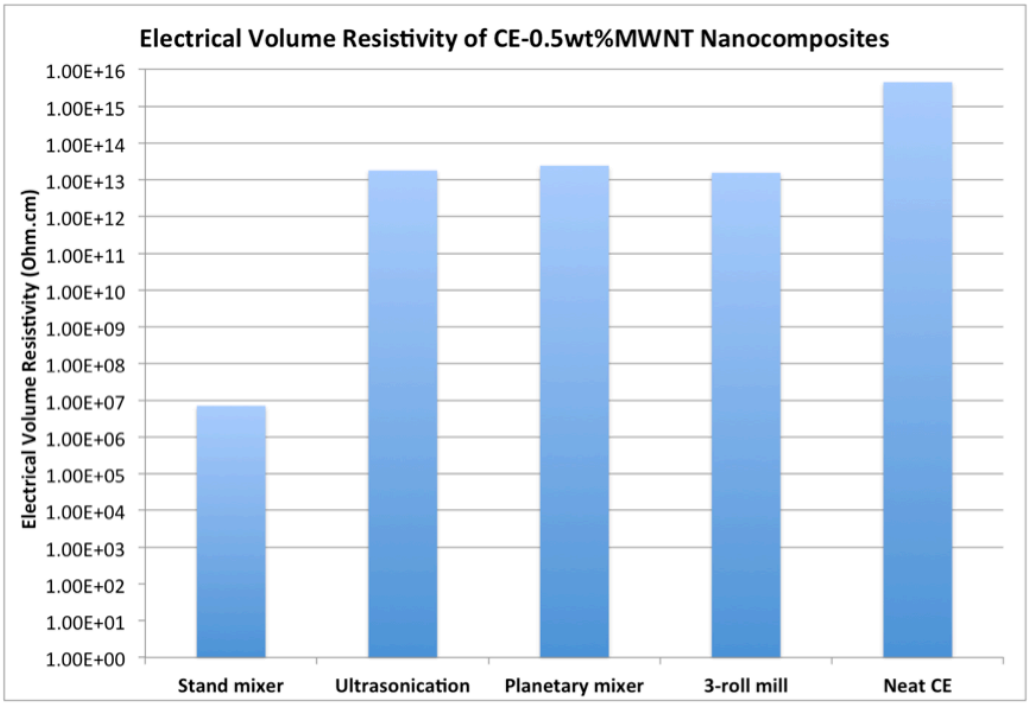

Figure 4.53. Electrical resistivity of CE-0.5%MWNT-5 (with 200ppm Fe^{3+} catalyst) polymer nanocomposites processed by five different processing techniques (*Number of samples per processing technique, N = 1)*.

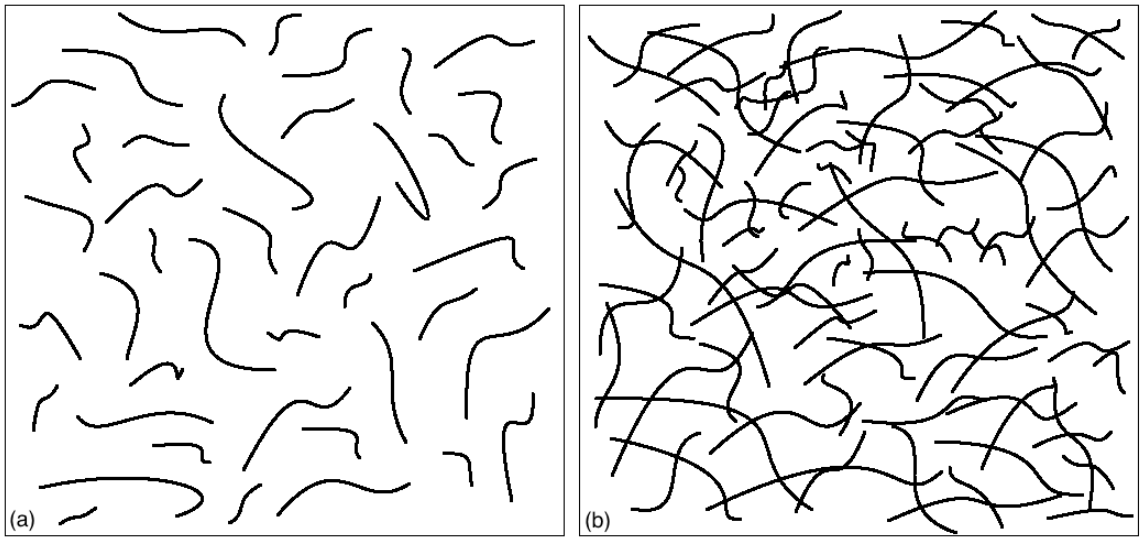

Figure 4.54. Illustration showing correlation of degree of dispersion and electrical conductivity; (a) more de-bundled and better dispersed nanotubes may not form continuous conductive path and (b) conductive path may form in polymer matrix with lower degree of nanotubes dispersion.

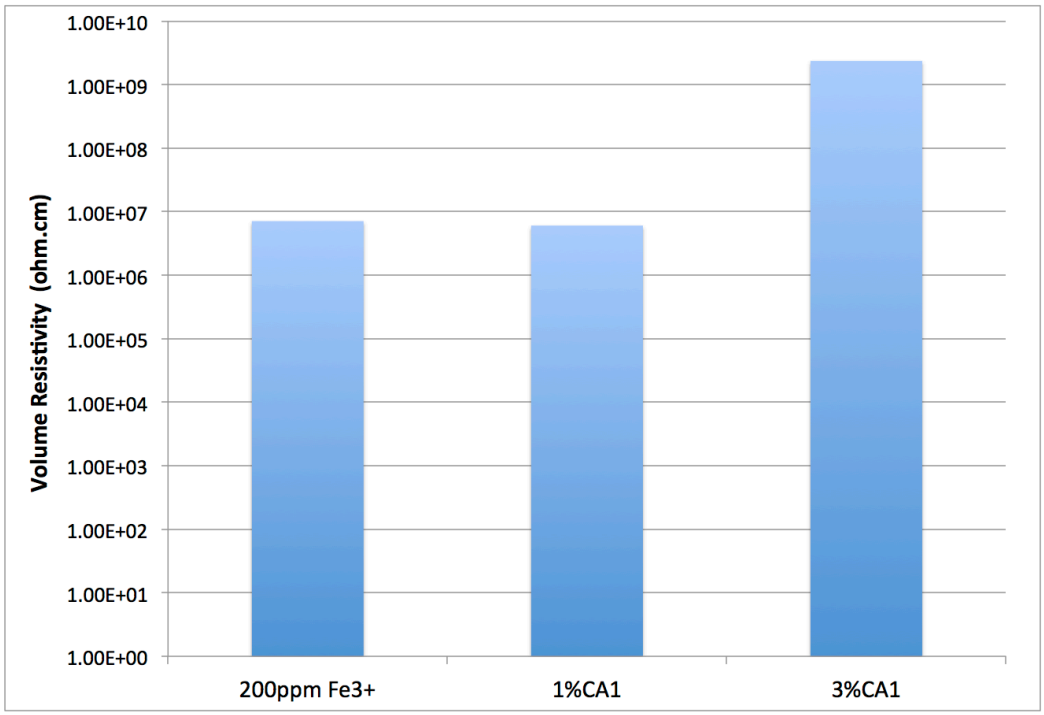

Figure 4.55. Electrical resistivity of CE-0.5%MWNT-5 polymer nanocomposites, cured with Fe^{3+} catalyst (200 ppm) or coupling agent CA-1 (1 or 3%)), and processed by stand mixer (*Number of samples per resin modifier, N = 1).*

Summary

Morphology of the CE-MWNT-5 nanocomposites was characterized by SEM and TEM. Quality of MWNTs dispersion was examined using both visual observation and a method of quantification. Samples processed by different processing techniques show different aggregates sizes and various degrees of de-bundling with aggregates. Inconsistency exists between the visual observation and dispersion quantification methods and further work is needed. Dynamic mechanical analysis shows that both the catalyst and coupling agents had detrimental effects on the mechanical properties and glass transition temperatures of the CE-MWNT nanocomposites. However, the glass transition temperature is not affected by the mixing methods or weight loadings of MWNTs. The thermal stability of the nanocomposites was not significantly affected by the processing techniques or the weight loadings of the MWNTs. Microscale combustion calorimetry shows that the onset temperature of heat release rate remains unaffected by mixing techniques, modifiers, or weight loadings of MWNTs. Electrical resistivity of CE was reduced by the incorporation of MWNTs. Sample processed by the stand mixer has the lowest electrical resistivity among those processed by other techniques.

REFERENCES

1. JEOL Serving Advanced Technology, "A Guide to Scanning Microscope Observation," p.5, 2013.
2. T. Glaskova, M. Zarrelli, A. Aniskevich, M. Giordano, L. Trinkler, and B. Berzina, "Quantitative Optical Analysis of Filler Dispersion Degree in MWNT-Epoxy Nanocomposite," *Composites Science and Technology*, 72: 477-481, 2012.
3. H. Sul, J. R. Youn, and Y. S. Song, "Quantitative Dispersion Evaluation of Carbon Nanotubes Using a New Analysis Protocol," *Carbon*, 49: 1473-1478, 2011.
4. X. Fu, J. Wang, J. Ding, H. Wu, Y. Dong, and Y. Fu, "Quantitative Evaluation of Carbon Nanotube Dispersion Through Scanning Electron Microscopy Images," *Composites Science and Technology*, 87: 170-173, 2013.
5. M. Yourdkhani, and P. Hubert, "Quantitative Dispersion Analysis of Inclusions in Polymer Composites," *Applied Materials & Interfaces*, 5: 35-41, 2013.
6. ASTM D2663-08, Standard Test Methods for Carbon Black – Dispersion in Rubber.
7. M. D. Haslam, and B. Raeymaekers, "A Composite Index to Quantify Dispersion of Carbon Nanotubes in Polymer-Based Composite Materials," *Composites: Part B*, 55: 16-21, 2013.
8. Z. P. Luo and J. H. Koo, "Quantifying the Dispersion of Mixture Microstructures," *Journal of Microscopy*, 225(2): 118-125, 2007.
9. Arkema Graphistrength® C100 Materials Data Sheet.
10. U.S. Department of Transportation, "A Microscale Combustion Calorimeter," NTIS, report, Feb 2002.
11. K. Liang, G. Li, H. Toghiani, J. H. Koo, C. U. Pittman Jr., and C. Dave, "Cyanate Ester/Polyhedral Oligomeric Silsesquioxane (POSS) Nanocomposites: Synthesis and Characterization," *Chemistry of Materials* (2006), 18(2), 301-312.
12. H. S. Cho, K. Liang, S. Chatterjee, and C. U. Pittman Jr., "Synthesis, Morphology, and Viscoelastic Properties of Polyhedral Oligomeric Silsesquioxane Nanocomposites with Epoxy and Cyanate Ester Matrices," *Journal of Inorganic and Organometallic Polymers and Materials* (2006), Volume Date 2005, 15(4), 541-553.
13. K. Liang, H. Toghiani, G. Li, C. U. Pittman Jr., and C. Dave, "Synthesis, Morphology, and Viscoelastic Properties of Cyanate Ester/Polyhedral Oligomeric Silsesquioxane Nanocomposites," *Journal of Polymer Science, Part A: Polymer Chemistry*, 43(17), 3887-3898, 2005.

14. Fundamentals of Electrostatic Discharge, Part One—An Introduction to ESD, ESD Association, Rome, NY, 2010.

15. 15. Hu, N., Z. Masuda, and H. Fukunaga. 2009. Carbon Nanotubes: New Research, Nova Science Publishers, Inc., New York, USA. pp. 175-222.P.

16. P.-C. Ma, N. A. Siddiqui, G. Marom, and J.-K. Kim, "Dispersion and Functionalization of Carbon Nanotubes for Polymer-based Nanocomposites: A Review," *Composites: Part A*, 41: 1345-1367, 2010.

Chapter 5

Carbon Fiber-reinforced Composites

Cyanate ester resin is often used as a structural adhesive or composite for aerospace applications due its good thermal stability, flammability properties, and dielectric properties. Cyanate ester composites reinforced by carbon fibers are useful and attractive in primary structures, high impact resistance and space applications due to their radiation resistance and thermal stability [1]. The fabrication techniques, conditions, and methodologies of carbon fiber-reinforced cyanate ester composites are often poorly described in most studies. Moreover, the cyanate ester used reported in the literature are different from the one selected in this study.

A preliminary study on the fabrication of the carbon fiber-reinforced composite with the PT-15 cyanate ester and cyanate ester nanocomposites was conducted and results are reported in this chapter. It can serve as a basis for the future work for the study on the carbon fiber-reinforced CE-MWNT nanocomposites. Properties characterization, such as tensile strength, electrical resistivity, and morphology were performed.

Based on the results from Chapter 4, three formulations were chosen for further studies of carbon fiber-reinforced composites (Table 5.1).

Table 5.1 Formulations of CE-MWNT Nanocomposites Chosen for the Fabrication of Carbon Fiber-reinforced Nanocomposites

Sample	CA1 (wt%)	MWNT-5 (wt%)
1	0	0
2	3	0
3	3	0.5

CA1 was selected over Fe^{3+} catalyst, because it had a lesser effect on the CE's glass transition temperature. Due to the low percolation threshold achieved by the stand

mixer processing technique, it was used to incorporate 0.5 wt% of MWNT-5 into the CE resin. A bi-directional woven carbon fiber fabric (Pyrofil® TR30S 6K) was used. A hand layup process was used in this fabrication.

CARBON FIBER-REINFORCED COMPOSITES PANEL FABRICATION

A study on the cure condition was performed. Neat CE, CE+CA1, or CE+CA1+MWNT mixture was brushed on a single layer of carbon fiber. The weight ratio of resin/carbon fiber is 35/65. To account for the loss of resin during the hand lay-up process, in which the brush will absorb some resin, more resin (+5 wt%) was prepared. Weights of the carbon fibers were measured before and after the brushing of the CE resin to confirm the weight ratio of the resin/carbon fiber. It was then placed into a furnace to determine the temperature and time when the CE resin in the carbon fibers was partially cured (B-stage), as the prepreg became tacky but not completely harden. It was found that the sample with neat CE reaches B-stage after being heated at 170°C for 25 minutes while the sample with CE+CA1 / CE+CA1+MWNT at 150°C for 50 minutes.

To investigate the composite fabrication parameters (i.e., temperatures and pressures required for compression molding), layers of carbon fiber brushed with the CE polymer resin or mixture were stacked and placed between the heated platens of the compression machine (Wabash MPI Genesis 30 Ton) until the polymer resin/mixture reached the B-stage. Pressure was then applied and temperature was raised until the polymer resin/mixture cured, followed by a post cure step. Table 5.2 summaries the compression molding conditions for each sample.

Table 5.2 Conditions for the Fabrication of Carbon Fiber-Reinforced CE Nanocomposites with Compression Molding Machine

Step	Conditions	Sample 1	Samples 2 and 3
1	**Temperature (°C) / Time (min)**	170 / 25	150 / 50
	Pressure (psi)	0	0
2	**Temperature (°C) / Time (min)**	200 / 15	200 / 15
	Pressure (psi)	30	30
3	**Temperature (°C) / Time (min)**	200 / 15	200 / 15
	Pressure (psi)	300	300
4	**Temperature (°C) / Time (min)**	250 / 60	250 / 60
	Pressure (psi)	700	700

A 8” x 10” x 0.125” panel using ten plies of carbon fibers was made for mechanical property testing while a thinner 4” x 4” x 0.04” panel of three plies was fabricated for electrical resistivity measurement. The resin/nanocomposite was heated into molten state and brushed onto each layer of carbon fibers evenly. Brushed carbon fibers were then layered or stacked by hand and cured with the compression molding machine using the cycle shown in Table 5.2. Table 5.3 shows the compositions of the composites, and Figure 5.1 shows a cured Sample 1.

Table 5.3 Composition of Carbon Fiber-Reinforced CE Nanocomposites

Sample	CE Resin		CE/Carbon Fiber (wt%/wt%)
	CA1 (wt%)	MWNT-5 (wt%)	
1	0	0	35/65
2	3	0	35/65
3	3	0.5	35/65

Number of samples per composite type, N = 1

Figure 5.1. A thin panel of CE carbon-reinforced composite of three plies of carbon fibers (Sample 1) for electrical resistivity measurement.

CHARACTERIZATIONS

Tensile specimens were cut from the thicker panel, while specimens for electrical resistivity specimens were cut from the thinner panel, using waterjet cutter.

Mechanical Testing

Tension test was performed in accordance with ASTM D638 with a platen displacement rate of 5mm/min. Table 5.4 shows the ultimate tensile strength and tensile strength at fracture of the three samples. Five specimens from each panel were used for each tensile testing. After the tension testing, delamination in the reduced section of Sample 1 tensile specimens, without fracture, was observed as shown in Figure 5.2. This could be the reason why both the ultimate tensile strength and the tensile strength at fracture of Sample 1 are only half of those of Samples 2 and 3. Samples 2 and 3 fractured

at the reduced section of the tensile specimens, as shown in Figure 5.3. Both their ultimate tensile strength and tensile strength at fracture are similar (differences ≤5%).

Table 5.4 Tensile Strength of Carbon Fiber-reinforced CE Nanocomposites (ASTM D638, 5mm/min).

Sample	**Ultimate Tensile Strength (MPa)**		**Tensile Strength at Fracture (MPa)**	
	Average	S.D. (±)	Average	S.D. (±)
1	305	21	270	61
2	588	8	534	9
3	566	25	564	26

Number of tensile specimens per composite panel, N = 5

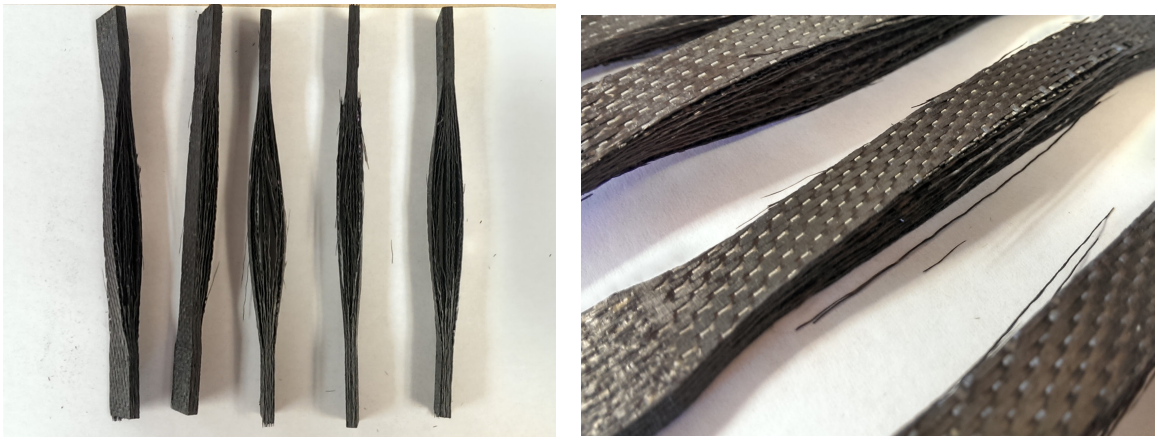

Figure 5.2. Pictures of tested Sample 1 tensile specimens showing delamination after tensile testing to failure (ASTM D638, 5mm/min).

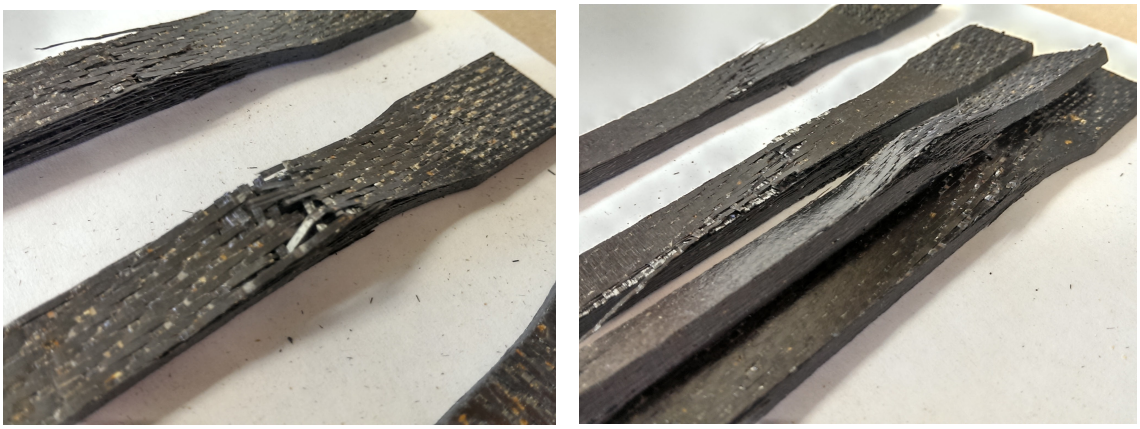

Figure 5.3. Pictures showing tested specimens of Sample 2 (left) and Sample 3 (right) (ASTM D638, 5mm/min).

Electrical Resistivity Measurement

The electrical resistivity of carbon fiber-reinforced CE-MWNT nanocomposites of 1 mm thick was measured using the same instrument and method used on the CE-MWNT nanocomposites in Chapter 4. The volume resistivity was measured through thickness of the composite laminates. Figure 5.4 shows the results. Since carbon fibers are conductive, the electrical resistivity of the Sample 1 (neat CE) and Sample 2 (CE + CA1) is much lower than the neat CE (>1 $x10^{16}$ohm.cm), while the electrical resistivity of Sample 1 and Sample 2 is similar. Sample 3 shows a resistivity 40% lower than that of Samples 1 and 2 which may be due to the MWNTs connecting some of the carbon fibers layers providing better path for electrons to travel through the composite. Moreover, as mentioned in Chapter 4, the requirement for ESD is $1x10^{11}$ ohm.cm or below so all three samples pass the ESD requirement.

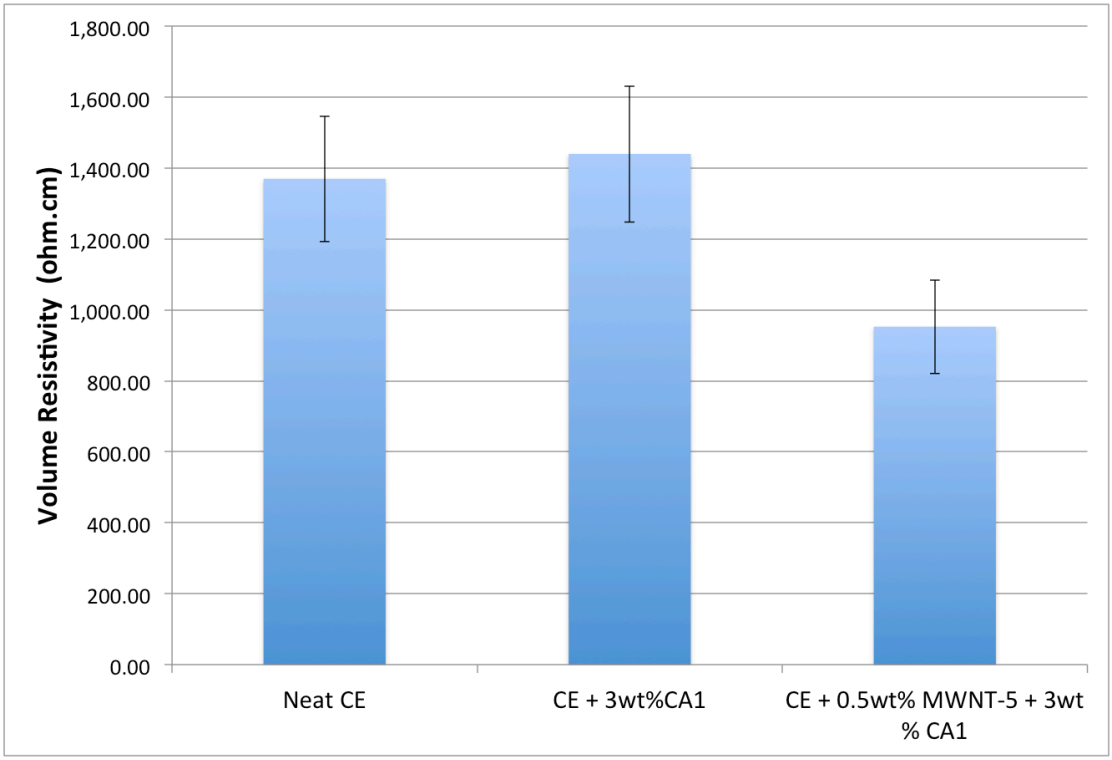

Figure 5.4. Electrical resistivity of the carbon fiber-reinforced CE nanocomposites. One specimen was tested per sample, and ten readings were measured at different locations on each sample.

Structural Morphology

The microstructure of the carbon fiber-reinforced CE composites were examined by SEM. Images of the cross section of the samples, cut by waterjet cutter, were obtained and shown in Figures 5.5 – 5.8. Figure 5.5 shows the representative images of microstructure of Sample 1. The microstructures of the untested specimens look very similar in all Samples 1, 2, and 3. Layers of carbon fibers are packed and intact, and no voids are observed. Cyanate ester resin can be seen on the image with higher magnification. Figures 5.6 – 5.9 show the cross sections of the tension tested specimens. Delamination of most layers of carbon fibers is observed in Sample 1 while fracture of fibers along the tension direction is observed in all three samples. Delamination is also observed in Samples 2 and 3 but it happens mainly in layers closer to the top and/or bottom surfaces of the specimens.

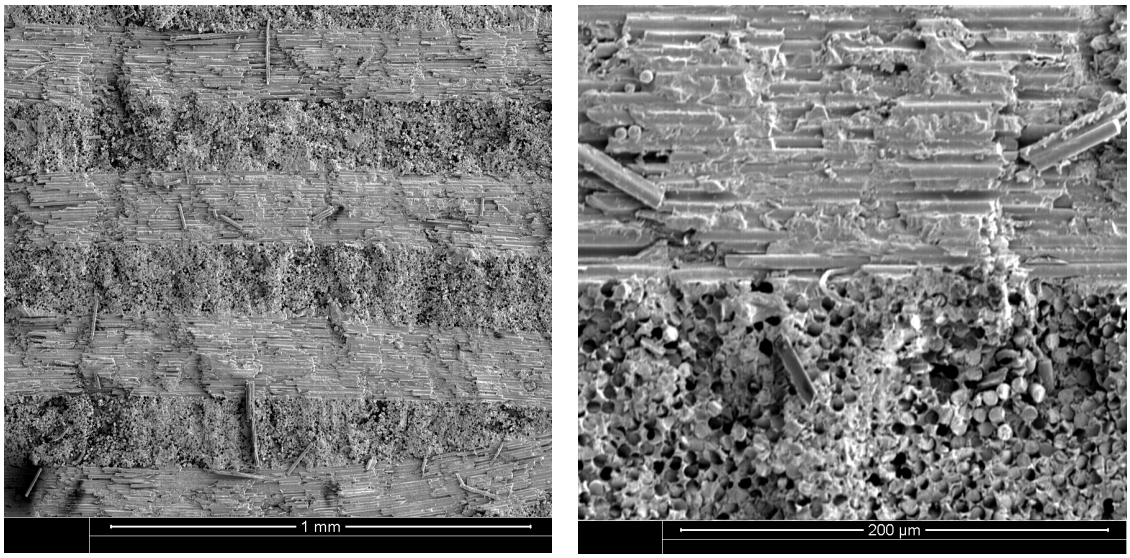

Figure 5.5. SEM images of Sample 1 carbon fiber-reinforced CE composites, in lower (left) and higher (right) magnification (length bar: 1mm left, 200µm right).

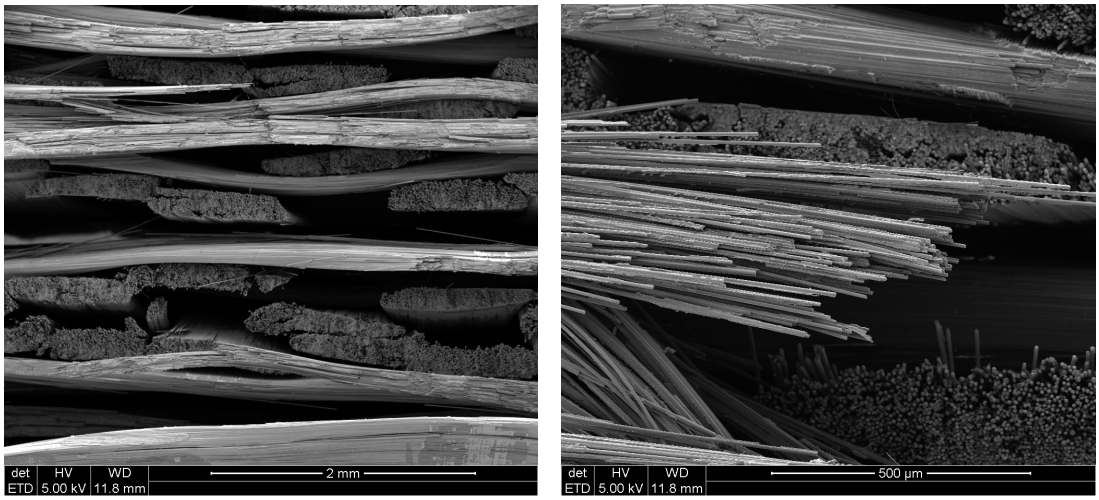

Figure 5.6. SEM images the cross section of tested carbon fiber-reinforced CE composites (Sample 1) showing (left) delamination of layers and fracture of carbon fibers along the tension direction and (right) higher magnification of the fractured carbon fibers (length bar: 2mm left, 500µm right).

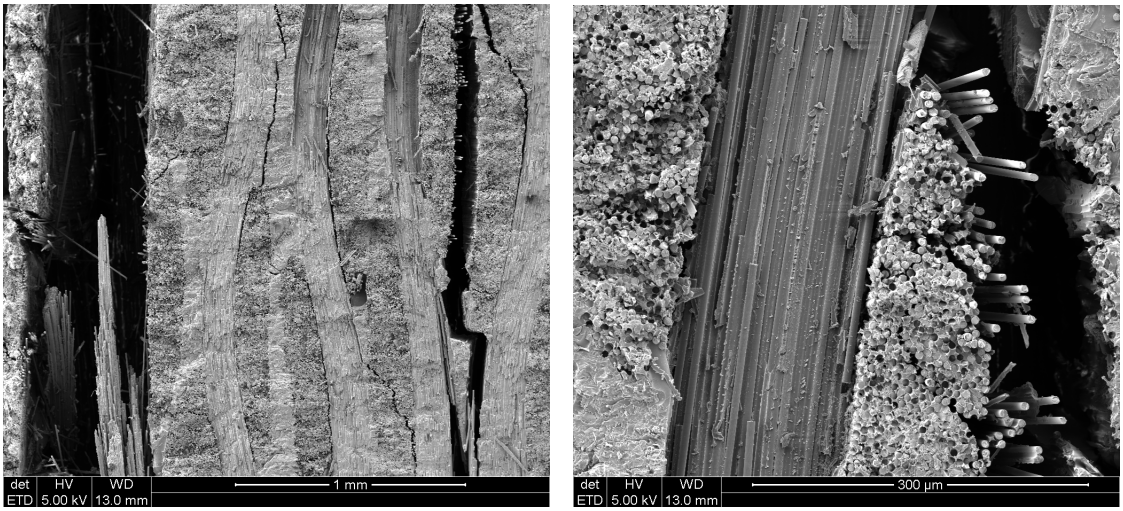

Figure 5.7. SEM images of the cross section of tested carbon fiber-reinforced CE+CA1 composites (Sample 2) close to the fracture site showing (left) delamination of some layers and fracture of carbon fibers and (right) higher magnification image of the fibers (length bar: 1mm left, 300µm right).

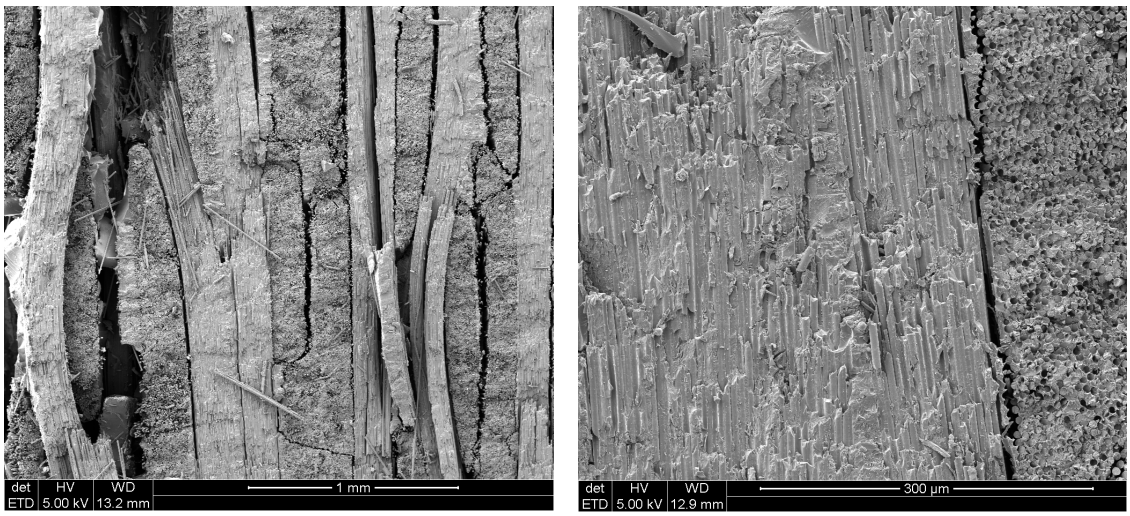

Figure 5.8. SEM images of the cross section of tested carbon fiber-reinforced CE+CA1+MWNT nanocomposites (Sample 3) close to the fracture site showing (left) delamination of some layers and fracture of carbon fibers and (right) higher magnification image of the fibers (length bar: 1mm left, 300µm right).

SUMMARY

Carbon fiber-reinforced CE-MWNT nanocomposites were successfully fabricated although the cure conditions used may not be optimum. A conclusion regarding the enhancement/effects of mechanical properties of the composite materials due to the incorporation of CA1 and/or MWNTs cannot be drawn due to the delamination of Sample 1. Further study is needed to find out the reason of the delamination. However, it is evident that MWNT lowers the through thickness electrical resistivity of the carbon fiber-reinforced composite materials.

REFERENCES

1. R. B. Durairaj, *Resorcinol: Chemistry, Technology and Applications*, Springer, 2005. p. 393.

Chapter 6

Summary and Future Work

SUMMARY

Cyanate ester multiwall carbon nanotube nanocomposites were fabricated using five processing techniques, namely, (1) ultrasonication, (2) low-speed mechanical mixing (using a stand mixer), (3) high shear mixing, (4) three-roll milling, and (5) revolving and centrifugal mixing (using a planetary centrifugal mixer). A direct comparison of various processing techniques, which was not reported by other studies, was made in this study.

MWNT phase separation from the CE resin during cure was solved by incorporating either (1) a Fe^{3+} catalyst, which enabled lowering of the cure temperature, or (2) a coupling agent, designed to enhance the adhesion between the CE resin and MWNTs.

Microstructural morphology characterizations by SEM and TEM show that various degrees of dispersions of MWNTs were obtained by the different mixing techniques. An attempt to quantify the MWNT dispersion was made, although the results appear to be inconsistent between the visual observations from the microscopy images. Further study is needed to resolve the apparent inconsistency.

Different processing techniques lead to varying degrees of electrical resistivity enhancement. Electrical resistivity of samples processed by both stand mixer and three-roll mill passes the ESD requirement; however, the MWNT percolation thresholds by the two techniques are different. The results indicate that better MWNTs dispersion (as in samples processed by three-roll mill) is not always desired. Enhancement of material

properties such as the electrical conductivity requires a relatively worse MWNTs dispersion, or a MWNT network in the polymer resin.

Thermal analysis shows that the addition of the Fe^{3+} catalyst or the coupling agent lowers the glass transition temperature and the mechanical properties (e.g., storage modulus, tangent of phase angle delta) of the CE resin. On the other hand, processing techniques only affect the mechanical properties of the resin.

Thermal stability of CE is only slightly affected by different processing techniques, as well as the addition of MWNTs. Much more significantly, flammability characterization shows that the incorporation of either the Fe^{3+} catalyst or the coupling agent substantially increases the PHRR relative to the neat CE resin value.

Preliminary study on carbon fiber-reinforced CE-MWNT nanocomposites was performed and the composites were successfully fabricated. Tensile test, electrical resistivity measurement, and structural morphological study were conducted. The carbon fiber-reinforced CE composite with neat CE (Sample 1) shows delamination after the tensile test, so whether or not the incorporation of coupling agent and/or MWNTs enhance/affect the mechanical properties of the composite materials is inconclusive. Further study is needed to determine the cause of the delamination. Nonetheless, the electrical resistivity of the composite materials is lowered by the incorporation of MWNTs.

FUTURE WORK

Additional work should be conducted to identify methods to enhance the dispersion of MWNTs. For instance, the combination of ultrasonication with three-roll

milling, planetary centrifugal mixer or stand mixer might result in smaller and looser (more de-bundled) MWNT aggregates in the CE resin.

Investigation on the optimum amount of Fe^{3+} and coupling agent used should also be performed to lower the adverse effect they have on the mechanical properties, the glass transition temperature, and particularly the flammability properties.

The incorporation of higher weight loadings of MWNTs in the composite materials should also be studied. As it stands, incorporating even modest amounts (0.5 wt%) of MWNTs into the relatively inviscid, heated CE resin was a real challenge.

Improving the method to quantify of the degree of MWNT dispersion would help the community. More characterizations, such as mechanical (compression, flexural, and shear), thermal stability, flammability, and ablation properties, on the composite materials should be conducted.

Cure and fabrication procedures for the carbon fiber-reinforced CE-MWNT nanocomposites are far from being optimized. That said, it is an extremely complex, coupled process that will not easily yield to optimization.

The potential of manufacturing multifunctional carbon fiber-reinforced CE-MWNT nanocomposites is significant. Currently, Mitsubishi Aldila Composite Materials is planning to scale up this technology for Raytheon Company's aerospace applications.

References

J. H. Koo, Polymer Nanocomposites: Processing, Characterization, and Applications, McGraw-Hill, New York, 2006.

J. Leng, and A. K. Lau, Multifunctional Polymer Nanocomposites, CRC Press, Boca Raton, 2011.

J. Cheng, S. Lao, J. Yong, J. H. Koo, P. Ferreira, L. Pilato, G. Wissler, and Z. P. Luo, "Cyanate Ester-Buckytubes Nanocomposites: Processing and Characterization," Proc. SAMPE 2007 ISSE, SAMPE, Covina, CA (2007).

K. A. Watson, J. G. Smith Jr., and J. W. Connell, Soc. Adv. Mat. Proc. Eng. Ser., 48: 1145, 2003.

D. A. Scola, "Polyimide Resins," ASM Handbook, Composites, 21: 105-119, 2001.

S. Ghose, K. A. Watson, H. A. Elliott, D. C. Working, J. M. Criss, K. L. Dudley, E. J. Siochi, and J. W. Connell, "Fabrication and Characterization of High Temperature Resin/Carbon Nanofiller Composites," Proc. Multifunctional Nanocomposites 2006, Sept 20-22, Honolulu, HI, 2006.

Y. Lu, M. Zhan, and W. Zheng, "Preparation and Properties of T300 Carbon Fiber-Reinforced Thermoplastic Polyimide Composites," J. Appl. Polym. Sci., 102: 646- 654, 2006.

T.-C. Mo, H.-W. Wang, S.-Y. Chen, and Y.-C. Yeh, "Synthesis and Characterization of Polyimide/Multi-Walled Carbon Nanotube Nanocomposites," Polymer Composites, 29(4): 451-457, 2008.

D. Kohli, R. Mayhew, S. L. Peake, M. Bucchi, T. Vuong, F. Riel, and E. Delaney, Proc. SAMPE 1993 ISSE, 25: 318-326, SAMPE, Covina, CA (1993).

L. Christodoulou and J. D. Venables, "Multifunctional Material Systems: the First Generation," Journal of Materials, 55: 39-45, 2003.

M. Moniruzzaman and K. I. Winey, "Polymer Nanocomposites Containing Carbon Nanotubes," Macromolecules, 39: 5194-5205, 2006.

D. Dean, M. O. Abdalla, S. Ganguli, M. Jose, S. Campbell, J. Gillman, W. H. Awad, and R. Vaia, "High Temperature Thermoset Nanocomposites," Proc. SAMPE 2003 ISSE, SAMPE, Covina, CA (2003).

I. Hamerton, Chemistry and Technology of Cyanate Ester Resins, Blackie Academic & Professional, New York, 1994, p. 122.

Primaset® PT-15 Brochure. Lonza Inc. Fair Lawn, NJ.

K. Shivakumar, F. Abali, R. Sadler, and J. McCoy, "Development of Cyanate Ester Based Carbon/Carbon Composites," Proc. SAMPE 2000 ISESE, SAMPE, Covina, CA (2000), p. 1005.

F. Abali, K. Shivakumar, N. Hamidi, and T. Sadler, "An RTM Densification Method of Manufacturing Carbon-Carbon Composites Using PT-30 Resin," Carbon, 41 (5), 893 (2003).

Koo et al. "Thermo-Oxidative Studies of Nanomodified Carbon/Carbon Composites," The University of Texas at Austin, Dept. of Mechanical Engineering, Austin, TX. Proc. SAMPE 2004 ISSE, SAMPE, Covina, CA (2004).

Koo et al. "Nanomodified Carbon/Carbon Composites for Intermediate Temperature: Processing and Characterization," Texas A&M University, Dept. of Mechanical Engineering, College Station, TX. Proc. SAMPE 2003 ISTC, SAMPE, Covina, CA (2003).

S. Ganguli, D. Derrick; K. Jordan, G. Price, and R. Vaia, "Cyanate Ester Resins - A Candidate for High Temperature Space Applications," TCAM, Tuskegee University, Tuskegee, AL. Proc. NATAS Annual Conference on Thermal Analysis and Applications (2001), 29th, 250-256.

D. Dean, M. O. Abdalla, S. Ganguli, M. Jose, S. Campbell, J. Gillman, W. H. Awad, and R. Vaia, "High Temperature Thermoset Nanocomposites," Tuskegee-Center for Advanced Materials, Tuskegee University, Tuskegee, AL. PMSE Preprints (2003), 89, 729-732.

S. Ganguli, D. Dean, K. Jordan, G. Price, and R. Vaia, "Chemorheology of Cyanate Ester-Organically Layered Silicate Nanocomposites," Polymer (2003), 44(22), 6901-6911.

D. R. Dean, S. Ganguli, M. Abdalla, S. Campbell, R. Vaia, and M. Jose, "High Temperature Thermoset Nanocomposites," Tuskegee University, Tuskegee, AL. 226th ACS National Meeting, New York, NY, September 7-11, 2003 (2003), PMSE-433.

S. Ganguli, D. Dean, K. Jordan, and G. Price, "Structure Processing Property Relationships of Cyanate Ester-Organically Layered Silicates Nanocomposites," Center for Advanced Materials, Tuskegee University, Tuskegee, AL. Proc. SAMPE 2003 ISSE, 48 (Advancing Materials in the Global Economy--Applications, Emerging Markets and Evolving Technologies, Book 1), 1132-1144.

S. Ganguli, D. Dean, K. Jordan, G. Price, and R. Vaia, "Mechanical Properties of Intercalated Cyanate Ester-Layered Silicate Nanocomposites," Polymer (2003), 44(4), 1315-1319.

J. W. Gilman, R. H. Harris, Jr., C. L. Jackson, A. B. Morgan, L. D. Brassell, and D. L. Hunter, "Phenolic Cyanate Ester Clay Nanocomposites: Effect of Ammonium Ion

Structure on Flammability and Nano-dispersion," Polymeric Materials Science and Engineering, 82: 276-277, 2000.

Y. Lin, M. Song, C. A. Stone, and S. J. Shaw, "A Comprehensive Study on the Curing Kinetics and Network Formation of Cyanate Ester Resin/Clay Nanocomposites," Thermochimica Acta, 552: 77-86, 2013.

P. Yongzheng, Y. Xu, L. An, H. Lu, Y. Yang, W. Chen, and S. Nutt, "Hybrid Network Structure and Mechanical Properties of Rodlike Silicate/Cyanate Ester Nanocomposites," Macromolecues, 41(23): 9245-9258, 2008.

T. Wooster, S. Abrol, and D. R. MacFarlane, "Rheological and Mechanical Properties of Percolated Cyanate Ester Nanocomposites," Polymer, 46: 8011-8017, 2005.

H. Lu, and Z. Zhou, "Research on Cyanate Ester Modified Epoxy Resin/Clay Nanocomposites," Wuhan Ligong Daxue Xuebao, 31(21): 89-92, 97, 2009.

S. Nagendiran, C. K. Chozhan, M. Alagar, and I. Hamerton, "Inorganic/Organic Hybrid Nanocomposites Involving OMMT clay and Cyanate Ester-Siloxane-Modified Epoxy Resin: Thermal, Dielectric and Morphological Properties," High Performance Polymers, 20(3): 323-347, 2008.

S. Nagendiran, S. Premkumar, and M. Alagar, "Mechanical and Morphological Properties of Organic, Inorganic, Hybrid, Clay-filled, and Cyanate Ester/Siloxane Toughened Epoxy Nanocomposites," Journal of Applied Polymer Science, 106(2): 1263-1273, 2007.

K. Dinakaran, and M. Alagar, "Preparation and Characterization of Epoxy-Cyanate Ester Interpenetrating Network Matrices/Organoclay Nanocomposites," Polymers for Advanced Technologies, 14(8): 574-585, 2003.

K. Liang, G. Li, H. Toghiani, J. H. Koo, C. U. Pittman Jr., and C. Dave, "Cyanate Ester/Polyhedral Oligomeric Silsesquioxane (POSS) Nanocomposites: Synthesis and Characterization," Chemistry of Materials (2006), 18(2), 301-312.

H. S. Cho, K. Liang, S. Chatterjee, and C. U. Pittman Jr., "Synthesis, Morphology, and Viscoelastic Properties of Polyhedral Oligomeric Silsesquioxane Nanocomposites with Epoxy and Cyanate Ester Matrices," Journal of Inorganic and Organometallic Polymers and Materials (2006), Volume Date 2005, 15(4), 541-553.

K. Liang, H. Toghiani, G. Li, C. U. Pittman Jr., and C. Dave, "Synthesis, Morphology, and Viscoelastic Properties of Cyanate Ester/Polyhedral Oligomeric Silsesquioxane Nanocomposites," Journal of Polymer Science, Part A: Polymer Chemistry (2005), 43(17), 3887-3898.

J. Seetharaman, D. Subramani, R. V. Muthukumaraswamy, C. Ayyavu, A. K. Achimuthu, and A. Muthukaruppan, "Thermal, Thermomechanical and Morphological Behavior of Octa(maleimidophenyl) Silsesquioxane (OMPS)

Cyanate Ester Nanocomposites," High Performance Polymers, 24(5): 379-388, 2012.

Z. Zhang, G. Liang, X. Wang, S. Adhikari, and J. Pei, "Curing Behavior and Dielectric Properties of Amino-functionalized Polyhedral Oligomeric Silsesquioxane/Cyanate Ester Resin Hybrids," High Performance Polymers, 25(4): 427-435, 439, 2013.

Y. Lin, J. Jin, M. Song, S. J. Shaw, C. A. Stone, "Curing Dynamics and Network Formation of Cyanate Ester Resin/Polyhedral Oligomeric Silsesquioxane Nanocomposites," Polymer, 52(8): 1716-1724, 2011.

S. Rakesh, C. R. Sakthi Dharan, M. Selladurai, V. Sudha, P. R. Sundararajan, and M. Sarojadevi, "Thermal and Mechanical Properties of POSS®-Cyanate Ester/Epoxy Nanocomposites," High Performance Polymers, 25(1): 87-96, 2013.

C. Ayyavu, D. Kanniyan, A. K. Achimuthu, and A. Muthukaruppan, "Synthesis and Characterization of Epoxy modified Cyanate Ester POSS Nanocomposites," High Performance Polymers, 24(5): 405-417, 2012.

K. Liang, H. Toghiani, and C. U. Pittman, Jr., "Synthesis, Morphology and Viscoelastic Properties of Epoxy/Polyhedral Oligomeric Silsesquioxane (POSS) and Epoxy/Cyanate Ester/POSS Nanocomposites," Journal of Inorganic and Organometallic Polymers and Materials, 21(1): 128-142, 2011.

Z. P. Zhang, J. Z. Pei, C. Q. Fang, and S. F. Chen, "Enhanced Thermal Properties of Cyanate Ester Resin by Epoxy-Functionalized POSS," Advanced Materials Research, 549: 647-650, 2012.

M.-L. Sham and J.-K. Kim, "Surface Functionalities of Multi-wall Carbon Nanotubes after UV/Ozone and TETA Treatments," Carbon, 44: 768-777, 2006.

D. D. Dominguez, M. Laskoski, and T. M. Keller, "Modification of Oligomeric Cyanate Ester Polymer Properties with Multi-Walled Carbon Nanotube-Containing Particles," Macromolecular Chemistry and Physics, 210: 1709-1716, 2009.

J. Wang, G. Liang, H. Yan, and S. He, "Mechanical and Thermal Properties of Functionalized Multiwalled Carbon Nanotubes/Cyanate Ester Composites," Polymer Engineering & Science, 49(4): 680-684, 2009.

C. Han, A. Gu, G. Liang, L. Yuan, "Carbon Nanotubes/Cyanate Ester Composites with Low Percolation Threshold, High Dielectric Constant and Outstanding Thermal Property," Composites: Part A, 41: 1321-1328, 2010.

Y. Lin, C. A. Stone, S. J. Shaw, and M. Song, "Effect of Carbon Nanotubes on the Curing Dynamics and Network Formation of Cyanate Ester Resin," Journal of Polymer Research, 20: 106, 2013.

E. Taha, J. Wu, K. Gao, and L. Guo, "Preparation and Properties of Fumed Silica/Cyanate Ester Nanocomposites," Chinese Journal of Polymer Science, 30(4): 530-536, 2012.

P. Badrinarayanan, and M. R. Kessler, "Zirconium Tungstate/Cyanate Ester Nanocomposites with Tailored Thermal Expansivity," Composites Science and Technology, 71(11): 1385-1391, 2011.

W. Sun, J. E. D. Leon, C. Ma, X. Tan, and M. R. Kessler, "Novel Si/Cyanate Ester Nanocomposites with Multifunctional Properties," Composites Science and Technology, 72: 1692-1696, 2012.

P. Badrinarayanan, M. K. Rogalski, and M. R. Kessler, "Carbon Fiber-Reinforced Cyanate Ester/Nano-ZrW_2O_8 Composites with Tailored Thermal Expansion," Applied Materials & Interfaces, 4: 510-517, 2012.

C. D. Blasi, C. Branca, A. Galgano, R. Moricone, and E. Milella, "Oxidation of a Carbon/Glass Reinforced Cyanate Ester Composite," Polymer Degradation and Stability, 94: 1962-1971, 2009.

W. K. Goertzen, and M. R. Kessler, "Thermal and Mechanical Evaluation of Cyanate Ester Composites with Low-Temperature Processability," Composites Part A, 38: 779-784, 2007.

K. Chung, and J. C. Seferis, "Evaluation of Thermal Degradation on Carbon Fiber/Cyanate Ester Composites," Polymer Degradation and Stability, 71: 425-434, 2001

Lonza Primaset® PT-15 Technical Data Sheet, Lonza Inc., Fair Lawn, NJ.

F. Abali, K. Shivakumar, N. Hamidi, and R. Sadler, "An RTM Densification Method of Manufacturing Carbon-Carbon Composites Using PT-30 Resin," Carbon, 41(5): 893, 2003.

R. E. Myers, US Patent # 07/447751, 1992.

J. H. Koo, S. C. Lao, et al., "Morphology and Thermal Characterization of Carbon-based Nanomaterials," Proc. SAMPE 2011 ISSE, SAMPE, Covina (2011).

S. Ghose, K. A. Watson, H. A. Elliott, D. C. Working, J. M. Criss, K. L. Dudley, E. J. Siochi, and J. W. Connell, "Fabrication and Characterization of High Temperature Resin/Carbon Nanofiller Composites," Proc. Multifunctional Nanocomposites 2006, Sept 20-22, Honolulu, HI, 2006.

J. Lee, Agency of Defense Development, Daejon, South Korea.

ILjin Nanotech Co., Ltd., Seoul, South Korea (www.iljin.co.kr).

The CM-95 neat MWNT was functionalized with hydroxy (-OH), carboxyl (-COOH), and amine (-NH_2) groups using plasma technology supplied by Dr. Lee of Agency for Defense Development (ADD).

Arkema, Lacq, France (www.graphistrength.fr).

Bayer MaterialScience (www.baytubes.com).

Cheap Tubes Inc., Brattleboro, VT (www.cheaptubes.com).

G. Wang, Z. Tan, X. Liu, V. Samuilov, and M. Dudley, "Preparation and Electrical Properties oft he MWNT/Polymer Nanocomposite Fibers," Proc. MRS 2006 Fall Meeting, Boston, MA, 693 (2006).

Plastics News Online Directory, Ken-React® Coupling Agents (V) (http://www.plasticsnewsdirectory.com/).

ChemBlink, Zicronate Coupling Agent Ken-React® NZ 97 (http://www.chemblink.com/products/111083-78-4.htm).

Emerson Industrial Automation, Branson 1510 (http://www.bransonic.com/).

Breville USA (http://www.brevilleusa.com/stand-mixer.html).

THINKY USA Inc. (http://www.thinkymixer.net/commentary/jiten-kouten.html).

IKA, Inc. (http://www.ikaprocess.com/Products/Inline-disperser-dispersing-machine-high-shear-cph-6/DISPAX-REACTOR-DR-csb-DR/#).

Exakt Technologies, Inc. (http://www.exaktusa.com/products/exakt_E.html)

P.-C. Ma, N. A. Siddiqui, G. Marom, J.-K. Kim, "Dispersion and Functionalization of Carbon Nanotubes for Polymer-based Nanocomposites: A Review," Composites: Part A, 41: 1345-1367, 2010.

ASTM 7309, "Standard Test Method for Determining Flammability Characteristics of Plastics and Other Solid Materials Using Microscale Combustion Calorimetry."

S. Choi, Y. Jeong, G.-W. Lee, and D. H. Cho, "Thermal and Mechanical Properties of Polypropylene Filaments Reinforced with Multiwalled Carbon Nanotubes via Melt Compounding," Fibers and Polymers, 10(4): 513-518, 2009.

Z. Li, S. J. Wilkins, K. S. Moon, and C. P. Wong, "Carbon Nanotube/Polymer Nanocomposites: Improved or Reduced Thermal Stabilities?" Materials Science Forum, 722: 77-86, 2012.

K. A. Wepasnick, B. A. Smith, K. E. Schrote, H. K. Wilson, S. R. Diegelmann, and D. H. Fairbrother, "Surface and Structural Characterization of Multi-walled Carbon Nanotubes Following Different Oxidative Treatments," Carbon, 49: 24-36, 2011.

XPS analysis conducted and data provided by Zsolt E. HORVATH, Hungarian Academy of Sciences, Jul 2011.

D. A. Shirley, "High-Resolution X-Ray Photoemission Spectrum of the Valence Bands of Gold," Phys. Rev. B., 5: 4709-4714, 1972.

F. Abali, K. Shivakumar, N. Hamidi, and R. Sadler, "An RTM Densification Method of Manufacturing Carbon-Carbon Composites Using PT-30 Resin," Carbon, 41(5): 893, 2003.

R. E. Myers, US Patent # 07/447751, 1992.

S. Ghose, K. A. Watson, H. A. Elliott, D. C. Working, J. M. Criss, K. L. Dudley, E. J. Siochi, and J. W. Connell, "Fabrication and Characterization of High Temperature Resin/Carbon Nanofiller Composites," Proc. Multifunctional Nanocomposites 2006, Sept 20-22, Honolulu, HI, 2006.

J. Lee, Agency of Defense Development, Daejon, South Korea.

ILjin Nanotech Co., Ltd., Seoul, South Korea (www.iljin.co.kr).

The CM-95 neat MWNT was functionalized with hydroxy (-OH), carboxyl (-COOH), and amine (-NH_2) groups using plasma technology supplied by Dr. Lee of Agency for Defense Development (ADD).

Bayer MaterialScience (www.baytubes.com).

Cheap Tubes Inc., Brattleboro, VT (www.cheaptubes.com).

G. Wang, Z. Tan, X. Liu, V. Samuilov, and M. Dudley, "Preparation and Electrical Properties oft he MWNT/Polymer Nanocomposite Fibers," Proc. MRS 2006 Fall Meeting, Boston, MA, 693 (2006).

Plastics News Online Directory, Ken-React® Coupling Agents (V) (http://www.plasticsnewsdirectory.com/).

ChemBlink, Zicronate Coupling Agent Ken-React® NZ 97 (http://www.chemblink.com/products/111083-78-4.htm).

Emerson Industrial Automation, Branson 1510 (http://www.bransonic.com/).

Breville USA (http://www.brevilleusa.com/stand-mixer.html).

THINKY USA Inc. (http://www.thinkymixer.net/commentary/jiten-kouten.html).

IKA, Inc. (http://www.ikaprocess.com/Products/Inline-disperser-dispersing-machine-high-shear-cph-6/DISPAX-REACTOR-DR-csb-DR/#).

Exakt Technologies, Inc. (http://www.exaktusa.com/products/exakt_E.html)

ASTM 7309, "Standard Test Method for Determining Flammability Characteristics of Plastics and Other Solid Materials Using Microscale Combustion Calorimetry."

S. Choi, Y. Jeong, G.-W. Lee, and D. H. Cho, "Thermal and Mechanical Properties of Polypropylene Filaments Reinforced with Multiwalled Carbon Nanotubes via Melt Compounding," Fibers and Polymers, 10(4): 513-518, 2009.

Z. Li, S. J. Wilkins, K. S. Moon, and C. P. Wong, "Carbon Nanotube/Polymer Nanocomposites: Improved or Reduced Thermal Stabilities?" Materials Science Forum, 722: 77-86, 2012.

K. A. Wepasnick, B. A. Smith, K. E. Schrote, H. K. Wilson, S. R. Diegelmann, and D. H. Fairbrother, "Surface and Structural Characterization of Multi-walled Carbon Nanotubes Following Different Oxidative Treatments," Carbon, 49: 24-36, 2011.

XPS analysis conducted and data provided by Zsolt E. HORVATH, Hungarian Academy of Sciences, Jul 2011.

D. A. Shirley, "High-Resolution X-Ray Photoemission Spectrum of the Valence Bands of Gold," Phys. Rev. B., 5: 4709-4714, 1972.

JEOL Serving Advanced Technology, "A Guide to Scanning Microscope Observation," p.5, 2013.

T. Glaskova, M. Zarrelli, A. Aniskevich, M. Giordano, L. Trinkler, and B. Berzina, "Quantitative Optical Analysis of Filler Dispersion Degree in MWNT-Epoxy Nanocomposite," Composites Science and Technology, 72: 477-481, 2012.

H. Sul, J. R. Youn, and Y. S. Song, "Quantitative Dispersion Evaluation of Carbon Nanotubes Using a New Analysis Protocol," Carbon, 49: 1473-1478, 2011.

X. Fu, J. Wang, J. Ding, H. Wu, Y. Dong, and Y. Fu, "Quantitative Evaluation of Carbon Nanotube Dispersion Through Scanning Electron Microscopy Images," Composites Science and Technology, 87: 170-173, 2013.

M. Yourdkhani, and P. Hubert, "Quantitative Dispersion Analysis of Inclusions in Polymer Composites," Applied Materials & Interfaces, 5: 35-41, 2013.

ASTM D2663-08, Standard Test Methods for Carbon Black – Dispersion in Rubber.

M. D. Haslam, and B. Raeymaekers, "A Composite Index to Quantify Dispersion of Carbon Nanotubes in Polymer-Based Composite Materials," Composites: Part B, 55: 16-21, 2013.

Z. P. Luo and J. H. Koo, "Quantifying the Dispersion of Mixture Microstructures," Journal of Microscopy, 225(2): 118-125, 2007.

Arkema Graphistrength® C100 Materials Data Sheet.

U.S. Department of Transportation, "A Microscale Combustion Calorimeter," NTIS, report, Feb 2002.

K. Liang, H. Toghiani, G. Li, C. U. Pittman Jr., and C. Dave, "Synthesis, Morphology, and Viscoelastic Properties of Cyanate Ester/Polyhedral Oligomeric Silsesquioxane Nanocomposites," Journal of Polymer Science, Part A: Polymer Chemistry, 43(17), 3887-3898, 2005.

Fundamentals of Electrostatic Discharge, Part One—An Introduction to ESD, ESD Association, Rome, NY, 2010.

Hu, N., Z. Masuda, and H. Fukunaga. 2009. Carbon Nanotubes: New Research, Nova Science Publishers, Inc., New York, USA. pp. 175-222.P.

R. B. Durairaj, Resorcinol: Chemistry, Technology and Applications, Springer, 2005. p. 393.